INTERROGATION OF THE LIMITATIONS AND CAPABILITIES OF THE MODEL-GEL-TISSUE ASSAY AND APPLICATION TO SOFT TISSUE MODULUS EVALUATION

By

Stephanie Lynne Barnes

Dissertation

Submitted to the Faculty of the

Graduate School of Vanderbilt University

in partial fulfillment of the requirements

for the degree of

DOCTOR OF PHILOSOPHY

in

Biomedical Engineering

May, 2011

Nashville, Tennessee

Approved:

Professor Michael I. Miga

Professor John C. Gore

Professor Robert J. Roselli

Professor Alissa M. Weaver

Professor Thomas E. Yankeelov

TABLE OF CONTENTS

Page

ACKNOWLEDGEMENTS

First and foremost, I want to thank my family. To my hubby-to-be, Adam, who is my best friend, my relief from the day, and who is often the inevitable bearer of my frustration – thank you for your love and support, and the many late nights spent hanging out with me in the lab while I squished gels and scanned samples. I can't express with words how much you mean to me and how lucky I am to have you. Thank you to my mom and dad, my brother Jeff, and my sisters Courtney and Julie. My family has served as my rock, giving me unwavering love and support and ensuring my confidence. I always know that I can turn to you guys in good times and in bad, and that is a luxury of which I am greatly appreciative. I love you all, and I hope I say it frequently enough, but thank you for everything.

My gratitude also goes to my advisor, Dr. Miga. He has provided me with insight, aided in problem solving, and been a constant source of enthusiasm and support for this research. I thank you for your confidence and your constant willingness to help me succeed. Also, to my committee members, Dr. Gore, Dr. Roselli, Dr. Weaver, and Dr. Yankeelov: thank you for your patience and guidance throughout this process. Especially thank you to Dr. Yankeelov who guided the direction of the final portion of this research and to Jennifer Whisenant who put up with me through the incessant emailing and many late nights of tissue collection.

Thank you to the members of BML and SNARL and all of my friends and confidants within Biomedical Engineering. The willingness to help that is eminent in all of the individuals within this department is amazing, and I am truly appreciative to have been a part of this department. Additionally, thank you to everyone who has helped me

in some way over the course of my years at Vanderbilt, including the machine shop, members of VUIIS, specifically Jarrod True who dealt graciously with all of my questions and issues, and Daniel Perrien who was always immediately available to help with the CT, and the BME administrative staff.

Finally, this research would not have been possible without the funding provided by the NSF Graduate Research Fellowship and the Vanderbilt University Discovery Grant.

LIST OF TABLES

LIST OF FIGURES

CHAPTER I

INTRODUCTION AND BACKGROUND

Introduction

Biological tissue mechanical property evaluation is generally concentrated on load-bearing tissues such as bone and skin. However, recent effort has been directed toward understanding the mechanical properties of soft tissue due mainly to motivations in the areas of modeling and disease evaluation. In regards to modeling, soft tissue models are used in a variety of applications, from predictive strategies such as surgical planning, to teaching methodologies such as surgical simulations [1-4]. In order generate accurate models, a precise input of the soft tissue properties is required. Due to this recent need for accurate assessment of tissue modulus values, attempts have been made to develop robust frameworks for soft tissue measurements. However, due to the difficulties associated with soft tissue mechanical property evaluation, specifically regarding sample shape and consistency, standard evaluation techniques have proven elusive and highly variable.

The more prevalent motivating reason for evaluating the mechanical properties of soft tissue is in regards to disease assessment. Disease in soft tissues generally results in a restructuring of the normal tissue components, which manifests as a change in the elastic modulus (the common mechanical property to observe in evaluation) of the tissue [5]. In most cases, the tissue tends to stiffen with disease (an elevated elastic modulus), though in some cases it can soften; regardless of directionality, changes in modulus have

been observed in many different pathological conditions which could potentially be used as a macroscopic evaluation of disease. A common example of elastic modulus as an indicator of disease is in the case of breast and prostate tissue, where a physical exam consisting of palpation of the affected area is utilized as a preliminarily evaluation of the presence of cancerous tissue [6, 7]. A change in mechanical properties has similarly been identified in many other pathological conditions, including hepatic fibrosis, arterial disease, myocardial infarction, thyroid disease, and skin cancer, among others [7-21]. Noninvasive methods of tissue evaluation, which rely on the correspondence between tissue modulus and pathological condition, are being devised to mediate the necessity for painful, invasive tissue evaluation methods; specifically, methods such as elastography have been developed to non-invasively assess tissue modulus [7, 11, 22-28]. However, in order for these methods to reach their full diagnostic potential, a baseline 'normal' value for the tissue modulus must be established as well as an understanding of the discriminatory power that mechanical properties might provide in characterizing disease.

As a further consideration, since disease correlates to changes in the microstructure, the elastic modulus of a tissue could potentially serve as a biomarker of microscopic changes within the tissue. This prospective correlation is indicated by work investigating the biological and molecular mechanisms of metastasis [29-32]. Work of this nature has indicated that, in tumors with a propensity to metastasize, there tends to be a dysregulation of extracellular matrix (ECM) gene expression [33]. Specifically, invasiveness has been associated with degradation of the ECM by enzymes such as metalloproteases [34, 35]. Additionally, many procollagen genes have been shown to be altered in highly metastatic tumors [33]. These genes have been associated with

metastatic progression via remodeling of the tumor microenvironment and in promoting cellular adhesion and motility [33, 36-39]. In breast cancer, fibrotic foci and desmoplasia have been associated with the transition from localized tumor to invasive tumor [40, 41]. All of these observed microstructural phenomena could potentially affect the bulk modulus of the tumor tissue, thus eliciting the consideration that a change in the tumor state, such as the propensity to metastasize, could be observed through noninvasive evaluation of the tissue modulus.

With the increasing interest in soft tissue modulus evaluation, an adaptable and consistent soft tissue modulus evaluation technique is desirable. A system that is compatible with noninvasive modulus evaluation techniques for validation purposes yet could serve as a standalone parameterization technique would serve to fill a void in the link between noninvasive diagnostic procedures and soft tissue modulus evaluation. The hypothesis presented here is that an adaptable soft tissue modulus evaluation system can be developed that allows for a simple tissue preparation and combines material testing with computational modeling which could be amenable to elastographic validation as well as independent modulus evaluation.

Specific Aims

The goal of the work presented here is the development, validation, and rigorous examination of a soft tissue modulus evaluation technique developed with the purpose of evaluating the elastic modulus of biological tissue samples which were not amenable, either due to size, shape, or consistency, to traditional material testing methods. To this avail, the method termed the MGT assay is described, which was developed with specific

consideration of the flexibility and practicality of the modulus evaluation procedure. Additionally, this work serves to test the feasibility of the assay as a modulus evaluation technique. Towards this end, the specific aims of this research are as follows:

1. Develop a soft tissue modulus evaluation technique that is amenable to tissue size and shape and adaptable in technique, thus allowing validation of non-invasive modulus evaluation techniques.
2. Validate MGT assay relative to traditionally accepted modulus evaluation techniques.
3. Investigate propensity of modulus evaluation as an indicator of microstructural differences in tissue.
4. Utilize the MGT assay to investigate the prospect of tissue elasticity as a biomarker for tumor responsiveness.
5. Examine the sensitivity and repeatability of the MGT testing protocol by assessing four different aspects:
    a. Consistency of modulus between gels generated simultaneously.
    b. Effect of background modulus on the evaluated tissue modulus.
    c. Reliability and repeatability of embedded modulus reconstruction.
    d. Embedded specimen interface effect on evaluation.

Background

Different basic modulus evaluation techniques include indentation, compression, torsion, shear, and tension testing. Of these, the most utilized techniques for soft tissue

evaluation evolved in the categories of compression and indentation testing. When considering the body of research that has been conducted concerning the mechanical properties of biological soft tissues, one will notice the magnitude of different methods for material testing and modulus calculation. Beyond the initial type of testing performed (i.e. compression versus indenter), the testing protocol can vary from simple linear compression to sinusoidal excitation to complex variations and combinations of approaches, and the model used to describe the tissue behavior can be elastic, viscoelastic hyperelastic, or some other more complex category. The combination of the plethora of options leads to a wide variety of testing and characterization approaches, thus creating a discrepancy in the literature concerning material testing of biological tissues as well as a discord among the resulting modulus values.

Compression Testing

Traditional compression testing is a direct compression of the tissue between two parallel plates. If the tissue is assumed to be elastic, isotropic, and near incompressible, then the linear response can be characterized solely by the elastic modulus. However, the method requires a uniform sample shape, in that the top and bottom surfaces need to be parallel in order to implement standard compression testing. The sample shape stipulation can prove difficult for soft tissues, as they are often hard to cut into a desired shape. Though the shape requirements are tedious, the calculations associated with modulus evaluation through compression testing are relatively simple in comparison to other techniques, lending to the use of variations of compression testing in literature.

Chen et al. utilized uniaxial compression for testing bovine muscle and liver tissue samples [42]. The research involved using a cylindrical punch for compression that had a diameter that was larger than any given sample diameter, so that uniform compression was applied to the surface. In addition, a lubricant was applied to the specimen surface to guarantee unconfined compression during testing and linear elasticity was assumed. The material testing results presented are compared to ultrasound measurements made using a transducer with a diameter of 3.18 cm, which was not always larger than the sample size. The authors recognize the inconsistency of using these two conflicting testing methods and compensate for the differences using numerical analysis. A correction factor is implemented for the ultrasound data that takes into account both the radius of the compressor relative to the tissue radius as well as the confined compression that is induced by the surrounding tissue on the tissue directly below the compressor. The authors note that the soft tissues behave linearly for strains up to 5% and react nonlinearly for strains above 10%. To calculate the average Young's modulus, a least squares fit to the linear portion (<5% strain) of the curve was used. The results showed an average compression value and ultrasound measurement of 2.12±0.91 kPa and 1.53±0.31 kPa, respectively, for the muscle tissue and 0.62±0.24 kPa and 0.94±0.65 kPa for the liver.

Yeh et al. also used a compression-based testing system to evaluate the elastic modulus of human fibrotic liver tissue [10]. In order to account for the necessary shape restrictions, tissue samples were cut into cubes using a surgical blade. Cyclic compression tests were utilized with varying amounts of prestrain (5, 10, and 15%) applied prior to the cyclic compression. A linear evaluation of the upswing of the cyclic

stress-strain values was then used to calculate the modulus of the tissue. The tissue samples were subjected to histology after material testing in order to grade the fibrosis of the samples. The authors found that at the 5% prestrain level, the average modulus value ranged from 0.640 to 1.650 kPa for the range of fibrosis scores. For 10% precompression the values jumped to 1.080 to 4.930 kPa, and at 15% the values reached 2.000 to 19.980 kPa.

Hoyt et al. investigated the viscoelastic properties of human prostate tissue using compression testing [43]. Similarly to previously mentioned work, a custom-made coring tool was utilized to cut the samples. Cancerous and normal tissue samples were cut into cylinders and then subjected to unconfined compression testing. The test consisted of a compression to 5% strain followed by a dwell for 700 seconds. The stress-relaxation curves were fit to a Kelvin-Voigt fractional derivative (KVFD) model by nonlinear least squares in order to obtain the three parameters (E_0, η, and α), from which the frequency-dependent complex Young's modulus was calculated. Results showed a contrast of approximately 2 to 1 in the stiffness of cancerous to normal tissue. At 0.1 Hz, the complex Young's modulus for normal tissue was 3.8 kPa while the cancerous tissue was 7.8 kPa. At 150 Hz, the normal tissue averaged 16.0 kPa while the cancerous tissue was 40.6 kPa.

Kiss et al. also used the KVFD model to analyze the modulus of canine livers [44]. As before, a custom tool was used to cut cylindrical specimen, and then some specimen were ablated to create lesions to analyze differences in modulus values. Unconfined compression was achieved by applying mineral oil to the platens, and a 2% pre-strain was applied. The samples were then cyclically compressed an additional 2% at

frequencies ranging from 0.1 to 400 Hz. The Levenberg-Marquardt method for nonlinear least squares fitting was used to evaluate the KVFD constants. Results showed an average modulus value of 1.995 kPa for normal liver tissue, with lesion values ranging from 10.00 kPa to 26.60 kPa.

This brief review of the compression testing literature illuminates two main points. First, in almost all of the cases, the investigators utilize a specially devised coring tool to create a relatively uniform shape of the samples. This approach is feasible when the sample size is large enough or the tissue is stiff enough to allow for the use of the coring device. However, in the case of a small sample, such as that obtained during a biopsy, or a soft tissue sample, the tissue manipulation approach could prove difficult if not impossible. The second point of interest is the breadth of approach utilized in analyzing the tissue modulus values. In most cases a precompression is applied, though the magnitude of the precompression typically varies. The testing protocol implemented after the initial precompression varies greatly across investigations. Additionally, the model of the tissue domain varies; specifically, some investigators consider the linear portion of the testing curve, while some investigators specifically target the viscoelastic nature of the tissue. The approach utilized is investigator dependent, and usually is chosen so as to highlight a specific, desired aspect of the tissue. However, the different testing protocols lead to different modulus values for similar tissues; hence for validation purposes of a method it would be necessary to maintain a consistent approach across testing protocols.

Indentation Testing

Indentation testing is another common testing method for biological tissues. Indentation testing is more flexible concerning the shape of the specimen, and thus proves easier to implement in soft tissues; however, stipulated dimensional ratios often have to be obtained in order to validate the assumptions of the equations associated with indentation analysis. For example, many types of indentation testing assume an infinite elastic medium for the soft tissue; hence it is necessary that the tissue diameter be significantly larger than the indenter diameter. Though indentation testing is more amenable to irregular tissue shape, the calculations involved in evaluating the modulus value can be difficult and tedious, and may change depending on the specifications of the testing protocol. Specifically, different calculations are performed if a cylindrical punch indenter is used as opposed to a spherical-tip indenter.

Krouskop et al. used uniaxial compression to test prostate and breast tissue [7]. However, the diameter of the compressor was only 4.83 mm, which was smaller than the tissue sample radius, necessitating the consideration of the work as indentation. The tissue was assumed to be linear and isotropic and the testing setup was modeled as a uniform load applied over a portion of the top boundary of a semi-infinite elastic solid. This approach required cutting the tissue into slab-shaped pieces, with height that was no more than one-quarter of the diameter. The excitation pattern was sinusoidal, with three different frequencies (0.1, 1.0, and 4.0 Hz) and the tissue was modeled as linear elastic, though the cyclic loading was used to characterize any viscoelastic behavior. The researchers found that at the experimental strain rate and strain range (20 to 30 percent), the tissue was sufficiently linear. Two sets of precompression were evaluated for each

tissue; for the breast tissue precompression levels of 5 and 20% were evaluated, and for the prostate precompression levels of 2 and 4% were used. For the breast tissue, the modulus did not change with applied frequency but did change with precompression level. Normal fat tissue had an average modulus of 19.7 kPa and 21.3 kPa, normal glandular tissue was 32 kPa and 57 kPa, and fibrous tissue was 106.3 kPa and 231.3 kPa for 5 and 20% precompression, respectively. Ductal carcinoma in situ was 24.3 kPa and 299.67 kPa and invasive ductal carcinoma was 73.7 kPa and 502.7 for 5 and 20% precompression. For the prostate tissue, it was also found that modulus did not change with loading frequency but did vary with precompression level. Normal anterior tissue had average modulus values of 58.7 kPa and 62 kPa and normal posterior tissue had values of 65.3 kPa and 69.7 kPa for 2 and 4% precompression. Tissue from regions of benign prostatic hyperplasia was 37.3 kPa and 39 kPa and tissue from cancerous regions was 98.3 kPa and 230.7 kPa for 2 and 4% precompression. In another paper, Kallel et al. used the same testing setup on ovine kidney samples [45]. It was found that the elastic modulus of the kidney ranged from about 10 kPa at low strains (<10%) to as high as 55 kPa at high strains (30%) for tissue obtained from the renal sinus, and from 20 kPa to 70 kPa for tissue obtained from the renal cortex.

Erkamp et al. also utilized indentation testing for modulus evaluation of canine kidney tissue [46]. In the system, a cylindrical sample was constrained laterally using a mold coupled with gelatin-agarose to fill the space between the sample and the mold. A set of single step indentations was performed using a step motor and a cylindrical punch, and the resulting data was converted to modulus values by means of a conversion factor that was obtained experimentally and validated by finite element modeling. The resulting

modulus values ranged from 10 kPa to 50 kPa depending on the amount of strain applied (0 to 9%). In other work, Carter at al. examined the modulus of pig liver and spleen and human liver [47]. The work utilized a round-tip indenter that was 4.5 mm in diameter as well as a cylindrical punch which was significantly larger at 30 mm in diameter. The work utilized a nonlinear elasticity description of the tissue in the form of an exponential stress-strain law, which contained two tissue parameters, γ and μ. The round-tip indenter was used for basic stress-strain calculations, wherein the force and displacement values were converted to stress and strain by dividing by the area of the indenter tip and the thickness of the tissue, respectively. The cylindrical indenter data was used to calculate γ and μ. An average porcine liver modulus of 4 MPa was obtained, and the average porcine spleen modulus was 0.11 MPa. The human liver had an average modulus of 0.27 MPa. In comparing the exponential stress-strain description to the data obtained from the cylindrical punch, the equation was representative of the physical data, matching the curve well. The resulting parameter values were 0.08 for γ and 0.12 for μ.

Samani et al. have performed extensive evaluations of breast tissue modulus using indentation techniques and an assumed linear elasticity of the tissue [6, 48, 49]. In the earlier work, Samani et al. evaluated breast tissue samples using unconfined indentation [48]. Tissue specimens were cut into a relative block shape using an apparatus devised by the authors that utilized an agarose gel encasement of the tissue to prevent deformation during the cutting process. Cyclic indentation was performed on the tissue block using a cylindrical indenter, force-deformation data acquired, and the elastic modulus was calculated using a conversion factor determined experimentally and validated by finite element evaluation. Three tissue samples were tested, one of adipose

tissue, one of fibroglandular tissue, and one of a high grade ductal carcinoma. The calculated modulus values were 1.9, 1.8, and 12.0 kPa, respectively. This system of modulus evaluation was adapted for use in ex vivo breast tissue tumors [49]. However, in this work, the authors calculated the elastic modulus by means of an iterative inversion technique as opposed to the direct conversion factor used previously. The technique used a finite element simulation of the tissue indentation to iteratively calculate a conversion factor and consequently modulus of the tumor tissue. Four different tumor types were evaluated: fibroadenoma, high grade ductal carcinoma in situ (DCIS), infiltrating lobular carcinoma (LC), and invasive ductal carcinoma (DC). The average modulus values were 11.42, 14.15, 18.57, and 22.55 kPa, respectively. The authors then applied both of the previously mentioned methods to investigate normal and pathological breast tissue specimens [6]. For normal breast tissue, the average modulus was 3.245 kPa. For diseased samples, the values ranged from 6.41 to 42.52 kPa, depending on the disease.

As with compression, the indentation literature serves to highlight the lack of data available regarding the modulus of various tissue types as well as to indicate the variety of approaches attempted by investigators. In the case of the indentation testing, the approach does not vary so much in the actual material testing protocol, but rather in the method of interpreting the resulting force-displacement data. As previously mentioned, indentation testing requires a more rigorous evaluation method due to the unusual geometries and the interaction of these geometries; the evaluation approach selected can vary greatly among investigators. This again makes it inherently difficult to compare results among investigators, and also impedes the use of these results as verification of other modulus evaluation techniques.

Microstructural Change

Histological analysis of tissue biopsies has been well established and remains the 'gold standard' for disease evaluation and diagnosis. However, the methods for biopsy collection are inherently invasive and often painful for the patient. Additionally, temporal tracking of the disease requires repetitive evaluations of the tissue, which is often not feasible due either to the invasiveness of the procedure or the amount of tissue available. Acknowledgment of this problem has led to the development of diagnostic techniques that aim to noninvasively differentiate diseased and normal tissue, often based on the elastic modulus. Assuming a link exists between microstructure and/or microstructural environment and macroscopic parameters, such as modulus, it is feasible to conceive of a non-invasive modulus evaluation technique as an evaluation of microstructural changes that could serve as a predictor of events such as tumor progression or tumor invasion.

Recent research has focused on the microenvironment and changes within it that contribute to and/or are driven by tumorigenesis and metastasis. Specifically, a series of recent papers have identified the importance of stress cues on the behavior of the cell and the resulting effect on the tissue microstructure. Paszek and Weaver provide a review of mechanical homeostasis, discussing the concept of tensional homeostasis and the effect that the tensional state of the tissue microenvironment has on the development and potential transformation of the mammary epithelial cells [50]. The paper explores the necessary function of physical forces on the development of the embryo and subsequent mammary gland development. The authors then identify ongoing work indicating that substrate compliance regulates cell shape, mammary tumor morphogenesis, and

endogenous basement membrane assembly. Considering the situation of perturbed homeostasis and the malignant transformation of the breast, the authors indicate that, given the changes in tissue tension and the difference in force sensing experienced by transformed cells that is associated with tumorigenesis, it is likely that altered mechanotransduction and loss of tensional-homeostasis account for a pivotal mechanism regulating the pathogenesis of epithelial tumors. Specifically, the microstructural changes that occur during tumorigenesis and the subsequent cellular changes form a positive feedback loop wherein the reaction of the cells to the increased forces results in responses that perpetuate the diseased state and promote increased tumorigenesis. This paper touches not only on the importance of mechanical reciprocity between the microenvironment and the cell in the development of the cell, but also identifies the tumorigenic 'journey' of the collective tissue and how force cues and mechanical changes in the microenvironment potentiate cancer progression.

Regarding the specific changes in the microstructure that result in an altered tensional state, a considerable body of research has been performed that explores the changes in the extracellular matrix corresponding to tumorigenesis and tumor progression. The paper by Butcher et al. summarizes the observed remodeling of the extracellular matrix in tumors [51]. Specifically, the extracellular matrix is affected by increased deposition of fibronectin, tenascin, collagen types I, III, and IV, and proteoglycans, overexpression of matrix metalloproteinases (MMPs) resulting in MMP-dependent cleavage, and increased levels of LOX-dependent matrix crosslinking. These factors result in a progressive increase in the stiffness of the tissue and the extracellular matrix. Additionally, the authors indicate that, in both in vitro and in vivo studies,

induced stiffening of the matrix promotes mammary epithelial cell transformation and associated increased mechanosignalling from the cells, perpetuating the positive-feedback loop suggested by Paszek and Weaver.

The paper by Levental et al. also addresses the matrix remodeling associated with tumor progression, and, specifically, the effect of collagen crosslinking on the stiffness and subsequent signaling [52]. The authors found that the transition of the mammary gland from normal to premalignant to invasive cancer was paralleled by an incremental stiffening of the tissue, as measured by unconfined compression and rheological testing, which could be correlated to increased collagen crosslinking. The authors also showed that ECM stiffening, in the presence of oncogenes such as ErbB2, promotes invasive behavior of the mammary epithelium. Additionally, the authors provide data indicating that focal adhesions, which serve as the force signaling pathways between cells and the stroma, are elevated in the stiffened tissue state, and that the adhesions promote mammary epithelial cell invasion, which resonates with the concept that force plays a role in tumor progression.

Beyond the information available in the literature regarding changes in the tumor stroma, an abundance of information also exists regarding the effect of these changes on the behavior of the tumor. A paper by Lo et al. translates the changing stiffness of the substrate into a locomotive effect on the cell [53]. Their work shows that ECM stiffness affects the migration of cells within the substrate and enhances cell growth and survival. In other work, Ramaswamy et al. evaluated the gene-expression profiles of various metastatic and primary tumors to identify genes that distinguished the two [31]. In this work, the authors found that collagen genes were upregulated in tumors with metastatic

potential, indicating that increased expression of collagen is associated with metastatic behavior.

This evaluation of the literatures serves as a brief but salient investigation of the many papers concerning the altered conditions of the tumor stroma and the effect that these have on tumor progression and potential invasion. Given the remodeling of the extracellular matrix, the deposition and crosslinking of collagen, the overall increase in tissue stiffness generally observed, and the subsequent correlation between these changes and the behavior of the tumor tissue, it is reasonable to conceptualize that certain events (such as progression or invasion) which relate to changes in the microstructure of the tissue may potentially be observable though the modulus of the tissue.

Introduction to this Thesis

The initial goal of this project was to develop an evaluation technique to quantify the modulus of soft tissue in a manner which was compatible with non-invasive modulus evaluation techniques for verification purposes. Specifically, the objective was to use a mechanically-based modeling evaluation technique to verify the quantification of fibrotic liver tissue modulus by means of ultrasound elastography, and thus the modulus evaluation technique was conceived as a complementary component of an elastographic technique. As the assay developed, the utility of it as a modulus evaluation technique that could be utilized to investigate ex-vivo soft tissue samples became apparent. Soft tissue modulus evaluation has historically proven difficult due to the irregular surfaces of the tissue and the difficulty in manipulating the tissue to create a normal shape which is generally required for basic mechanical testing techniques. Further, disease development

and progression often affects the microstructure and hence the modulus of the tissue in a manner that is discernable from the surrounding, non-diseased tissue. Hence a modulus evaluation method that would allow the tissue to be utilized in its natural, irregular shape would prove useful as the correlation between modulus and disease is further investigated. The assay described in this work serves to fill this need as it is an adaptable system which could be utilized for soft tissue modulus evaluation under a variety of preparation conditions. The skeleton of the system is a gel-embedding process by which the tissue sample is embedded in a polyacrylamide gel. This coupled with a mechanical testing protocol, imaging of the tissue-gel system, and modeling of the system resulted in what has been termed the Model-Gel-Tissue (MGT) assay.

This thesis is the concatenation of work that focuses on the development, utilization, and evaluation of the MGT assay. Chapter II focuses on the details of the development of the MGT assay. This chapter provides information on the experimental protocol for using the MGT assay. Additionally, it contains specifics regarding each component of the evaluation of a modulus of interest utilizing the assay.

The next three chapters explore the application of the MGT assay to soft tissue modulus evaluation ex-vivo. In the Chapter III, murine livers were utilized as the tissue of interest, and the testing protocol consisted of 14 fibrotic livers, 3 control livers, and 3 normal livers. Two lobes from each liver were submerged in polyacrylamide and evaluated using the MGT assay. A separate liver lobe was utilized in direct indentation testing, which provided a baseline comparison for the results of the MGT assay. The model-calculated modulus, though not equivalent to the indenter modulus, demonstrated a high correlation to the indenter modulus, indicating a relationship between the two

testing methods. The results also showed a clear difference between non-diseased and diseased livers.

Chapter IV describes the transition from the evaluation of liver tissue to the evaluation of tumor tissue. Though still in the murine environment, this work demonstrated the utility of the assay in evaluating various tissue types with inherently different consistencies. The mouse mammary tumor virus polyomavirus middle T (PyV-mT) transgenic model of breast cancer served as the system of interest. The tumors were allowed to grow to a prescribed size, at which point they were resected and sectioned. A portion of the tumor was utilized in the MGT assay, while a second portion was analyzed for collagen content. The model-evaluated modulus values were correlated quantitatively to type I collagen content of the tissue samples, providing a first consideration of the link between the bulk modulus as evaluated by the MGT assay and the microstructural composition of the tissue. The results demonstrate a strong linear correlation between tumor mechanical properties and collagen content.

Chapter V revolves around the quantification of a third tissue type using the MGT assay. In this evaluation, the modulus values of a HER2+ murine model of breast cancer were assessed. Two strains of the tumor line were utilized, one which is resistant to treatment with Herceptin, and one which is responsive to the treatment. The resistant and responsive lines simulate non-responders and responders in the human case, and the work aimed to gage the potential difference in modulus between the two cases for prognostic evaluation.

Finally, the last investigative chapter of this work contains other pertinent studies with a specific interest in the interrogation of the sensitivity and accuracy of the assay in

order to validate its use as a reliable soft tissue modulus evaluation technique. A series of tests were performed which examined the repeatability and accuracy of the assay, and the assumptions employed within the assay were considered.

Significance of this Thesis

The novelty of the work presented here lies in the method of tissue parameter evaluation coupled to model-based analysis and correlated with traditional cellular assays. As indicated by the material testing literature, an abundance of methods exist by which the mechanical parameters of soft tissue can be evaluated. This leads to a discordance regarding the published modulus values for soft tissues. Additionally, manipulating the soft tissue, especially when the sample is on the scale of a biopsy specimen, has proven difficult and often requires specialized equipment. The MGT assay allows for the utilization of the soft tissue in its native state, without extensive and tedious manipulation which could, quite feasibly, affect the integrity and structure of the tissue, and hence the measured modulus. The method utilized within the MGT assay allows for ease of manipulation of the tissue specimen while maintaining adaptability to tissue size and shape. In regards to a unified protocol, the MGT assay allows integration of a preferred testing protocol and provides flexibility regarding mechanical model of the tissue domain. Concisely, a rigorous skeleton of the soft tissue evaluation protocol is defined by the MGT assay, which can then be customized to reflect the testing environment.

Additionally, the treatment of the soft tissue of interest which is presented by the MGT assay is a novel approach. As presented in the review of the material testing

literature, the majority of the approaches utilize a manipulation of the soft tissue in order to normalize the size and shape of the sample. Depending on the location of origin of the tissue, manipulating the sample can prove tedious and difficult due to the consistency. Being that the accuracy of the modulus evaluation via mechanical testing can depend on the success of creating a normal surface, the manipulation proves very important. The approach presented within the MGT assay is a gel-embedding process, whereby the excised soft tissue is used in its native shape and state, thus eliminating the need for tedious manipulation. An approach such as this has not previously been utilized in soft tissue modulus evaluation techniques. As previously mentioned, Erkamp et al. used a gelatin to create a confined compression of the soft tissue of interest; however, in that case the gel was utilized as part of the material testing setup instead of serving as a contained portion of the sample. The gel-embedding approach indicated by the MGT assay is a novel approach to sample preparation and testing.

A prime example of the utility of this system is evident within the field of elastography. Techniques termed 'elastographic' have been developed which allow for noninvasive modulus evaluation of soft tissues. Though elastographic approaches can be varied in regards to imaging modality (i.e. ultrasound versus MRI) and in method of tissue evaluation (direct strain images versus inverse modulus evaluation) the theory is the same. Specifically, a prescribed stress is applied to the tissue, during which the internal displacements of the tissue are monitored. Using these deformations and assuming a mechanical behavior of the tissue, a spatial map of the elasticity of the tissue domain can be generated. In this manner, elastographic techniques can noninvasively evaluate tissues for areas of low strain or high stiffness, which is generally correlated to

disease. However, in most cases these techniques have not been rigorously validated regarding their assessment of modulus value, and though areas of interest can be identified, the accuracy of the assessment of tissue parameters has been elusive due to the non-invasive nature of the techniques. A system such as that conceived within the MGT assay would allow for a direct evaluation of elastographic techniques. The heterogeneous gel-tissue system is developed in such a way that it is readily amenable to modulus evaluation via elastographic techniques. The modulus evaluation could then also be performed using the combined mechanical testing and modeling approach outlined by the MGT assay, the specifics of which would be defined so as to mimic the deformation experienced in the elastographic evaluation. This would allow for direct comparison of the evaluated modulus between the two methods, providing a measure of the accuracy of the elastographic technique. Additionally, the MGT assay provides a heterogeneous system that is analogous to that which is evaluated by elastographic techniques. More specifically, when an in vivo soft tissue evaluation is performed using elastography, the tissue of interest is generally subdermal and at least semi-confined by other tissues which inherently impose boundary conditions on the tissue of interest. This environment is not accurately reflected in an ex vivo direct testing situation where either an indenter or compression test is utilized, as the external surfaces of the tissue are typically stress-free in these cases. A confined compression may more closely resemble the native environment, but realistically the confining substrate is likely to be far more stiff than the restraining soft tissues in vivo. The MGT assay serves to address this issue in that it begins to replicate the in vivo environment by embedding the tissue of interest within a gel of controllable modulus.

CHAPTER II

EXPERIMENTAL PROTOCOL

MGT Assay Overview

The MGT assay was developed as an adaptive soft tissue modulus evaluation technique that couples mechanical testing with modeling to achieve tissue parameterization. The system consists of three major components. The first is the gel-embedding process, whereby the soft tissue of interest is embedded in a cylindrical polyacrylamide gel of known and controllable height and diameter. This creates a heterogeneous system with normal surfaces amenable to direct material testing. A homogeneous gel is also created at this time, termed the reference gel. The reference gel is evaluated to obtain a modulus value of the polyacrylamide gel, which is then assigned as the background modulus in the heterogeneous gel-tissue system. The second component of the assay is the mechanical testing, which can be adapted so as to mimic the environment of interest in regard to the tissue. The final component of the three-part assay is the CT scan and modeling. Both the homogeneous gel and the heterogeneous gel-tissue system undergo a microCT scan. The resultant images are then segmented in order to create a 3D mesh of the sample. This allows for a model which accurately describes the shape, size, location, and surfaces of the tissue and gel. The mesh is utilized in a finite element model (FEM) description of the tissue domain with assumed modulus values, and boundary conditions are implemented so as to mimic the mechanical testing routine. The model-calculated force values are compared to the mechanical forces

achieved during material testing; optimization of the system results in an assigned tissue modulus value.

Gel Generation

The gel-embedding process is pivotal to the MGT assay as it allows the use of the soft tissue in its native state and shape without tedious manipulation. Additionally, the gel-embedding process allows the formation of external surfaces which are controllable in shape and size, hence increasing adaptability of the sample to various material testing protocols. The process for creating the gels begins with the production of a buffer solution consisting of all of the gel components with the exception of the contrast agent and the initiator. This solution is then utilized in the production of all individual gels. To create the buffer solution, deionized water, 1 molar Tris buffer, and 10% ammonium persulfate (BioRad Laboratories, Hercules, CA) are mixed in a specified proportion, the absolute volumes of which depended on the total volume of solution needed for gel generation (i.e. larger tissue samples or a greater number of samples would require a larger volume of bulk solution). Generally, 19.1 mL of deionized water, 0.65 mL of 1 molar Tris buffer, and 0.25 mL of 10% ammonium persulfate, or some multiple of these values, are utilized. A volume of the buffer solution is then combined with 30% Acrylamide/Bis-acrylamide (BioRad Laboratories, Hercules, CA) in a proportion which is dependent on the desired final polyacrylamide percentage, to yield a total combined volume of 16 mL (or some multiple of this volume). The combination of the buffer solution and the polyacrylamide constitutes the bulk solution, which is then used in each individual sample generation in order to enforce homogeneity across the samples. To

generate the individual gel, the desired volume of the bulk solution is transferred to the forming container. The container used to generate the individual gel can be varied depending on desired shape and size of the resulting sample. Optiray (Mallinckrodt Inc, Hazelwood, MO), a CT contrast agent, is subsequently added to the individual gels after allocation of the solutions. The object to be embedded is suspended by means of forceps in the gel solution while TEMED, the initiating agent, is added to the solution. The sample is pipette-mixed for approximately one minute as the solution begins to solidify in order to promote a uniform mixture. In addition to the heterogeneous, tissue-containing samples, a homogeneous reference gel is also produced during all gel generation instances. The homogeneous gel is generated from the same solution and in the same manner as the homogeneous gels, without the addition of the submerged tissue. This gel serves as the reference gel for evaluating the modulus of the polyacrylamide, which is then utilized as the assumed background modulus in the heterogeneous gel.

Material Testing

As indicated previously, the MGT assay is amenable to the use of any desired mechanical testing protocol. However, for this work, the same protocol was utilized in all tissue evaluations. Specifically, the protocol adopted in this work consists of a series of unconfined step compressions followed by a 60 second dwell which was implemented to allow the viscoelastic behavior of the gel and tissue to dissipate. This protocol was selected to create compatibility with elastography techniques as our initial liver work was designed as a comparison mechanism for ultrasound elastography evaluation of hepatic fibrosis. To perform the material testing, after gel generation the individual samples are

removed from their forming containers and placed on the lower platen of the Enduratec Electroforce 3100 tester (Bose, Enduratec Systems Group, Eden Prairie, Minnesota), which has been previously fitted with the appropriately sized force transducer, dependent on the size of the sample. Additionally, both platens are lubricated using an oil-based spray which allows the sample to displace laterally while being compressed. The system is tared after placing the sample so as to remove the weight of the sample from the evaluated force value. The lower platen is then raised until the tissue initially contacts the top platen. Contact is determined both visually and by a slight increase in the force reading. After establishing contact, a 0.3 mm precompression is applied and held for 60 seconds. The testing protocol then consists of consecutive step compressions from 0.35 mm to 0.65 mm in 0.05 mm increments. After each step a 60 second dwell is implemented to allow the transient behavior to dissipate.

Imaging and Mesh Creation

Imaging of both the homogenous gel and the heterogeneous gels is necessary in order to implement the modeling portion of the MGT assay evaluation, and thus computed tomography (CT) scans are collected of each sample. After collection of the CT images, image segmentation is performed using AnalyzeAVW (Mayo Foundation for Medical Education and Research). The addition of the contrast agent to the gel generation process allows for sufficient contrast between the gel-tissue and the gel-air interfaces such that thresholding based on pixel intensity and connectivity can be utilized to segment the images. A marching cubes surface extraction is then performed on the segmented images to create a surface description of the samples which is then used as a

bounding description for a custom-built tetrahedral mesh generator [54]. This results in a 3-dimensional mesh for each individual sample, which describes the size, shape, and boundaries of the polyacrylamide gel, as well as (in the heterogeneous gel) the size, shape, location, and boundaries of the embedded soft tissue.

Finite Element Model

A central concept of the MGT modulus evaluation assay is the finite element model (FEM) used to represent the domain of interest. In all work presented here, a linear elastic medium is assumed, so that the set of mathematical equations governing linear elastic deformations for this model is given by:

$$\nabla \cdot G\nabla\vec{u} + \nabla\frac{G}{1-2\nu}(\nabla \cdot \vec{u}) = 0 \qquad (1)$$

where $G = {}^{E}/_{2(1+\nu)}$ is the shear modulus, **ν** is Poisson's ratio, and $\vec{u}$ is the vector of Cartesian displacements. Given this equation, a numerical solution to the coupled set of linear partial differential equations is obtained using a weighted residual method. The method begins with standard residual weighting and integration:

$$\langle G\nabla\vec{u} \cdot \nabla\phi_i\rangle + \langle\frac{G}{1-2\nu}(\nabla \cdot \vec{u})\nabla\phi_i\rangle = \iint \tilde{\sigma}_s \cdot \vec{n}\,\phi_i dS \qquad (2)$$

where an integration by parts has taken place which reduces the basis function order requirement, and introduces the surface integral via the divergence theorem. In the previous equation, the ⟨ ⟩ operator indicates integration over the problem domain, and ϕ_i is the $\mathbf{i^{th}}$ member of a complete set of scalar functions of position. The particular functions used can vary, but this work utilizes the standard $\mathbf{C^0}$ local Lagrange polynomial interpolants associated with finite elements. Using the Galerkin approach, the unknown displacement vector is also expanded using a Lagrange basis function of position:

$$u(x,y,z) \approx \hat{u}(x,y,z) = \sum_{j=1}^{4} u_j \phi_j(x,y,z) \qquad (3)$$

The element used in this work was the standard linear tetrahedral element. Upon substituting the basis function, the local weighted residual expression for the i[th] equation and the j[th] set of displacement coefficients can be written as:

$$[K_{ij}]\{\vec{u}_j\} = \{\vec{b}_i\} \qquad (4)$$

where

$$[K_{ij}] =$$

$$\begin{bmatrix} G\left\langle \frac{2(1-\nu)}{1-2\nu}\,\delta_{xx} + \delta_{yy} + \delta_{zz} \right\rangle & G\left\langle \frac{2\nu}{1-2\nu}\,\delta_{yx} + \delta_{xy} \right\rangle & G\left\langle \frac{2\nu}{1-2\nu}\,\delta_{zx} + \delta_{xz} \right\rangle \\ G\left\langle \frac{2\nu}{1-2\nu}\,\delta_{xy} + \delta_{yx} \right\rangle & G\left\langle \delta_{xx} + \frac{2(1-\nu)}{1-2\nu}\,\delta_{yy} + \delta_{zz} \right\rangle & G\left\langle \frac{2\nu}{1-2\nu}\,\delta_{zy} + \delta_{yz} \right\rangle \\ G\left\langle \frac{2\nu}{1-2\nu}\,\delta_{xz} + \delta_{zx} \right\rangle & G\left\langle \frac{2\nu}{1-2\nu}\,\delta_{yz} + \delta_{zy} \right\rangle & G\left\langle \delta_{xx} + \delta_{yy} + \frac{2(1-\nu)}{1-2\nu}\delta_{zz} \right\rangle \end{bmatrix},$$

$$\{\vec{u}_j\} = \begin{Bmatrix} u_j \\ v_j \\ w_j \end{Bmatrix}, \qquad and \qquad \{b_i\} = \begin{Bmatrix} \vec{x} \cdot \oint \sigma \cdot \vec{n}\phi_i ds \\ \vec{y} \cdot \oint \sigma \cdot \vec{n}\phi_i ds \\ \vec{z} \cdot \oint \sigma \cdot \vec{n}\phi_i ds \end{Bmatrix}$$

and $\delta_{kl} = \frac{\partial \phi_j}{\partial k}\frac{\partial \phi_i}{\partial l}$. The contribution from each tetrahedral element can thus be determined, and a global stiffness matrix can be constructed. Boundary conditions are then assigned either as displacement boundary conditions or as applied stresses, the location and magnitude of which are determined by the material testing protocol. Corresponding to the material testing protocol previously described, the boundary conditions at the top surface of the gel in this work are:

$$u_n = -d, \sigma_{t1} = 0, \sigma_{t2} = 0 \qquad (5)$$

where d is the displacement at the step compression of interest. At the bottom surface of the gel, the boundary conditions are:

$$u_n = 0, \sigma_{t1} = 0, \sigma_{t2} = 0 \qquad (6)$$

In order to ensure solution uniqueness, at least one Dirichlet condition is required in the lateral directions. To achieve this, the approximately 10 nodes on the top and bottom surface that are closest to the center-line are fixed on each surface to restrain their movement laterally. The remaining boundary conditions for the sides of the gel are stress-free:

$$\sigma_n = 0, \sigma_{t1} = 0, \sigma_{t2} = 0 \qquad (7)$$

The matrix system is then assembled and solved using an iterative matrix solver which uses a biconjugate gradient solver with an incomplete LU preconditioner, resulting in a displacement solution for the domain of the mesh.

Once the displacement solution is calculated from the matrix system, the unused Galerkin equations on the compressing model surface (the Dirichlet, or Type I, conditions on the top surface) can be used to estimate the average surface stress applied. To be specific, after the evaluation of the displacement solution, the finite element equation:

$$\iint \tilde{\sigma}_s \cdot \vec{n}\phi_i dS = \sum_j \vec{u}_j \langle G\nabla\phi_j \cdot \nabla\phi_i \rangle + \sum_j \vec{u}_j \langle \nabla\phi_j \frac{G}{1-2\nu} \nabla\phi_i \rangle \qquad (8)$$

is available at nodes where a Dirichlet boundary condition was implemented. The right-hand-side of the equation can be constructed using the displacement solution, allowing for the solution of the left-hand-side surface integral for the local normal stress distribution. This provides a surface stress description for the gel based on the defined compression and the prescribed modulus value. The surface stress can subsequently be averaged and multiplied by the model-based surface area for comparison to the respective mechanically-tested average force value.

Optimization Procedure

The process of evaluating the elastic modulus of the embedded tissue sample is achieved via an inverse evaluation of the previously described FEM wherein the resulting stresses are known and the input modulus values are to be determined. This inverse evaluation of the modulus values is achieved by the implementation of an iterative optimization technique which minimizes the difference between the resultant model forces and the measured mechanical forces. The optimization is initialized using an estimate of the modulus value (E) to perform a forward evaluation of the model forces. The unknown modulus value is then optimized iteratively using a custom-built Levenberg-Marquardt non-linear optimization algorithm. The optimized modulus value occurs when the error between the model-derived force values and the experimental force values is minimized. Thus, the objective function of consideration is the sum of squares of the difference between the model force values and the experimental force values, and is given by:

$$S(E) = \sum_1^N (F_{exptl}(\varepsilon_i) - F_{model}(\varepsilon_i, E))^2 \qquad (9)$$

where F_{exptl} is the set of experimental force values at each strain level, F_{model} is the set of model-calculated force values at each strain level for the current modulus value, and N is the number of strain levels. To optimize for the modulus value E which minimizes the objective function, the derivative of the objective function is taken with respect to the modulus of interest and set equal to zero:

$$\frac{dS}{dE} = 0 = \sum_1^N (F_{exptl}(\varepsilon_i) - F_{model}(\varepsilon_i, E)) \frac{\partial F_{model}(\varepsilon_i, E)}{\partial E} \qquad (10)$$

or,

$$\left\{\bar{F}_{exptl} - \bar{F}_{model}\right\}[J]^T = 0 \qquad (11)$$

where $[J]^T$ is the transpose of the Jacobian matrix J, which is the matrix consisting of the first-order partial derivatives of F_{model} with respect to the modulus. Applying a standard Newton-Raphson root-finding approach to equation 11 results in:

$$E_{k+1} = E_k - \frac{[J]^T\{\bar{F}_{exptl} - \bar{F}_{model}\}}{[J]^T J} \qquad (12)$$

from which the parameter update can be calculated using a standard Levenberg-Marquardt approach,

$$([J]^T[J] + \alpha I)\Delta E = [J]^T\{\bar{F}_{exptl} - \bar{F}_{model}\} \qquad (13)$$

where $\Delta E = E_{k+1} - E_k$, I is the identity matrix, and α is a regularization parameter utilized to improve the conditioning of the iterative procedure:

$$\alpha = (\lambda * \text{trace}([J]^T[J]) * SSE^2)^{\frac{1}{2}} \qquad (14)$$

In the definition of α, λ is an empirical factor and SSE is the sum squared error between measured and calculated forces [55]. Optimization of the modulus value occurs by a series of iterative parameter updates, calculated using Eq. 13. The optimization proceeds until the relative error between iterations is below a set tolerance or until the objective function is static and a unique solution is obtained.

Tissue Modulus Evaluation

With the components of the MGT assay in place, the evaluation of the tissue modulus takes place in a series of defined steps. First, the homogeneous and heterogeneous gels are generated, tested, and imaged as previously described. The CT scans are segmented and a tetrahedral mesh is generated for each sample. The FEM is then utilized in the Levenberg-Marquardt optimization procedure to perform the modulus evaluation. The homogeneous reference gel is evaluated first, and the optimization

procedure is implemented with the material testing data in order to obtain the modulus value of the polyacrylamide gel. The optimized gel modulus value is then used as the assigned background gel modulus in the heterogeneous sample. This reduces the two parameter system (gel modulus and tissue modulus) to one unknown modulus value. The heterogeneous sample is subsequently evaluated, using its associated material testing data, and an optimized tissue modulus value is assigned.

CHAPTER III

EX VIVO LIVER STUDY

Introduction and Contribution of Study

This paper was the first publication regarding the MGT assay, and the murine liver work presented here represents the initial development of the MGT assay as well as the first implementation of the assay as a modulus evaluation technique. This study addressed proof of concept of the assay in regards to its feasibility and application. The combination of the gel-embedding, mechanical testing, and modeling proved to be successful in evaluating the modulus of a soft tissue sample in its resected shape, without alteration. The introduction and some of the methods may be repetitive in regards to Chapter II due to the necessity of presenting a detailed description of the MGT in this principal paper. Beyond the details of the assay, this paper served as the first evaluation of a soft tissue specimen via the MGT assay and provides validation of the assay-assigned modulus in comparison to indentation testing, thus verifying its utility as a modulus evaluation technique. The motivation for this work was to develop a correlative technique for soft tissue modulus evaluation that could be used in conjunction with ultrasound elastography. The need for a sample preparation method that was compatible with both ultrasound imaging and mechanical evaluation techniques led to the development of the gel-embedding system utilized in the MGT assay. The development of the assay serves to connect the material testing literature and the evaluation of elastographic techniques. Additionally, this work adds to the material testing literature

by presenting a novel approach to soft tissue modulus evaluation that can be adapted to suit the nature of the specific interrogation. This work was published in *Medical Physics* in November of 2007.

Experimental Study

DEVELOPMENT OF A MECHANICAL TESTING ASSAY FOR FIBROTIC MURINE LIVER

Appearing in
Medical Physics, Volume 34, Number 11, November 2007

Abstract

In this article, a novel protocol for mechanical testing, combined with finite element modeling, is presented that allows the determination of the elastic modulus of normal and fibrotic murine livers and is compared to an independent mechanical testing method. The novel protocol employs suspending a portion of murine liver tissue in a cylindrical polyacrylamide gel, imaging with a microCT, conducting mechanical testing, and concluding with a mechanical property determination via a finite element method analysis. More specifically, the finite element model is built from the computerized tomography (CT) images, and boundary conditions are imposed in order to simulate the mechanical testing conditions. The resulting model surface stress is compared to that obtained during mechanical testing, which subsequently allows for direct evaluation of the liver modulus. The second comparison method involves a mechanical indentation test performed on a remaining liver lobe for comparison. In addition, this lobe is used for histological analysis to determine relationships between elasticity measurements and

tissue health. This complete system was used to study 14 fibrotic livers displaying advanced fibrosis (injections with irritant), three control livers (injections without irritant), and three normal livers (no injections). The moduli evaluations for non-diseased livers were estimated as 0.62±0.09 kPa and 0.59±0.1 kPa for indenter and model-gel-tissue (MGT) assay tests, respectively. Moduli estimates for diseased liver ranged from 0.6–1.64 kPa and 0.96–1.88 kPa for indenter and MGT assay tests, respectively. The MGT modulus, though not equivalent to the modulus determined by indentation, demonstrates a high correlation, thus indicating a relationship between the two testing methods. The results also showed a clear difference between non-diseased and diseased livers. The developed MGT assay system is quite compact and could easily be utilized for controlled evaluation of soft-tissue moduli as shown here. In addition, future work will add the correlative method of elastography such that direct controlled validation of measurement on tissue can be determined.

Introduction

Investigating the mechanical properties of soft tissue has important impact on many application fronts within biomedical engineering. The nature of soft tissue is that of a composite material whereby collagen and elastin fibers contribute most substantively to its mechanical properties. Hepatic fibrosis is an example of a disease where the elastic properties generally increase as the disease progresses due to elevated deposition of collagen. Though the distribution of the scar tissue within the liver will vary based on the cause of the fibrosis, the response is the same for all types; i.e. a cascade of events occurs that cause stellate cells to become activated, and in turn, contract, and produce scar tissue.

A process known as fibrogenesis degrades the liver's normal matrix, and release cytokines which cause inflammation. All of these effects result in disruption of the liver's normal function [56, 57]. Quantifying the mechanical properties with novel testing assays or imaging techniques could be an excellent way to stage disease and outcomes. In recent years, noninvasive imaging techniques have been a very active area of research, i.e. the field know as elastography [28, 58-61]. Within this domain, some example applications using mechanical properties to assess organ health have been forthcoming including breast [25, 62-66], prostate [67, 68], thyroid [69], and intravascular evaluations [70, 71].

While the recognition that mechanical properties may be important for tissue characterization, detailed quantitative experimental systems correlating imaging modality and independent assessment have been difficult with real tissue. For example, one popular method of mechanical property interrogation is compression testing and consists of compressing a known geometric sample between two plates and measuring the applied displacements and resulting forces [42]. From this data, various mathematical constitutive models of the tissue can be generated that relate the stress, strain, and rates thereof. While this testing is quite routine, the tissue sample preparation can be a challenge especially with respect to small irregularly shaped samples. Due to this restriction, mechanical indentation techniques have become a popular method for modulus assessment also. A variety of different approaches to indentation testing have been cited in the literature [46, 47, 72-74]. However, eliciting a modulus value from indenter testing requires significant experimental assumptions, the basis of which is dependent on many factors, such as sample size and shape, indenter type, and boundary

conditions. This complexity in testing makes a uniform testing protocol for different tissue samples equally as challenging as the sampling issue above. In addition, as the results in this paper indicate, some variability between tests is possible based on the mechanism of disease onset. In any case, the need for controlled independent testing that can be directly verified with noninvasive imaging techniques is evident.

This paper presents a novel ex vivo model-gel-tissue (MGT) assay system that combines mechanical testing, imaging, and finite element modeling to monitor the changes in mechanical properties of a murine liver fibrosis model. The purpose of this protocol was to provide an independent tissue evaluation system that could be adapted to a variety of applications and that would assist in quantifying elastography techniques. The protocol calls for tissue samples to be embedded in a cylindrical gel which is used in compression testing for modulus analysis and is equally amenable to elastography evaluation. In order to develop this system, the ability of the assay to accurately assess the modulus of the embedded tissue must be verified. Thus, to qualify our results, separate indentation testing was performed and compared to the MGT assay technique. While many previous studies have been predominantly concerned with human or large animal evaluations, this protocol is focused on small animal models (i.e. rodent). The obvious advantage of targeting small animal applications is that it allows for rapid evaluation of many subjects, multi-modal image registration (magnetic resonance, computed tomographic, positron emission tomography, bioluminescence, etc.), access to numerous disease models, and the ability to test pharmacological therapeutics within these systems. This paper serves as a description of the testing protocol as well as an initial evaluation of its capabilities based on the modulus assessment of 14 fibrotic and 6

non-diseased livers. The separate indentation tests were consistent with the MGT assay results for control and normal livers. While stiffening of the tissue was measured by both MGT assay and indentation tests, there was inconsistency among the absolute values established for fibrotic livers (consistency for the normals/controls). Interestingly though, the offset between the values among the two testing methods was correlated. It is also shown that statistical differences in modulus values for fibrosis and controls can be detected in both the MGT assay and indentation tests. In addition, the results from the liver testing seem to correlate with those found in the literature for normal and fibrotic human liver testing post mortem [57].

Methods

The protocol used to evaluate fibrotic and non-diseased murine liver involves a series of steps as shown in Figure 1. This three-pronged investigation sought to characterize liver tissue in three distinct ways: (1) mechanical testing with an ex vivo MGT assay, (2) mechanical testing by indentation, and (3) tissue characterization for disease progression via histochemical staining. This system of tissue evaluation allows for an investigation of the abilities of the proposed MGT assay by comparison with traditional indenter testing technique, while correlating elasticity measurements with normal and diseased subjects.

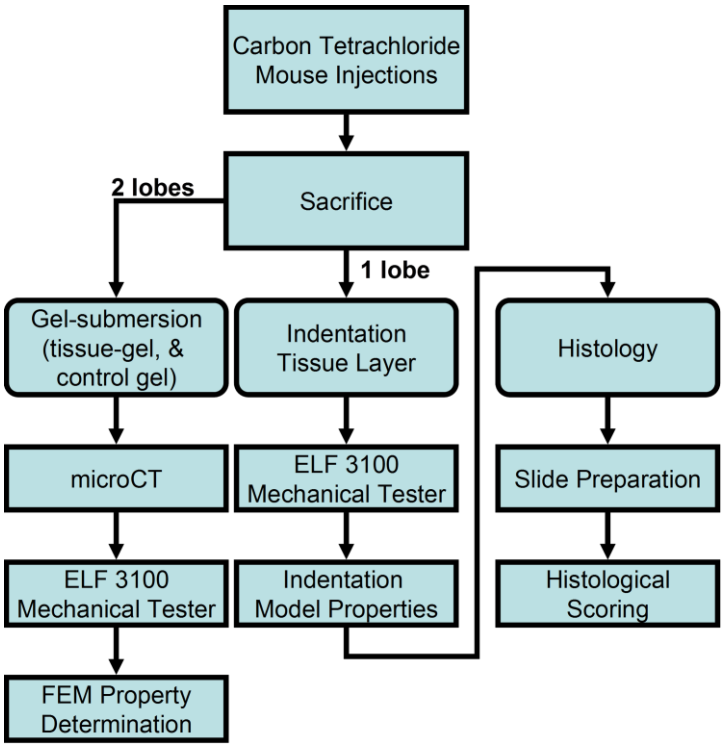

Figure 1. General mechanical testing framework for murine liver system.

Fibrosis Model & Disease Scoring

Adult C57 mice (18-20 g, 8-10 weeks of age) purchased from Jackson Laboratory were housed in cages with a 12-hour light/dark cycle (6 a.m. to 6 p.m.) and provided with rodent chow and tap water ad libitum. All animals received humane care in compliance with the institution's guidelines, and animal procedures were approved by the Institutional Animal Care and Use Committee, which is certified by the American Association for Accreditation of Laboratory Animal Care. The animals were divided into three groups – *fibrosis, controls, and normals*. The *fibrosis* group of mice consisted of fourteen animals that received weekly intraperitoneal (IP) injections of carbon

tetrachloride (Sigma Chemical, St. Louis, MO) mixed with olive oil (Sigma Chemical, St. Louis, MO) in a 1:4 ratio, respectively. Each dose of CCl_4 was 1 ml/kg per injection. The second group of mice consisted of three animals and was the *control* group. This group received weekly IP injections of pure olive oil. The third group, the *normal* group, consisted of three animals and did not receive IP injections (of note these mice were several weeks older than groups 1 and 2). Diseased mice were sacrificed at variable time points between 2 and 10 weeks of treatment. Using histological assessment, only mice that were of an Ishak fibrosis scores of 3 or 4 (advanced fibrosis) were selected for comparison. A control mouse was sacrificed after five, six, and eight weeks of treatment. The liver was removed and divided into three sections. The first, and largest, section consisted of two of the four lobes, and was embedded in the polyacrylamide gel. The third lobe was preserved for use in indenter testing and histological analysis, and the fourth lobe was frozen for future analysis.

Histological analysis of the liver tissue was performed using the liver lobe designated for indenter testing. After indenter testing, the tissue was fixed in 10% buffered formalin, dehydrated in graded ethylic alcohol, and embedded in paraffin. Sections were generated with a thickness of 5 micrometers and were stained with hematoxylin/eosin (H/E) or 0.1% Sirius red. The H/E stained sections were analyzed under light microscope for histopathological assessment. The Sirius red stained sections were used for fibrosis evaluation. These specimens were scored using Ishak (score 0-6) systems, which is commonly used in clinical pathology. The Ishak system grades mild fibrosis as 0-1, advanced fibrosis as 2-4, and cirrhosis as 5-6 [75].

Model-Gel-Tissue (MGT) Assay Construction

In order to provide a controllable evaluation technique, a system of embedding extracted murine livers in a cylindrical gel has been developed. This gel-matrix provides a reference material for evaluation, provides a measurable contrast in elasticity between the gel and liver, and allows for use of true tissue shape by building a model based on microCT scans of the gel. In addition, the cylindrical gel could easily be utilized in multiple imaging modalities for possible elastography assessment. The gel-tissue samples also needed to be appropriately shaped for both imaging applications and material testing. In order to make the system amenable to compression testing, this meant a small sample size with a uniform shape. To achieve this, the gel samples were generated in Petri dishes that had a known diameter. This created a cylindrical shape with a measurable surface area and a consistent height. The process of tissue submersion involved a simultaneous tissue resection and mixing of base components of the polyacrylamide gel (BioRad Laboratories, Hercules, CA). The components were 1 molar Tris buffer, deionized water, and ammonium persulfate (APS). Graphite flakes (Sigma-Aldrich Chemie GmbH, Buchs, Switzerland) were also added to the base solution; these were necessary to provide ultrasound contrast (although this will not be reported in this work at this time) for imaging. During liver resection, the buffer solution was mixed as indicated in Table 1. Once the liver was removed and sectioned, the portion dedicated to the gel sample was weighed using a digital balance. In order to generate the individual gel sample, the buffer solution and acrylamide/polyacrylamide were mixed in a Petri dish according to the proportions indicated in Table 1. To provide a perceivable distinction between the liver and gel in the CT scans for segmentation purposes, a computed

Table 1. Polyacrylamide gel recipe utilized for the liver evaluations.

Polyacrylamide Gel Recipe	
Buffer Solution	**Individual Gel Recipe (5% Polyacrylamide)**
38.2 mL deionized H_2O	6.67 mL buffer solution
1.3 mL 1 M Tris buffer	1.33 mL 30% Acrylamide/Polyacrylamide
0.5 mL 10% APS solution	0.2 mL Optiray CT contrast
1.5 g graphite	0.07 mL TEMED

tomography (CT) contrast agent, Optiray (Mallinckrodt Inc, Hazelwood, MO), was included in the gel mixture. The liver sample was then suspended in the liquid gel using forceps and TEMED was added, which initiates the polymerization reaction to cause solidification of the gel. The solution was agitated during the solidification process, which required approximately two minutes, using pipette mixing; the agitation prevented settling of the graphite flakes. This process was performed for the fibrosis liver, the control liver, and the normal liver; gels with a fibrotic liver embedded are referred to as *fibrosis gels*, gels with a control liver embedded are referred to as *control gels*, and gels with a normal liver are referred to as *normal gels*. In addition, a *reference gel* was generated, which was produced as described above, without the addition of the liver sample. This *reference gel* was utilized in material testing in order to evaluate the modulus of the polyacrylamide gel generated on the occasion of each fibrotic liver evaluation. Fourteen fibrosis gels, three control gels, and three normal gels were generated over the course of the research.

Imaging

After the gel had congealed, microCT scans were obtained using the Imtek microCAT II scanner (Concord/CTI, Knoxville, TN). The resolution of the microCT image voxel was 115 by 115 by 115 microns. These scans were later utilized for finite element model generation. The gel sample was placed on the scanner bed and made level by adjusting its positioning based on prescan information from the scanner. CT scans were obtained for fibrosis, control, and normal gels, as well as for the reference gels. After scanning, the gels were transferred to the material testing lab and immediately tested. The total time between sacrifice and testing ranged from 1 – 2 hours.

Indenter & Traditional Compressive Material Testing

Individual liver lobes obtained during resection of the liver were placed in 0.9% NaCl and refrigerated until testing could be performed, which was less than one hour. Indenter tests were performed on the liver lobes in order to acquire an elasticity value to which results from the MGT assay could be compared. All material testing was performed utilizing the Enduratec Electroforce 3100 tester (Bose, Enduratec Systems Group, Eden Prairie, Minnesota). The material tester setup is shown in Figure 2. A 50-g transducer (Honeywell Sensotec, Columbus, Ohio) was attached to the upper arm of the tester, the indenter tip was attached to the transducer using a coupling device manufactured for this purpose, and the tip was lubricated with non-stick oil-based lubricant spray. The testing configuration is shown in Figure 3. The indenter tip used in all tests was a spherical tip with a diameter of 1.5 mm. A spherical tip was chosen in

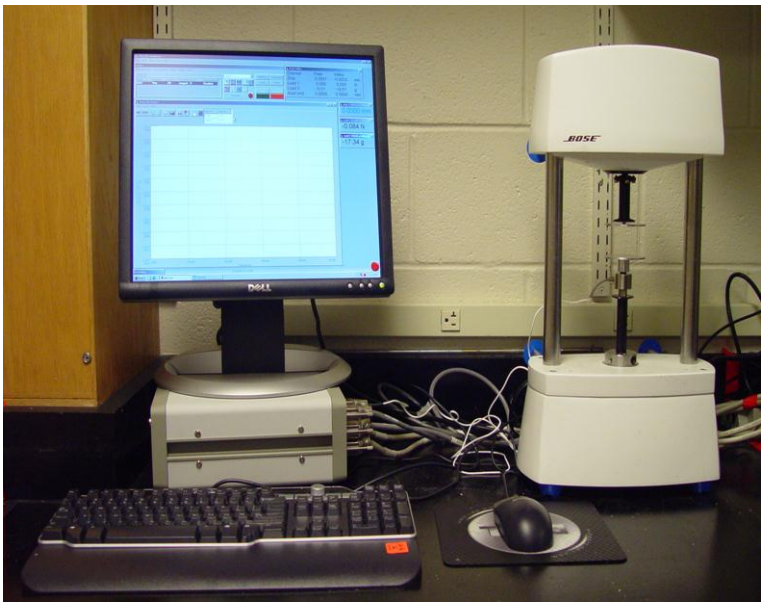

Figure 2. Material testing setup used in the MGT assay.

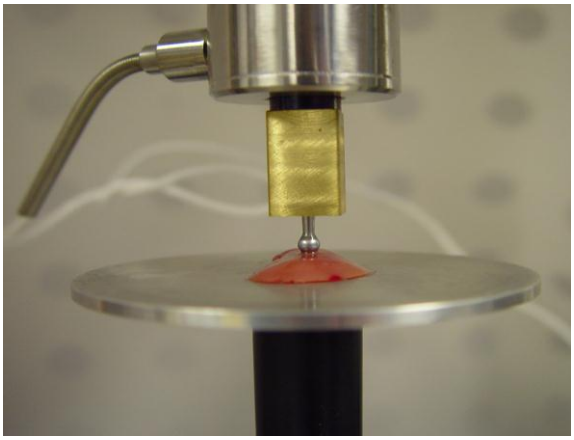

Figure 3. Close up of liver indentation setup. The liver was positioned so that contact with the indenter occurred at a point where the liver was uniform in height.

order to minimize damage to the tissue so that the liver lobes could subsequently be utilized for histological testing. The liver lobes were placed on the lower platen of the material tester, and the force and displacement values were zeroed prior to lowering the indenter. The indenter tip was manually lowered until it made contact with the liver

surface, which was determined by visual inspection and by observation of a sudden increase in the force values registered by the transducer. Contact between the liver and indenter was regulated between specimens by maintaining a force value between 0.01 and 0.03 g at initial contact. The liver lobe was situated on the platen relative to the indenter so as to provide a uniform surface for indentation. The indentation occurred at the thickest portion of the liver, in an area where there were no steep surface gradients.

Development of an indentation protocol that correlated to the compression protocol was necessary in order to generate results that could be analyzed relative to one another. However, in indentation testing, it is necessary that the depth of indentation not exceed the radius of the indenter tip to prevent aberrant behavior of the indentation model. In order to remain within the confines of the indenter system, the indentation protocol consisted of three indentations to a depth of 0.4 mm. Each indentation was held for a 60 second dwell period, which allowed the viscoelastic effects to dissipate, and then released. The indenter returned to zero position, and remained there for 60 seconds, at which point another indentation occurred in the same manner. In addition, each liver was measured after testing using a digital caliper to determine the thickness of the specimen at the region of indentation for use in modulus calculation.

The gel-tissue cylindrical specimen was tested using traditional compression. Due to the increased size of the specimen, the load cell used was a 250 gram transducer (Honeywell Sensotec, Columbus, Ohio). Figure 4 illustrates the setup for compression testing. Each gel was weighed using an analytical balance and measured using digital calipers (diameter and height) prior to testing. Both platens of the material tester were lubricated, again using the non-stick oil-based lubricant spray. The material tester was

zeroed after placing the gel specimen on the platen, so that the weight of the gel was not considered in the measured force. The platen was then raised until initial contact with the gel surface. This was determined by visual cues as well as a negligible increase in the force reading. For the compression case, the initial force values were limited to between 1 and 2 grams. A precompression of 0.3 mm was applied to each gel prior to testing in order to ensure full contact with the gel surface (~3-5% prestrain). The testing protocol consisted of a series of step compressions, applied in 0.05 mm increments, from 0.35 mm to 0.65 mm (~max strain 6.5-9%). After each step, the compression dwelled for 60 seconds, as was implemented in the indentation, to allow the force to reach steady state. The test was performed twice for each gel.

Figure 4. Gel compression testing setup.

Computational Model for Indentation and Model-Gel-Tissue Assay

With respect to the indentation testing data, the mechanical properties were determined using the correlation model suggested by Stevanocić et al. which concerned the contact between a rigid sphere and an elastic layer bonded to a rigid substrate [76]. The assumption is that the boundary defined between the liver and the bottom platen experiences no-slip conditions, and hence the liver can be modeled as an elastic medium bonded to the rigid platen. Stevanocić et al. developed a set of equations that was able to normalize the data presented by Chen and Engel [77] for a variety of varying modulus combinations by utilizing a dimensionless radius and layer thickness, which caused all of the curves to collapse onto one normalized curve. The correlation equation derived by Stevanocić et al. is:

$$\frac{a}{a_L} = 1 - c_3 e^{c_1\left(\frac{t}{a}\right)^{c_2}} \qquad (15)$$

where c_1,c_2, and c_3 are correlation coefficients, which, based on the analysis by Stevanocić et al., are defined as -1.73, 0.734, and 1.04, respectively, a represents the contact radius, a_L is the contact radius corresponding to an infinitely thick elastic layer, and t is the layer thickness. The contact radius, a, for a spherical indenter can be calculated from:

$$a = \sqrt{2\rho d} \qquad (16)$$

where ρ is the radius of the spherical indenter tip and d is the penetration depth of the indenter. To calculate the contact radius for an infinitely thick elastic layer, the Hertz relation must be consulted:

$$a_L = \sqrt[3]{\frac{3}{4}\frac{(1-\upsilon^2)}{E}F\rho} \qquad (17)$$

where E denotes the elastic modulus of the medium, υ the Poisson's ratio, and F the applied load. For this research, if a Poisson's ratio is assumed for the tissue, all of the elements of equation 3 are known except for Young's Modulus of the tissue. In past work, it has shown that for general soft tissue organs 0.45 has captured 1st order elasticity effects for liver and brain reasonably well [78-81]. This value would correlate with a 9:1 ratio of the Lamé constants (λ:G with G the shear modulus, and λ the bulk modulus) which is reasonably below the convention for Poisson locking which is important for the MGT assay (sometimes called mesh locking and typically has λ»G, or ν→0.5). Substituting equations 16 and 17 into equation 15 and solving for the modulus gives:

$$E = \frac{3}{4}(1-\upsilon^2)F\rho\frac{\left(1-c_3e^{c_1\left(\frac{t}{a}\right)^{c_2}}\right)^3}{\sqrt[3]{2\rho d}^2} \qquad (18)$$

The modulus for each liver lobe was calculated for each of the three indentations. The indentation depth and applied force were both calculated as the average respective value over the last 20 sampling points of the dwell, at which time the viscoelastic response had dissipated. The three calculated modulus values were then averaged to obtain the final elastic modulus value for each liver.

For the traditional compression test, a more complex model analysis was performed. Finite element analysis was combined with physical material testing to determine the modulus of interest. A critical component in this analysis was the selection of the model to represent the continuum of interest. In this work a Hookean elastic solid was chosen. This model assumes a symmetric, isotropic, specimen in equilibrium under small strains. These assumptions linearize the strain tensor and simplify Cauchy's law from 36 stiffness constants to 2 (Young's modulus E, and Poisson's ratio ν) and use the

traditional mechanical equilibrium equation. Similar to the indentation tests, Poisson's ratio was assigned to be 0.45. However, sensitivity tests with respect to Poisson's ration and the models associated with indentation and model-gel analysis are summarized at the end of this section.

Based on the equations for linear elastic deformation, a finite element system was developed for the gel-tissue domain. An iterative matrix solver was used to solve the sparse FE system which used a biconjugate gradient solver with an incomplete LU preconditioner [82]. To construct the domain, microCT image volumes were acquired prior to compression. In all experiments, the control, normal, and fibrosis gel systems were imaged and the gel and tissue were segmented using AnalyzeAVW (Mayo Foundation for Medical Education and Research, Rochester, MN). Due to the doping of the gel with CT contrast, it was relatively simple to extract the liver volume using the standard morphometric operations of threshholding and region-growing. The segmented volumes were found to agree with estimated volumes based on an assumed liver tissue density and the measured mass of the tissue. Upon completion of the segmentation, a surface description was generated and used as a bounding description for a custom-built tetrahedral mesh generator [54]. Figure 5 illustrates the geometric model construction process with Figure 5a demonstrating a representative CT slice of the murine liver within a contrast-doped gel. Figure 5b illustrates a homogeneous gel tetrahedral mesh (as can be seen, small gel surface defects were even captured with the process). Figure 5c illustrates the extracted liver tetrahedral mesh within the gel system.

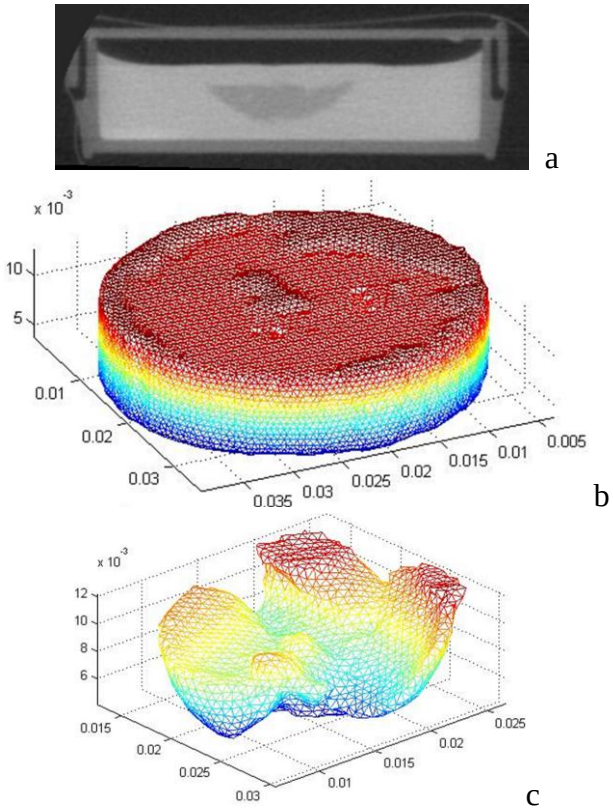

Figure 5. Computational domain construction with (a) liver microCT, (b) gel tetrahedral mesh, and (c) liver tetrahedral mesh extracted from gel/liver model.

The boundary conditions for the model reflected an unconfined compression that prescribed a fixed normal displacement (Dirichlet boundary conditions) on the majority of the top surface but was allowed to slip laterally (Neumann boundary conditions). This was achieved experimentally by placing a lubricant on the contact surfaces. More formally, the boundary conditions on the majority of the top surface were,

$$u_n = -d, \;\; \sigma_{t1} = 0, \;\; \sigma_{t2} = 0 \qquad (19)$$

where d is the fixed compressive displacement magnitude, *u* signifies a displacement, and σ signifies a stress. The subscript *n* indicates the normal direction and the subscript *t*

indicates a tangent-to-the-surface direction (subscript 1 or 2 indicates the two tangent axes associated with a right hand coordinate system). Similarly, at the bottom surface, the boundary conditions were,

$$u_n = 0, \;\; \sigma_{t1} = 0, \;\; \sigma_{t2} = 0 \qquad (20)$$

In order to ensure solution uniqueness, at least one Dirichlet condition is required in the lateral directions. To achieve this, nodes on the top and bottom surface that were within approximately 15 microns of the center-line (which translated to approximately 10 nodes) were fixed on each surface to restrain their movement laterally. The remaining boundary conditions for the sides of the gel were stress-free, i.e.

$$\sigma_n = 0, \;\; \sigma_{t1} = 0, \;\; \sigma_{t2} = 0 \qquad (21)$$

This paper serves to compare modulus estimates as provided by a novel MGT assay and that provided by indentation theory. In the model-based comparison method, the above model is compressed in simulation to a degree that matches the physical compression of its mechanically tested physical counterpart. As mentioned previously, for each gel with embedded liver, a corresponding homogeneous (reference) gel is also constructed. From the mechanical tester, an average force applied to either gel surface (homogeneous or liver-gel system) is recorded. By measuring the contact surface area, an average stress can consequently be determined. Similarly, in the simulation, a compression is prescribed according to (19), (20), and (21). Once the boundary conditions are prescribed, a solution is calculated which is based on an initial estimate of the gel and liver properties for each of the gel systems (homogeneous and liver-gel systems). Once the displacement solution is calculated, the unused Galerkin (weighted residual finite element technique) equations associated with implementing Dirichlet

conditions along the compressing surface can be used to estimate the boundary integral resulting from the standard weighted residual form, and subsequently the local boundary stress. This stress is averaged and multiplied by the surface area and then compared to the mechanical tester result. The determination of the liver modulus occurs in two steps. The reference gel (which is made at the same time as gel-tissue suspensions) is tested in the mechanical tester, and the modulus to match the model to the mechanical testing output is performed. Once determined, this is the assumed modulus of the gel within the heterogeneous liver-gel system. The properties of the liver are then determined by the same process of comparing measured to predictive average stresses.

As alluded to above, Poisson's ratio estimates were utilized in both the indenter modulus calculation and the finite element simulation for model modulus calculation. In order to assess the variability of the results based on Poisson's ratio selection, a range of Poisson's ratio in both calculations were tested. Based on previous experience, a value of 0.45 was assumed to be a reasonable estimation. From this assumption, it was opted to test a range of Poisson's ratio values from 0.43 to 0.49. For the indenter test calculations, the evaluation only required changing the Poisson's ratio that was utilized in the calculations for the modulus value. Each Poisson's ratio in the range was substituted into the equation and the resulting modulus value was recorded. This evaluation was performed for each of the tested livers (14 fibrotic, 3 control, and 3 normal). For the model calculation, the evaluation was performed using one of the sample fibrotic livers (analysis for #11). The range of Poisson's ratio values tested was from 0.43 to 0.48 (in the case 0.49, conditioning in the stiffness matrix was poor). For the liver of interest, the previously described modulus evaluation technique was performed a total of six times,

with each of the different Poisson's ratios. The modulus value obtained for each ratio was recorded for comparison.

Results

Figure 6 illustrates the average stress-strain behavior of the reference gels with the values extracted after the 60 second dwell period. Generating an estimate of the reference gel properties (which was created at the same time as the gel-tissue suspension) was important to the model-based characterization of mouse-liver properties. Figure 7 illustrates a similar stress-vs-strain application for a gel containing a murine liver, with data points again collected after the 60 second dwell. Figure 8 illustrates the excitation and dwell period of a typical indentation test.

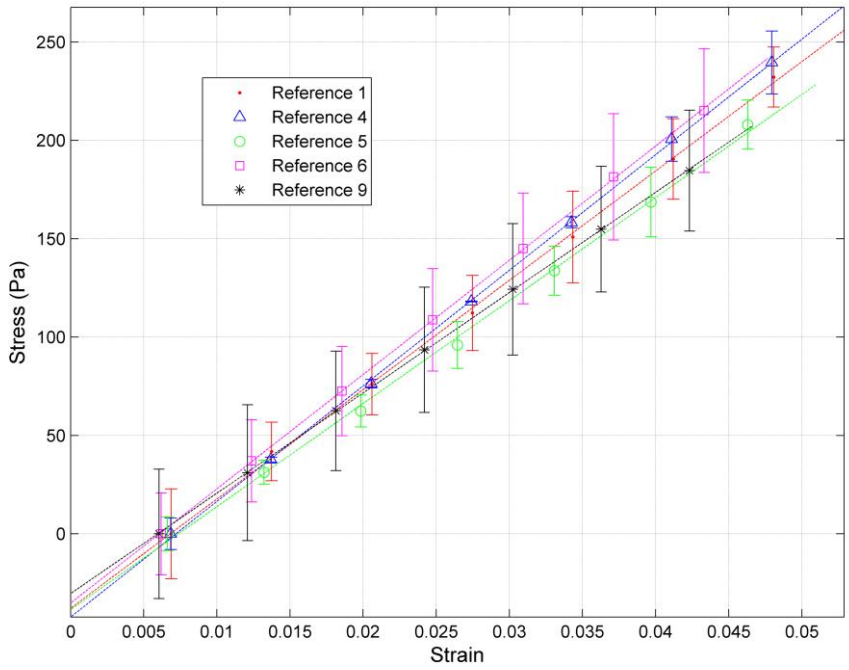

Figure 6. Stress-strain curves for reference gels from compression testing. A precompression of approximately 4% strain (0.3 mm) was applied prior to testing. The values are average values for the two compression tests performed on each gel, with error bars indicating the standard deviation of the two tests.

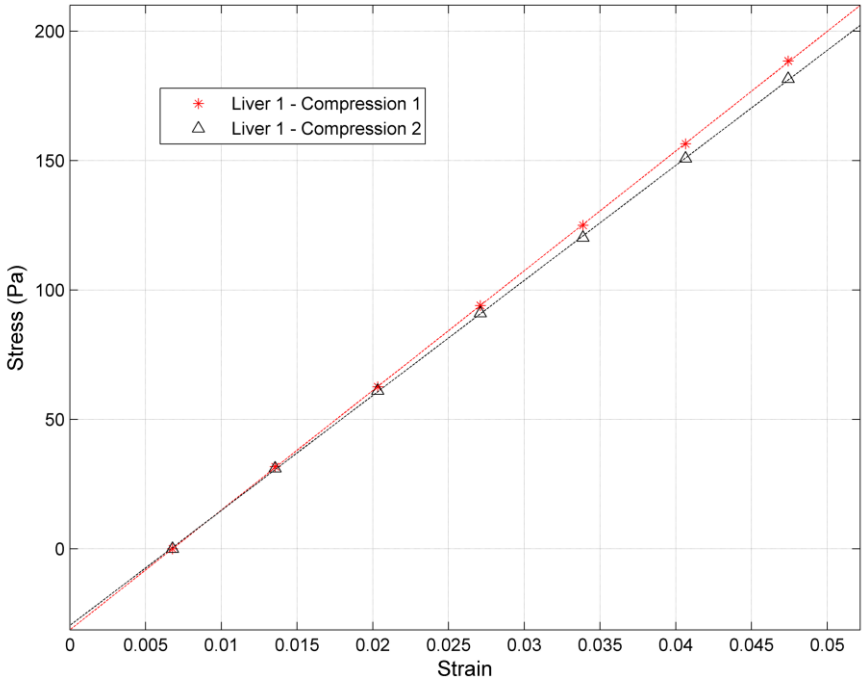

Figure 7. Stress-vs-strain behavior taken after the 60 second dwell for the gel-tissue system of a fibrotic specimen. The two curves represent the two compression tests. The data points represent the stress value after the dwell period at each step compression.

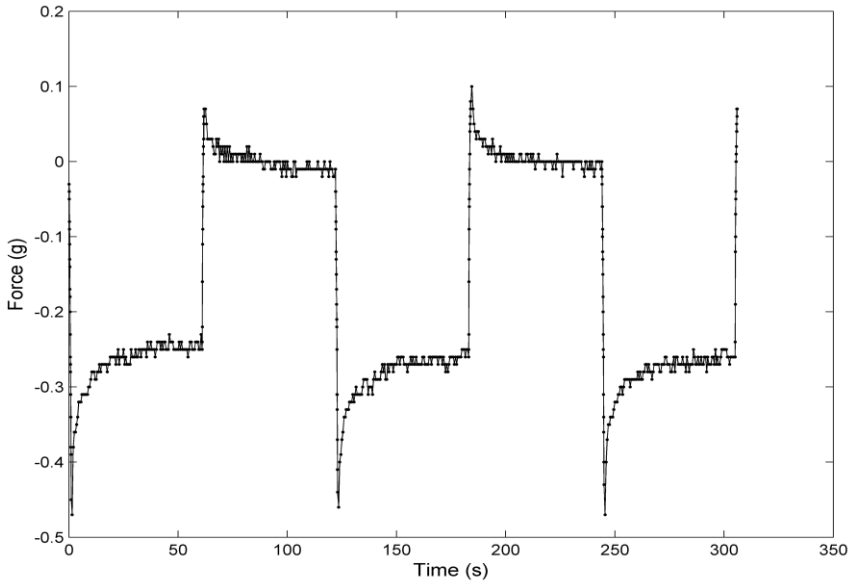

Figure 8. Example of force data obtained from liver indentation test. The temporal decay of the force data during sustained compression indicates the viscoelastic nature of the tissue. However, the effect dampens and a steady state has been approximately established at the end of the dwell.

The results from the indentation testing of the liver lobes are given in Tables 2, 3, and 4. Table 2 contains the data for the fibrotic livers. The values are given as the average of the three indentation tests for each liver. Table 3 contains the average modulus values and the standard deviations for the indenter assessment of the fibrotic livers. Table 4 contains the data for the control livers and the normal livers without treatment. The average value and standard deviation are given for the three controls, the three normals, and the non-diseased group, which contains all six control and normal livers. In each case, the standard deviation is small, indicating the variability of inter-sample moduli. The model-based calculation of fibrosis, control, and normal liver moduli are given in Tables 2, 3, & 4, also. For the model-based simulations, the control liver from liver 2 was not available so model data from only two control livers were used

to determine the control liver properties. In both the model-based and indenter cases, the control and normal moduli did not vary over the course of the experimentation. When considering the control/normal liver moduli as compared to the fibrosis liver moduli, both the indenter testing and the model results show a difference between groups. Fibrotic livers 6, 7, and 12 have indenter modulus values that are slightly lower than the others and are not distinct from the non-diseased average modulus, but the average fibrosis value for the indenter assessment is distinct from the average non-diseased value.

Table 2. Results from indenter material testing and model compression simulation for fibrosis and reference gels.

Liver Number	Ishak Grade	Indentation Modulus (kPa)	Model (Compression)		Indenter Percent of Model Modulus - Fibrosis
			Liver Modulus (kPa)	Reference Modulus (polyacrylamide) (kPa)	
1	4	**1.56**	**1.53**	6.12	101.9%
2	4	**1.26**	**1.70**	6.52	74.3%
3	4	**1.64**	**1.88**	6.69	87.5%
4	4	**1.18**	**1.53**	6.67	77.5%
5	4	**0.85**	**1.42**	5.84	59.9%
6	3	**0.70**	**0.96**	5.84	73.1%
7	4	**0.72**	**1.05**	5.84	69.0%
8	4	**1.06**	**1.39**	5.79	76.3%
9	4	**0.95**	**1.10**	5.79	85.9%
10	4	**1.07**	**1.31**	5.52	81.8%
11	4	**0.87**	**1.05**	5.66	82.6%
12	3	**0.60**	**0.97**	5.66	61.1%
13	4	**1.07**	**1.50**	6.20	71.3%
14	4	**1.08**	**1.60**	6.20	67.8%

Table 3. Average modulus values and standard deviations from indenter material testing and model compression simulation for fibrotic livers.

	Indenter	Model
Average	1.04	1.36
Standard Deviation	0.30	0.29

Table 4. Average modulus values and standard deviations from indenter material testing and model compression simulation for control gel.

	Indentation Modulus (kPa)	Model – Compression Modulus (kPa)
Control Average (kPa)	0.69 ± 0.06	0.66 ± 0.13
Normal Average (kPa)	0.55 ± 0.04	0.55 ± 0.06
Average Non-Diseased Modulus (kPa)	0.62 ± 0.09	0.59 ± 0.10

A correspondence is suggested between indenter and model-gel-tissue assays of modulus, as can be seen in Figure 9 and in the last column of Table 2. Figure 9 plots the model-based modulus for each fibrotic liver versus the indenter test modulus. A general trend exists between the two sets of measures, whereas the indenter modulus increases, so does the model modulus. This is again represented in the last column of Table 2, which gives the indenter modulus as a percentage of the model modulus. With exception of the liver 1 measurement, the modulus as measured by the indenter is consistently lower and represents an approximate mean of 76.4% ± 11.1%. As Figure 9 indicates, a discrete least squares approximation generates a reasonably good linear fit between the two methods.

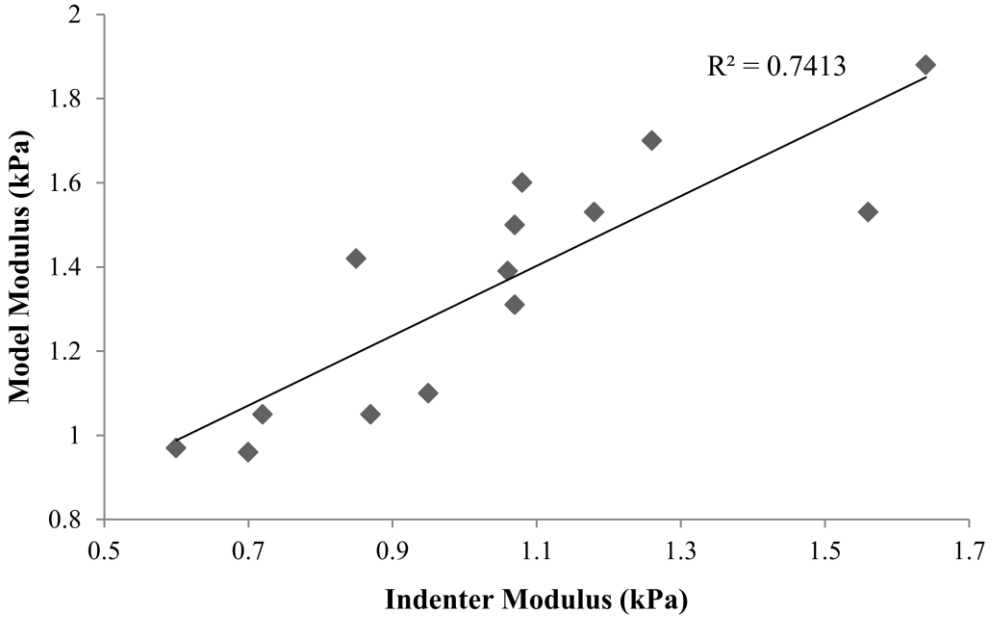

Figure 9. Liver model modulus as a function of indenter modulus for fibrotic samples. The correlation coefficient between the two sets (R^2=0.741, R=0.861) indicates a relationship between the two measures.

A test for normality was conducted on both the model and indenter modulus assessment data for the fibrotic livers. The Lilliefors test for normality was utilized, which allows analysis on continuous data with estimated mean and standard deviation [83]. In both cases, the null hypothesis of a normal distribution could not be rejected. A *t-test* analysis was performed to assess the difference in means between the non-diseased group and the fibrosis group for both the indenter analysis and the model analysis. In both cases, a difference was detected at a significance level of 0.01. A *t-test* was also utilized to assess the difference in means between the indenter and model analysis for the fibrosis group. The analysis indicated that the average indentation modulus was lower than the average model modulus for the fibrosis group at the 0.01 significance level. The

non-diseased results from the indenter analysis and the model analysis were compared using a *t-test*, and in this case, the null hypothesis of equal means could not be rejected. Finally, an outliers test was performed on the data point for liver 1, which is the only instance of the indentation modulus computed as larger than the model modulus. Grubb's test was performed on the data for the ratio of the indenter test to the model test, and the data point for liver 1 was found to be an outlier. Removing the data point for liver 1 from the correlation curve (figure 9) increases the correlation between the two curves, as shown in figure 10 below.

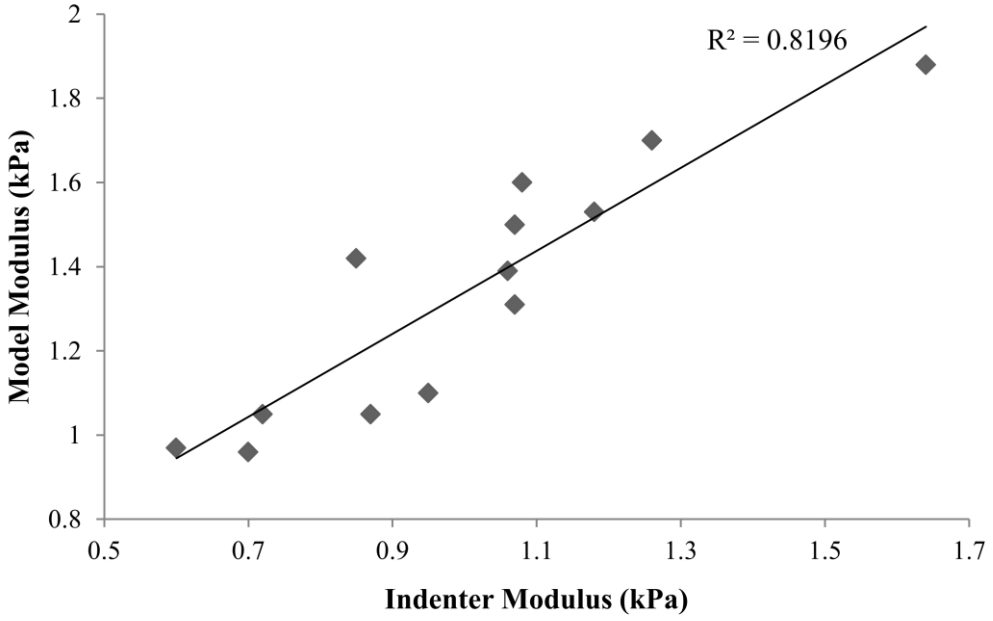

Figure 10. Liver model modulus as a function of indenter modulus for fibrotic samples. When the data point for liver 1 is removed, the correlation coefficient between the two sets increases (R^2=0.820, R=0.905).

In the Poisson's ratio evaluation, the effects were generally minimal from varying the Poisson's ratio. In the indenter case, the maximum difference in modulus for any of the livers was approximately 75 Pascals between Poisson's ratio values of 0.43 and 0.49. In the model evaluation, the maximum modulus difference was approximately 255 Pascals, between 0.43 and 0.48 (with 0.49 resulting in ill-conditioned stiffness matrix).

Discussion

Research has indicated that, in general, biological soft tissues are viscoelastic in nature, and, therefore, research commonly utilizes cyclic compressions to estimate the viscous reaction of biological soft tissue and isolate their elastic nature [84]. In contrast, some testing regiments institute a dwell period if they are concerned with factoring out such influences. When considering diagnostic processes such as elastography, in particular static-based methods which involve a prolonged state of compression, using the latter strategy to estimate properties would seem appropriate [28, 85]. When considering surgical loading conditions also, a static-based assessment is more suitable [78]. Thus, for compatibility reasons with research directions within the laboratory, a dwell period was instituted to factor out transient behavior and data was analyzed at these approximate steady state times. The dwell period length was chosen as 60 seconds for two reasons. First, this length of time was sufficient to approximate steady state as is indicated by Figure 8, which shows the force curve for a sample liver indentation under the protocol described above. Second, this time frame is relative to how long it takes to acquire an image in ultrasound elastography, or other elastography techniques, which is a current focus within the laboratory. There is little doubt that tissue is viscoelastic, and the force-

to-displacement behavior will change with increasing load rate. However, as with any material testing protocol, the loading environment concerned with the application must be taken into account. In addition, the same dwell period was implemented for both the indenter and compression tests in order to provide uniformity to the investigation. These dwell periods may be adjusted in the future depending on the application or if certain information regarding diseased tissue can be uncovered by looking at different loading events temporally. It should be noted that a linear regression was performed on the "steady-state" data to establish stress-to-strain relationships at these time points; in each case, a consistent correlation value of greater than 0.99 was determined thus indicating a reasonably robust analysis at this time point.

The main purpose of this research was to identify whether the MGT assay could be utilized to measure the stiffness of an embedded piece of tissue. As indicated by the correlation between the indenter and model modulus evaluations, the developed testing protocol delivered reasonable results for the elastic modulus of these trial samples. This is especially evident through the non-diseased analysis, in which case the model and indenter values are statistically indifferent. In addition, a chemically-induced liver fibrosis model was used to determine whether intuitive changes in these properties could be monitored. The dual-testing methodology allowed for independent confirmation of the MGT assay's measurement. It is interesting to note that while the control/normal mice values were statistically the same between testing methods, i.e. MGT and indentation assays, the fibrotic liver comparison indicated statistically different but correlated moduli values. The controls/normals would indicate fidelity exists between the two methods. However, the fibrotic discrepancy indicates that there is something

different with respect to the constituency of the tissue when performing indentation versus MGT, i.e. a smaller value. Statistical analysis among fibrotic livers indicated a difference in means between the indenter and MGT assay at a 0.01 level of significance, which may signify differing sensitivities in the model-based and indentation methods. One of the distinct differences between the two tests is the extent of the mouse liver used within each test. The two largest lobes are used in the MGT test, while one of the smaller lobes is used for the indentation. The other distinct difference is that indentation tests are measured on the surface of a liver lobe. It is quite possible that the outer parenchymal capsule associated with the liver may not have the same degree of fibrosis as the internal regions of the organ. Any heterogeneity with respect to the fibrosis in regions near the outer surface of the liver would inherently have a greater effect on indentation tests. The fact that the moduli values were less for these tests would be consistent with this assertion and the outer surface would be the most likely region to not have fully developed fibrosis. The MGT assay would be more representative of global organ fibrosis and the properties would reflect this.

There are several sources of error within the techniques that reflect limitations of this protocol. All methods herein represent an *ex vivo* methodology. Without linking the *in vivo* and *ex vivo* properties, it will be difficult to use this as a quantitative metric for *in vivo* changes. Nevertheless, the protocol does represent a reasonably robust technique to monitor changes under like conditions. It is interesting though that the values presented here correlate with other results within the literature for human liver. Yeh et al. measured normal and fibrotic livers in 19 fresh human cadaver livers using a standard compression test. At 5% strain normal and fibrotic livers had moduli values of 640 ± 80, and 1110 ±

170 Pascals, respectively. These are remarkably consistent with the values reported here. This may indicate that murine liver is a reasonably good model of human liver for mechanical properties; however, this should be tempered by the fact that Yeh's results were done 24-48 hours post-mortem (tissue was preserved) whereas the tests presented here are done 1-2 hours post-mortem; nevertheless, an interesting correlation.

Another possible source of error is the Poisson's ratio selection. A value of 0.45 was chosen based on two primary reasons. The first is that this value has been used in previous lab work and has proven successful in that application. The second is that this value provides a nearly incompressible description which is sufficiently elastic (as opposed to hyperelastic) to not invoke mesh-locking in the finite element solution. In addition, the testing of the Poisson's ratio range indicated that the indenter testing is somewhat insensitive to a small change in Poisson's ratio. The model is more sensitive to the changing Poisson's ratio; however, the effect is still small. The analysis was performed using a Poisson's ration of 0.45. Other research has utilized values higher than this. It is important to note, though, that the same Poisson's ratio was used in both analyses, which at the very least provides a very good relative comparison of moduli.

There are a myriad of other possible sources of error to include: segmentation, tetrahedral element choice, variability in disease model, subjectivity of disease grading, variability in pre-compression environment, etc. However, the independent method testing performed herein does provide confirmation regarding the detection of disease. The results also suggest that indentation and the MGT assay may provide information regarding fibrosis at both a local and more global level. Furthermore, it should be noted

that one advantage of the MGT assay is it would be amenable for calibrating elastography methods and conducting controlled experiments among different modalities.

Conclusions

The MGT method yielded results that could be correlated to indenter testing of the individual liver lobes. The control/normal liver modulus values are consistent for both the model and indenter tests. However, the fibrotic livers resulted in modulus values that were consistently higher in the model calculation than in the indenter calculation. Rather than thinking this is a limitation of either theory, it is hypothesized that this may be due to the indentation being performed at the liver surface, which is a region that may experience less fibrosis formation than the organ volume. The results reported here support this hypothesis thus far. The results demonstrated that normal and advanced fibrotic livers can be statistically identified with these techniques. Unfortunately, the Ishak scoring system is not specific enough to determine whether the extent of fibrosis can be correlated to the variability within modulus measurements. Future work would have to be focused at providing disease scoring that is more quantitative such as by image analysis. In addition, enhancements to the model regarding element-type and perhaps more complicated constitutive relations to match the transient properties would be appropriate for investigation. Despite some limitations though, the techniques and results produced herein should serve as a robust framework for testing elastography techniques as well as to monitor small-animal diseases systems that affect soft tissue architecture.

CHAPTER IV

EX VIVO TUMOR STUDY #1

Introduction and Contribution of Study

The work presented in this manuscript served to further the breadth of analysis of the MGT assay as well as to investigate the potential of linking microstructural content of tissue samples to evaluated modulus values. Continuing the work of the previous manuscript, this paper concerned the application of the MGT assay to tumor tissue evaluation, further demonstrating the capability of the assay as a soft tissue modulus evaluation technique. In addition, this paper served as an initial investigation into the relationship between microstructure and modulus. Specifically, collagen content of the samples was quantified and compared to the assay-evaluated modulus, and a correlation between the two measures was established. Finally, this work highlighted a potential limitation of the assay relative to the ratio of the size of the tissue specimen to the volume of the gel in which it is embedded, thus indicating the need to qualitatively evaluate the capabilities of the assay in order to ensure its application as a modulus evaluation technique. This work was initiated with the notion of evaluating the suspected mechanical differences between tumors with membrane-tethered TNF-α versus those with cytoplasmic TNF-α, which was being evaluated by a collaborator; the collagen content of the samples was also evaluated due to the expected effect of the TNF-α differences. The results showed that the TNF-α state of the tumors was not differentiated by either the MGT assay modulus or the collagen content of the tissue. However, the

collagen content and the modulus value demonstrated a correlation, which provided an interesting first observation of the potential quantitative link between microstructure and macroscopic property. This work was published in *Biomechanics and Modeling in Mechanobiology* in August of 2009.

Experimental Study

A NOVEL MODEL-GEL-TISSUE ASSAY ANALYSIS FOR COMPARING TUMOR ELASTIC PROPERTIES TO COLLAGEN CONTENT

Appearing in
Biomechanics and Modeling in Mechanobiology, Volume 8, Number 4, August 2009

Abstract

In previous work, a new assay was realized for determining soft-tissue mechanical properties. The method, named the model-gel-tissue (MGT) assay, couples material testing with a finite element model built from a micro-CT image acquisition of a gel-embedded tissue specimen to determine its mechanical properties. Given recent reports demonstrating that increased stromal collagen promotes mammary tumor initiation and proliferation, in this paper, the MGT assay is used to evaluate the modulus of murine mammary tumors and is subsequently correlated quantitatively to type I collagen content. In addition, preliminary testing of the assay sensitivity with respect to gel-volume to tissue-mass ratio is reported here. The results demonstrate a strong linear correlation between tumor mechanical properties and collagen content ($R^2 = 0.9462$). This result is important because mechanical stiffness as provided by the MGT assay is very similar to parameters under clinical investigation using elastographic imaging techniques. The

sensitivity tests indicated that an approximate gel-volume to tissue-mass ratio threshold of $16.5 mlg^{-1}$ is needed for successful analysis. This is an important result in that it presents guideline constraints for conducting this analysis.

Introduction

Assessment of tissue stiffness often plays an integral role in research and clinical diagnostics since it has been identified as an indicator of a variety of pathological conditions, including hepatic fibrosis, arterial disease, myocardial infarction, breast cancer, prostatic cancer, thyroid disease, and skin cancer, among others [7-21]. In addition, recently developed medical imaging modalities are attempting to render non-invasive measurements of these properties for disease screening (commonly cancer screening) and therapeutic applications [22, 24, 27, 86-91]. However, direct mechanical measurement of tissue for modulus assessment and method validation has proven difficult due to the inherent irregular tissue shape and the challenge of preparing them for traditional mechanical testing methods. However, some material testing methods have been developed that are applicable to a specific tissue configuration; for example, indentation testing for layered slab tissues. While a very common approach, the determination of elastic properties from this data is often based on certain geometric shapes, and boundary conditions. In the case of tissue resection and biopsy specimens, which are generally the gold-standard pathological sampling techniques, these tissue samples would routinely violate many of these assumptions. Thus, the development of a mechanical property assessment technique that can be adaptable to the uncertainty of

tissue size and shape and yet be quantitative would be an important contribution towards understanding biomarkers associated with tissue structure.

With respect to the macroscopic determination of mechanical properties, the two primary protein components that define mechanical stability of soft tissue are collagen and elastin. These proteins directly influence the structural integrity of tissue, and an assessment of the amount of collagen in a sample is a measure that reflects the load-bearing nature of tissue, and hence its stiffness. Changes to tissue health can lead to altered distributions of these particular proteins within soft tissue [5]. For example, in recent reports increased stromal collagen has been shown to increase tumor formation and proliferation in murine mammary tissue by threefold and has resulted in a more invasive phenotype with increased metastasis [92]. The possibility to use an assessment of collagen to predict tumorigenic behavior is intriguing but the interaction and change to the relationship between cellular structure and modulus in the diseased state is to some degree uncertain; and, it's relationship at clinically relevant diagnostic length scales is equally uncertain. The standard method used for collagen assessment is histological analysis; however, at best histological processing provides an indirect relationship to collagen's functional mechanical role, and it is this functional role that is critical in many ways to the use of mechanical properties as a biomarker. For example, breast cancer and liver fibrosis are often detected by palpation [93-96]. Other areas of study such as fracture repair and wound healing are also characterized by mechanical performance [97-101]. While these are important areas, it would also be interesting to extrapolate the role that mechanical properties or the monitoring of tissue architecture could play in cancer evaluation.

In this work, an ex vivo mechanical testing assay that was previously reported is used within the context of measuring mechanical properties of arbitrarily shaped tissue volumes from a murine mammary tumor model. The assay involves suspending freshly excised tissue volumes within a rapidly congealing gel, imaging the sample, evaluating mechanical performance using standard material testing equipment, and then implementing a model-fitting process for modulus assessment. The assay is called the model-gel-tissue (MGT) assay, and is used here to demonstrate the link between tissue mechanical properties and collagen content for mammary tumors. Preliminary work utilizing the assay within a liver fibrosis murine model has been reported [102]. In the work presented here, the utility of the assay to evaluate various tissue types is demonstrated, as a shift is made from fibrotic liver to mammary tumor tissue. This expansion of the assay analysis to other tissue types, in particular cancer-based, begins to provide a more quantitative understanding of the stiffness biomarker that is commonly used to detect breast cancer. In addition, the work presented here is concerned with the specific task of linking structural load bearing changes to a histological assessment of a murine breast cancer system. In doing so, a critical quantitative correlation to cellular microstructural content, which had not been realized in the previous work, is demonstrated. In addition to this considerable advance, the tissue specimen volume has been reduced by one order of magnitude such that it is now biopsy-relevant and a preliminary sensitivity study regarding gel-volume to tissue-mass ratios is explored.

Methods

The work reported herein concerns the analysis of the modulus of elasticity of nine murine mammary tumors as measured by the MGT assay previously reported. The mouse model was prepared with murine breast cancer $1x10^6$ cells derived from mouse mammary tumor virus polyomavirus middle T transgenic lines (PyV-mT; maintained in DMEM, 10% FCS, 5.0 ng ml^{-1} 17-β estradiol, 1 μg ml^{-1} progesterone) and were implanted contralaterally in FVB/nJ host mice in the 4^{th} mammary fat pad. Tumor tissues were collected after 30–40 days, which allotted growth to approximately 1 cm^3, and sectioned for analysis. The largest section was utilized for modulus evaluation in the MGT assay. Collagen content of the tumors was determined from the acid-hydrolyzed homogenate of a separate tumor segment. Amino-acid analysis of the derivatized hydrolysate yielded hydroxyproline and other amino acids to estimate both total and relative collagen content [5]. This value was then used as a comparison for the MGT assay evaluation of the tissue modulus. These tests were prepared in a blinded fashion from the MGT assay and were only available post MGT assay conclusion. In addition, a histological analysis was performed on tissue samples in order to ensure that the collagen present was predominantly type I. Tissue samples underwent standard immunohistological analysis, using rabbit anti-collagen I (abcam, Cambridge, MA), which has shown 100% specificity to collagen type I and less than 1% reactivity to other collagen types. The Dako Envision+ System, DAB/Peroxidase (DakoCytomation) was used to produce localized, visible staining of the collagen. For comparison purposes, adjacent sections of tumor were stained with Masson's Trichrome to visualize extracellular collagen deposition.

The MGT assay used to measure mechanical properties utilizes a gel-embedded tissue sample and combines finite element modeling of the gel-tissue composite with direct mechanical testing to evaluate the mechanical properties of the tissue sample. An outline of the assay is depicted below (Fig. 11).

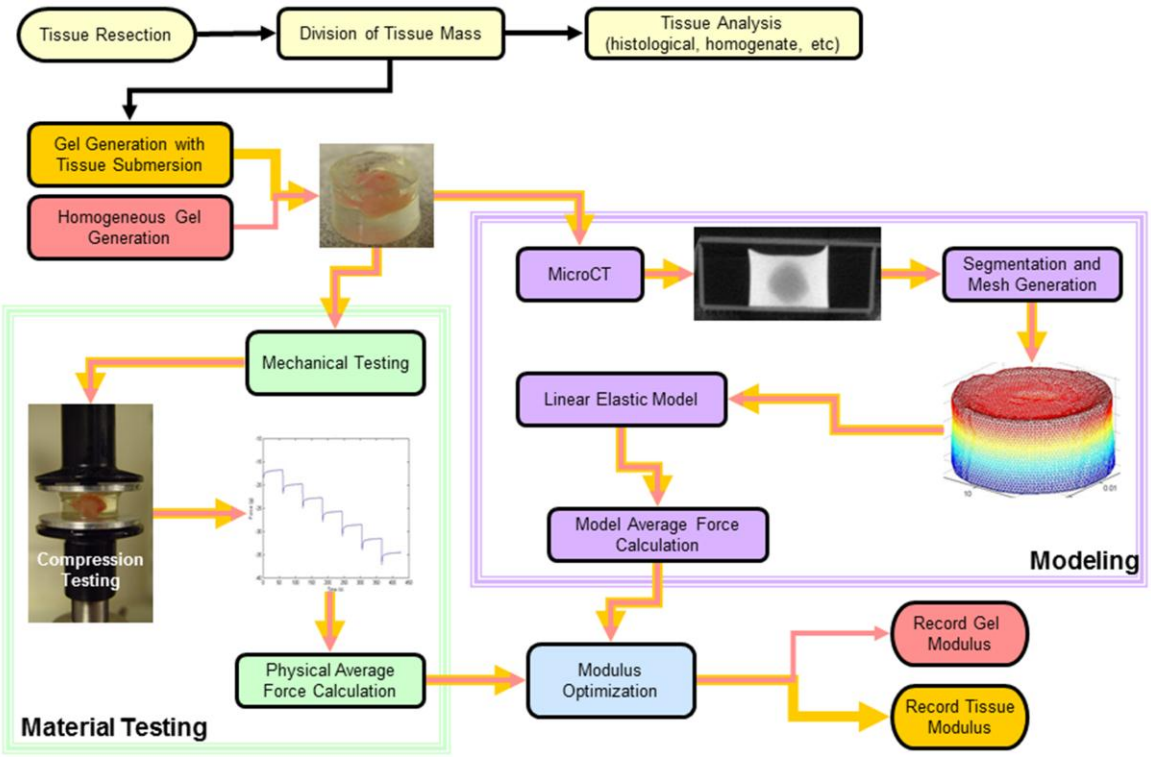

Figure 11. Assay outline.

Implementation of the MGT system required production of a uniform gel with embedded tissue sample as well as rigorously defined material testing protocols. The gel that proved most amenable to the demands of the system was a rapidly congealing polyacrylamide (PA) gel. The components of such a gel were 1 molar Tris buffer, 10%

ammonium persulfate (APS) solution, and 30% acrylamide/polyacrylamide (BioRad Laboratories). Since multiple samples could be generated during the course of one experiment, an initial solution was generated for use in all gel generation. For this research, a 4.5% polyacrylamide gel, which had a modulus of approximately 2.5 kPa, was utilized. It is necessary for the MGT assay that the modulus of the gel be similar to that expected for the tissue; if the gel is too stiff, the incremental effect of the tissue modulus on the composite system is undetectable. In addition, the ratio of gel-volume to tissue-mass proved pivotal in the effectiveness of the assay. In an attempt to compensate for the varying tumor tissue volumes across samples, we gradually varied the gel volume, resulting in gel-volume to tissue-mass ratios ranging from 4.43 to 32.68. The success of the assay appears to be linked to this ratio (Table 5). Based on this preliminary analysis, a volume of 1.4 mL of solution was generally used; however, this amount could be varied dependent on the tissue mass if necessary. With respect to setup, the diameter of the gel cylinder could be varied to accommodate different tissue shapes, but it was necessary that the gel completely envelop the tissue for the assay evaluation. In the mammary tumor case, well plates with a diameter of 16 mm proved sufficient for the extracted tissue size. To generate the gels, the desired volume of buffer/APS/PA solution was added to one of the wells. In addition, to provide a distinguishable boundary between the tissue and the gel in CT scans for the purpose of extracting the geometric shape for modeling (i.e. image segmentation), Optiray (Mallinckrodt Inc), a CT contrast agent, was added to the mixture. The tissue was then suspended in the liquid using forceps while the polymerization initiator, TEMED, was added to the well. Solidification of the gel was complete in approximately two minutes. In addition to the embedded tissue gels, a

homogeneous gel was generated at the same time for the purpose of estimating the mechanical properties of the gel itself. The homogenous gel was created following the same guidelines previously described, without suspension of the tissue. If multiple gel volumes were used in the experimentation, a homogeneous gel was generated for each volume instance.

After gel generation, the gel-tissue sample was imaged using the Imtek microCAT II scanner (Concord/CTI). Image segmentation of the CT images was performed using AnalyzeAVW (Mayo Foundation for Medical Education and Research). Upon completion of the segmentation, a surface description was generated and used as a bounding description for a custom-built tetrahedral mesh generator [54]. After imaging, the gel-tissue specimen was subjected to compression testing using the Enduratec Electroforce 3100 material tester (Bose, Enduratec Systems Group) with both force and displacement being acquired. Due to the small size of the samples, a 50-gram force transducer was utilized. The mechanical test consisted of a series of incremental unconfined step compressions to specified displacement levels, from 0.35 to 0.65 mm in 0.05 mm increments, followed by a 60 second dwell period which was implemented to dissipate the majority of the viscoelastic behavior of the tissue and gel. The compression testing was repeated twice for each gel sample. The unconfined nature of the compression was achieved experimentally by applying a lubricant to both the top and bottom surfaces of the gel.

After imaging and material testing was completed, the MGT assay modulus evaluation process took place in two steps. First, the homogenous gel sample was evaluated to determine its modulus. The finite element model generated for the

homogeneous gel was subjected to boundary conditions that matched the unconfined mechanical compression of the physical gel. Specifically, the top surface was subjected to a fixed normal displacement (Dirichlet boundary conditions) while being allowed to slip laterally (Neumann boundary conditions). The bottom surface of the gel experienced similar boundary conditions, with the difference being that the normal displacement was maintained at a constant zero value. Approximately ten nodes in the center of both the top and the bottom surfaces were confined laterally in order to ensure uniqueness of the computational solution. A modulus value was assumed for the gel in the model, and a forward evaluation of the displacements was calculated. From the displacement field, equivalent surface stress due to the specified compression level could be reconstructed. The resulting model stress was then converted to a force value based on the surface area of the specific gel and compared to the acquired force from the mechanical tester; the input gel modulus was varied until the model-calculated force value matched the measured force value, at which point the reference gel modulus was recorded. This value was then assumed to be the gel modulus in the gel-tissue sample evaluation. The method of tissue modulus estimation, as in the homogeneous case, was compressed according to the same mechanical testing conditions. The modeled and measured mechanical forces were compared, and the model's tissue modulus was adjusted until the two forces were equivalent, at which point the tissue modulus was assigned.

Results

The results of the volume regulation testing are presented below (Table 5), wherein the ratio of tumor gel-volume to tissue-mass is correlated to whether the MGT

assay was able to successfully analyze the tissue modulus. A successful analysis was achieved in the case where a modulus value could be evaluated for the tissue. An unsuccessful analysis was defined by an inability to differentiate the specimen from the background gel due to undetectable differential force resolution experienced when adjusting the tissue modulus. In cases where the gel-to-tissue ratio is approximately 16.5 or less the assay is able to successfully evaluate the tissue modulus. According to the available data, the maximum value at which the assay is no longer able to evaluate the tissue modulus is 18.92.

Table 5. Gel-to-tissue volume ratio.

Mammary Tumor Mass (g)	Gel Volume (mL)	Gel-to-Tissue Ratio (mL/g)	Positive Analysis?
0.3819	2	5.24	Yes
0.3580	2	5.59	Yes
0.4519	2	4.43	Yes
0.1057	2	18.92	No
0.0684	2	29.24	No
0.0912	1.5	16.45	Yes
0.0950	1.5	15.79	Yes
0.0459	1.5	32.68	No
0.1011	1.4	13.85	Yes
0.2221	1.4	6.30	Yes
0.1335	1.4	10.47	Yes
0.2554	1.4	5.48	Yes

The results from the murine tumor tissue assay analysis are compiled below (Table 6). The first column is the tumor number given for identification purposes. The

second column of the table is the modulus value as calculated by the MGT assay, and the third column is the collagen percentage as evaluated by acid-hydrolyzed homogenate analysis. A pictorial depiction of the data from Table 6 follows, wherein collagen percentage of the tumors is plotted versus the MGT assay modulus assessment for each tumor (Fig. 12). A linear regression was performed on the data, resulting in a correlation coefficient that demonstrates a strong linear correlation between the two variables (R^2=0.9462). In addition, two sets of predictive intervals (90% and 95%) are shown. These predictive intervals indicate the range of obtainable collagen percentage values correlating to a specific modulus value in future evaluations [103, 104]. In other words, these intervals depict the specificity of the assay in evaluating a correlation between the model modulus value and the analysis of collagen percentage.

Table 6. Assay and acid-hydrolyzed homogenate results

Tumor Number	Modulus (Pa)	Collagen Percentage
1	750	7.93
2	970	9.00
3	3840	33.48
4	2430	16.64
5	1050	11.76
6	2730	20.11
7	1840	16.37
8	890	7.07
9	650	4.49

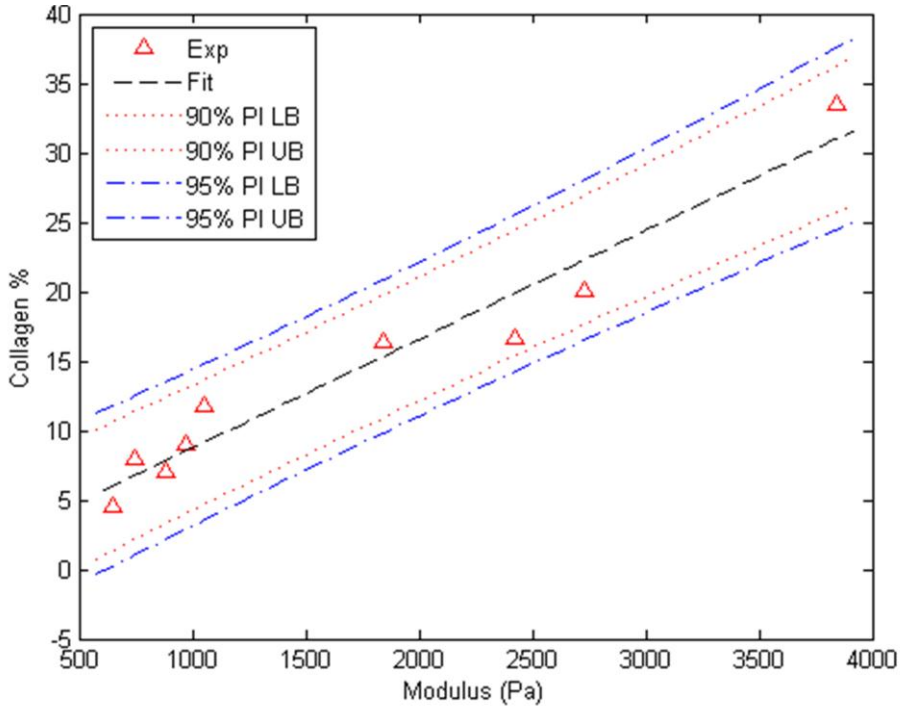

Figure 12. Collagen percentage as a function of tumor modulus for PyV-mT tumors. The black line is the linear regression to the data set, while the red line is the 90% confidence interval, and the blue line is the 95% confidence interval.

Results from the histological analysis of the mammary tumor tissue are shown in figures 13 and 14 below. Representative images at 10x and 20x magnification are shown for both the immunohistological analysis for collagen type I (Fig. 13) and the Masson's trichrome staining of adjacent slices (Fig. 14). In figure 13, the slides were lightly counterstained with Mayer's hematoxylin to tag collagen I with a slight brown color. In figure 14, the light pink areas are cellular cytoplasm, while the darker pink/brown areas are the nuclear component. Blues areas in figure 14 are extracellular collagen. Comparison of the brown-stained collagen type I (Fig. 13) to the blue-stained ECM

collagen (Fig. 14) indicates that most, if not all, of the collagen present in the tumor tissue is type I.

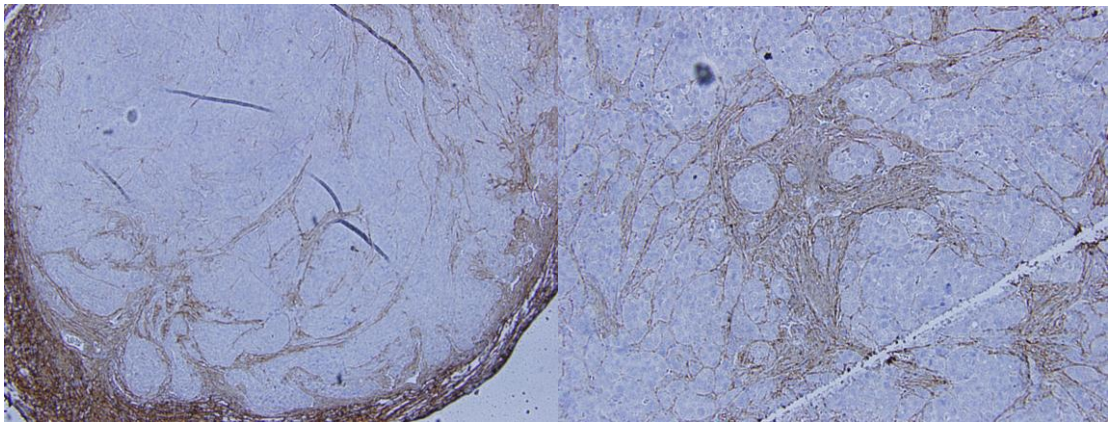

Figure 13. Representative slice from immunohistological analysis of murine mammary tumor tissue. The two images are the same slice, with the left being at 10x magnification and the right at 20x magnification.

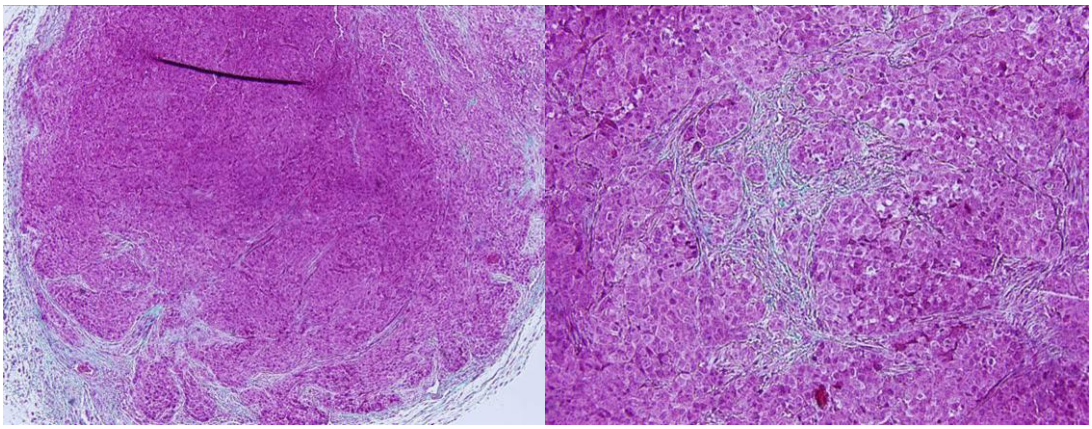

Figure 14. Representative slice from Masson's Trichrome staining of murine mammary tumor tissue. The two images are the same slice, with the left being at 10x magnification and the right at 20x magnification.

Discussion

One of the aims of this work was to demonstrate that the analytic capability of the MGT assay was not limited to a specific tissue type. To this avail, murine mammary tumor tissue was used, which, by dictation of the system, is a much smaller tissue volume than the murine liver. Thus, while we were able to show the applicability of the assay to other tissue types, this work also provided insight to the required assay parameters for tissue assessment using the MGT assay; namely, the required control of the gel-volume to tissue-mass ratio. In practice, the gel must completely surround the tissue. However, if the gel volume exceeds the tissue mass by too large a ratio, the gel mechanics will overwhelm the changes to the composite mechanics and the assay will be less sensitive to contributions from the soft-tissue. The realization of this volume regulation is evident from the data (Table 5). From this data, a threshold of the ratio is observed, above which the assay is not able to identify the tissue among the gel, which is important to recognize in order to ensure the fidelity of the assay. In cases where the gel-to-tissue ratio is approximately 16.5 or less the assay is able to successfully evaluate the tissue modulus. The implications are that since the tissue mass can only be minimally controlled (e.g. volume of the biopsy), control of the assay must be performed by modifying the gel recipe based on the measured mass of the resected tissue, i.e. the gel volume is dependent on the individual tissue samples.

With respect to cancer screening, a common clinical presentation is a change in the mechanical stiffness of tissue in a focal region such that it becomes more rigid (e.g. breast cancer). While for conditions such as liver fibrosis, the mechanism for altered mechanical properties is well understood, this process in cancer is mechanistically

unclear. As more information is uncovered regarding microstructural effects relating to tumorigenesis, such as that relating increased stromal collagen content to tumor formation and proliferation [92], the need to understand the underlying structure-function link is enhanced. This work demonstrates a distinct tracking of mechanical properties with respect to collagen content within this particular cancer model (Fig. 12). In addition, the immunohistological analysis performed indicates that the collagen content evaluated by the acid-hydrolyzed homogenate is representative of collagen type I. It is unclear if the apparent linear relationship will translate to other tumors or whether various cellular and molecular challenges will change this correlation. From a methodological standpoint, the breakthrough that the MGT assay makes is the ability to analyze mechanical properties of small animal tissue immediately post-mortem while allowing the sample size to be arbitrarily shaped and very small in volume. From the clinical standpoint, the breakthrough is twofold: (1) human biopsies are generally small and arbitrarily shaped, and hence the assay could presumably be utilized in biopsy evaluation, and (2) it is clear that the MGT assay combined with other cellular assays allows more detailed understanding of the elasticity signal commonly collected by clinical elastographic imaging methods, i.e. it illuminates the relationship between the cellular biomarker of collagen presentation and the mechanical abnormalities of the tumor at the macroscopic scale.

While the general behavior reported can be intuited, the contribution is in the absolute quantification – a definable metric to relate function to histological presence. In addition, it is interesting to begin to speculate how this type of analysis can be furthered. For example, the force-displacement data for this assay was fit to a linearly elastic

homogeneous computer model of the tumor. Time-varying changes were factored from the experiment by allowing sufficient time lapses to allow for a quasi-steady state force-displacement response. The reality is that these temporal behaviors have information regarding soft-tissue interstitial fluid dynamics and cell-to-cell mechanics. With more sophisticated models, and more sophisticated fitting procedures, other information regarding structure and function could possibly be determined. In addition to generating models to correlate the slow-varying transients, other altered material testing profiles could be utilized. For example, viscoelastic properties are often illuminated by testing specimens with cyclic loading; it would be interesting to put a mechanical excitation spectrum though the specimen and correlate the findings with very complex models. Another area that awaits further investigation is the enhancement of the imaging aspect to this experiment. Here, microCT was used to essentially capture the shape of the tissue specimen. One could envision using high-field MR techniques to get at the more fine structural heterogeneity; or perhaps, diffusion imaging could be used to highlight regions of the tumor that do not permit the traffic of interstitial fluid as readily. The ultimate triumvirate for relating structure to assessable modulus would be to combine structure-enhancing imaging sequences, sophisticated testing regimens, and detailed cell and molecular assays. The MGT assay is a first move in this direction.

CHAPTER V

EX VIVO TUMOR STUDY #2

Introduction and Contribution of Study

The study presented in this paper served to investigate a prognostic aspect of soft tissue modulus evaluation. In this work, the potential of early determination of responsiveness of a tumor to treatment by means of elastic modulus evaluation was considered. However, in the small cohort of tumors studied, a connection between the two could not be established. Subsequently, this work presented a second opportunity to consider the modulus as an indicator of microstructure, as the assay derived modulus values were evaluated relative to collagen content of the tissues. As in the previous study, a correlation was observed between sample collagen content and the elastic modulus. The rationale for this work pertained to the potential of a non-invasive evaluation of tissue modulus as an early prognostic indicator of tumor responsiveness to treatment. While current, invasive biochemical evaluations of tumor tissues can determine tumor classification and point to the indicated treatment, some tumors that are expected to respond to a given treatment unforeseeably will not. The literature indicates that work has been done to investigate genetically identifiable indicators of resistance, but these are not pertinent in all cases. Hence, in many cases, resistance cannot be determined prior to treatment. While almost all of the literature regarding resistance to treatment investigates resistance evaluation via genetic or cellular means, this work aims

to investigate mechanical differences as an indicator of resistance. This work will be submitted for publication.

Experimental Study

INVESTIGATION OF A MODULUS DEPENDENCE ON TREATMENT RESPONSIVENESS USING A MURINE MODEL OF HER2+ BREAST CANCER

To be submitted, 2011

Abstract

Screening and treatment for breast cancer has improved, thus increasing survival among patients. Additionally, genetic analysis of tumors can indicate preferential treatment regiments based on tumor class. However, even with knowledge of the tumor subtype and the associated treatment, patients do not respond equivalently to the same treatment. Methods for determining which patients are responsive and which are resistant to a specific treatment prior to treatment are not currently available, but would prove valuable in treatment planning. In this work, an association between the modulus of the tumor tissue and the responsiveness of the tumor to a specified treatment was investigated. The MGT assay was utilized to evaluate the modulus of Herceptin-responsive and Herceptin-resistant lines of a murine model of HER2+ breast cancer. Four responsive and four resistant tumors were evaluated; in this cohort of samples, a correlation between responsiveness of the tumor and tissue modulus could not be defined. The collagen content of the tissue was subsequently evaluated via histological staining and quantification using the Ariol SL-50 platform (Genetix). In regards to collagen content, a correlation between modulus and tissue collagen content was established, with

the exception of one of the samples, which was statistically identified as an outlier. Though a modulus/responsiveness relationship could not be elicited, the work serves to further validate the use of the MGT assay as a modulus evaluation technique. Additionally, it indicates the relationship between the microstructure (collagen content) and macroscopic parameter (modulus) of the tissue.

Introduction

Breast cancer is an extremely prevalent form of cancer in the United States, and is the second-leading cause of cancer-related death in women [105]. Though breast cancer is an inherently heterogeneous disease dependent on a plethora of factors, breast cancer subtypes have been identified based on gene expression. Of particular interest for therapeutic reasons are the subclasses of cancer that involve cellular receptors which are targets for therapy; specifically, estrogen receptor (ER), progesterone receptor (PR), and human epidermal growth factor receptor 2 (HER2). Tumors are classified as either positive or negative for overexpression of the protein or gene amplification in these cases. HER2, a member of the ErbB protein family, is a cell surface receptor tyrosine kinase and has been shown to be involved in pathways affecting cell growth and differentiation. Overexpression of HER2, or an amplification of the HER2/neu oncogene, occurs in approximately 25% of human breast cancers. A HER2+ tumor demonstrates increased cell growth and proliferation, and is generally indicated by a poor prognosis as it is correlated to a shorter time to relapse as well as a shorter overall survival [106]. Specifically, the signaling pathways implicated in HER2+ tumors have effects on cell division, migration, adhesion, differentiation, and apoptosis [107]. Trastuzumab

(Herceptin®, Genentech Inc., San Francisco, CA) is a monoclonal antibody that, through mechanisms that are currently not fully understood, targets the HER2 protein on the cell surface, elucidating an immune response as well as affecting the intracellular signaling [108]. While Herceptin has proven successful as a treatment in some HER2+ cases of breast cancer, a portion of HER2+ patients do not respond to the treatment. The mechanism for resistance is not well understood; while some cases can be described by a genetic signature, others are not identifiable. Currently, no clinically relevant biomarkers exist that can predict resistance to Herceptin, and hence it is not possible to discern between patients who will and will not respond to treatment prior to the treatment.

Though the mechanisms of resistance to Herceptin treatment are as of yet not understood, recent studies have resulted in speculated potential pathways. It has been observed that Herceptin binding to the HER2 extracellular domain does not prevent ligand-induced generation of HER2/HER3 and HER2/HER1 (or EGFR) heterodimers; these heterodimers can continue signaling via the mitrogen-activated protein kinase (MAPK) and phosphatidylinositol 3-kinase (PI3K) proliferative survival pathways, and thus, although Herceptin affects HER2 signaling, it may not affect signaling from the HER receptor family members, which may have an implication in conferring resistance to the drug [109, 110]. The PI3K and the MAPK pathways have also been indicated in Herceptin resistance due to activation by the insulin-like growth factor 1 receptor (IGF1R). Based on this observation, overexpression of IGF1R has been identified as a potential mechanism for Herceptin resistance [111-113]. Mutations in the PI3K pathway have also been investigated as potential mechanisms of Herceptin resistance. Specific mutations in the catalytic and kinase domains of the p110α subunit of PI3K activate

signaling and have been indicated in Herceptin resistance [114, 115]. Additionally, a decrease in, or loss of, the phosphatase and tensin homolog (PTEN), a tumor suppressor which acts to inhibit PI3K signaling, has also been indicated in conferring Herceptin resistance [115, 116]. However, even with this knowledge of molecular and cellular effects, the mechanism for resistance is incompletely defined and may potentially vary among patients. This lack of a priori knowledge unfortunately results in patients spending valuable time undergoing ineffective treatments. For this reason, differences between the responsive and the non-responsive (or resistant) cancers that can be illuminated prior to devising a treatment plan would prove invaluable.

It has been well established in many pathological conditions that the modulus of the affected tissue is perceivably different than the normal tissue; specifically, in many cases, disease affects the microstructure in such a way that it produces a lesion that is stiffer than the healthy tissue [7-21]. This discernable change in condition is the central concept behind physical palpation as a method of breast tumor detection. Though in many cases the mechanisms that impart resistance have not been identified or are not well understood, it is conceivable that these same mechanisms may also have an effect on the modulus of the tumor. This is especially prevalent when considering the literature regarding the role of tensional homeostasis on the progression of the tumor as well as the propensity to affect the remodeling of the extracellular matrix associated with tumor aggressiveness and invasiveness [32,51-54]. To examine the potential prognostic value of modulus assessment, the MGT assay was utilized to investigate the modulus of a Herceptin-responsive and a Herceptin-resistant strain of the BT-474 xenograft mouse model of breast cancer. BT-474 is a human-derived cell line originating from an invasive

ductal carcinoma that is HER2+ and conducive to growth in the murine environment. With the attempted development of imaging-based noninvasive modulus assessment techniques, a recognizable difference in stiffness between the resistant and the responsive tumor types could prove to be useful as a preliminary indicator of treatment success [24, 25, 27, 86, 87, 89-91, 117].

Methods

The Herceptin-responsive and Herceptin-resistant cell lines utilized in this work had been previously established by the Arteaga laboratory at Vanderbilt, and the methods described here were adapted from their protocol [118]. To generate the Herceptin-responsive line, BT-474 cells were obtained from the American Type Culture Collection and maintained in improved minimal essential medium (IMEM, Life Technologies Inc.) supplemented with 10% FCS at 37°C in a humidified, 5% CO_2 incubator. To devise the Herceptin-resistant line, $2x10^7$ BT-474 cells suspended in growth factor-reduced Matrigel were injected subcutaneously into the right flank of five week old BALB/c athymic nude mice (Harlan Sprague-Dawley) 24 hours after they had been implanted with 0.72 mg, 60 day release 17β-estradiol pellets (Innovative Research). The tumors were allowed to grow until they reached a volume of approximately 300 mm^3, at which point the mice were treated with Herceptin in a biweekly regiment. Tumors that responded completely to the treatment and then reoccurred with continuous treatment were harvested and processed to generate the Herceptin-resistant cell line. For this work, cells from each established line were obtained from the Arteaga laboratory. To develop the tumors utilized here, five week old BALB/c athymic nude mice were implanted with an estradiol pellet, and then, 24 hours later, were injected in the right flank with $1x10^7$ cells from the

appropriate cell line suspended in a 1:10 matrigel to media solution. Five mice were injected with Herceptin-responsive cells specifically for this work, while the mice implanted with the Herceptin-resistant strain were utilized in collaboration with another investigator. The tumors were allowed to grow until they reached approximately 200-250 mm^3, at which point the mice were euthanized and the tumors were resected for evaluation. A portion of the tumor was reserved for histology. The other portion of the tumor was immediately embedded in a 4.8% polyacrylamide gel and analyzed via the MGT assay protocol [1,2]. Four responsive mice and four resistant mice grew tumors of sufficient volume and were used in the evaluation.

Histological analysis was performed on a portion of the tissue from each tumor sample in order to quantify collagen content of the samples. Following resection, the tissue samples were placed in 10% formalin for 24 hours, after which the tissue was moved to 70% ethanol where it was kept until histological analysis was performed. To establish consistency among the staining, histological analysis was performed on all of the samples at the same time. Once all of the samples had been collected, they were paraffin-embedded and sliced at a thickness of 5 microns. Three slides were obtained from each tissue sample, one taken from each edge of the tissue volume and one taken from the core of the sample, in order to provide a representative sampling of the entire available volume. The slides were stained using Gomori's Trichrome and analysis of the slides was performed using the Ariol SL-50 platform (Genetix, New Milton, UK). The Ariol system obtains high resolution images of the slides in an automated manner that is specific to the individual tissue sample. The system is trained on one of the obtained images to identify the colors of interest (based on the staining procedure and tissue

components of interest), as dictated by hue, intensity, and saturation. After training, the system evaluates each of the slices by means of thresholding based on the previously established limits, generating data for the number of pixels in the sample for each indicated color. For this evaluation, the system was trained to identify two colors: the blue stain, indicating collagen, and the set of all colors, indicating the total tissue area. The amount of collagen in each histological sample was then quantified as the sum of the blue pixels in the sample. The percent collagen in each sample slice was calculated by dividing the total number of collagen pixels by the number of pixels of all colors, thus allowing for a calculation of the collagen in the sample normalized to the area of the tissue sample.

Results

The results for the breast tumor responsiveness testing are shown in Figures 15, 16, and 17. Figure 15 shows the assay evaluated modulus for the four responsive (BT) and the four resistant (HR) tumors. For the small sample size investigated here, there was no observed difference in stiffness between the Herceptin-responsive and the Herceptin-resistant samples; a t-test for the difference in means between the two groups indicated that there is no significant difference in the two means. Figure 16 depicts the tumor modulus value versus the percent collagen as calculated by the Ariol analysis. Figure 17 again shows the modulus versus percent collagen with a linear regression of the data, but excludes sample HR6-1. A Grubb's outlier test was performed on the data to determine if sample HR6-1 qualified as on outlier in the data set. The test indicated with a significance of 0.01 that the point was an outlier, and thus the data point was excluded

from the linear regression. The resulting correlation coefficient for the regression (R) is 0.89. Table 7 provides the percent collagen calculations for each of the three slides from each tumor sample as assessed by the Ariol system, as well as the average percent for the three slides. The evaluated percent collagen is consistent across the three slides, with an average standard deviation of 1.9%, except in the case of HR6-1. The highest slide for this sample registered at 30.82% collagen while the lowest equivocated to 8.44%. This spread caused a large standard deviation for the sample at 11.58%. Figure 18 shows the three histological images from sample HR6-1 corresponding to the three calculations in Table 7. Figure 19 contains the three images from sample HR6-3. The data point for sample HR6-3 was not considered an outlier, but as can be seen in Figure 17, it has one of the larger deviations from the correlation curve.

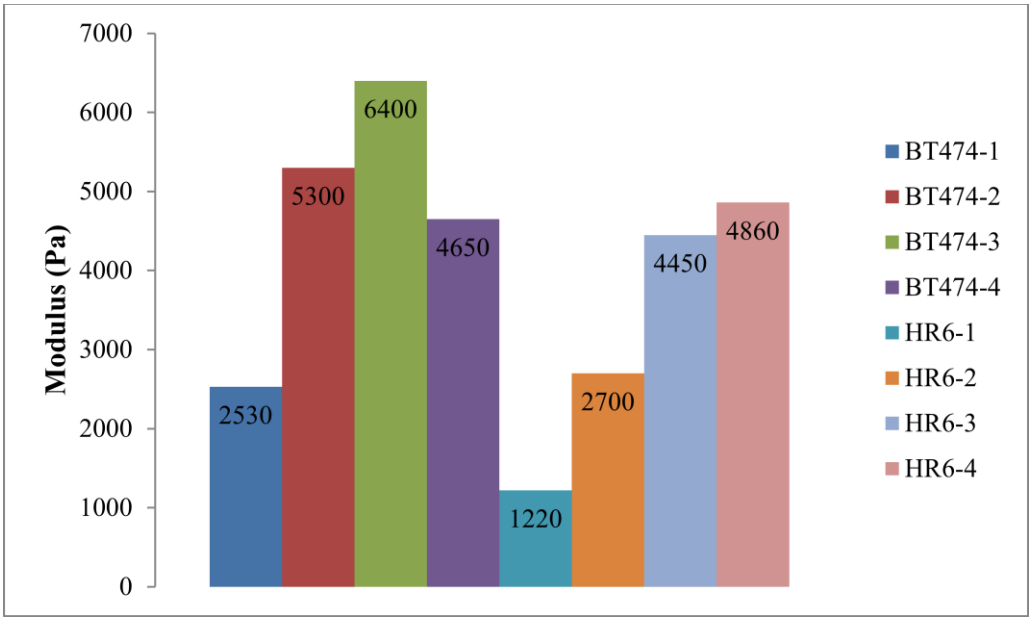

Figure 15. Modulus values for the Herceptin-responsive (BT) and Herceptin-resistant (HR) tumors.

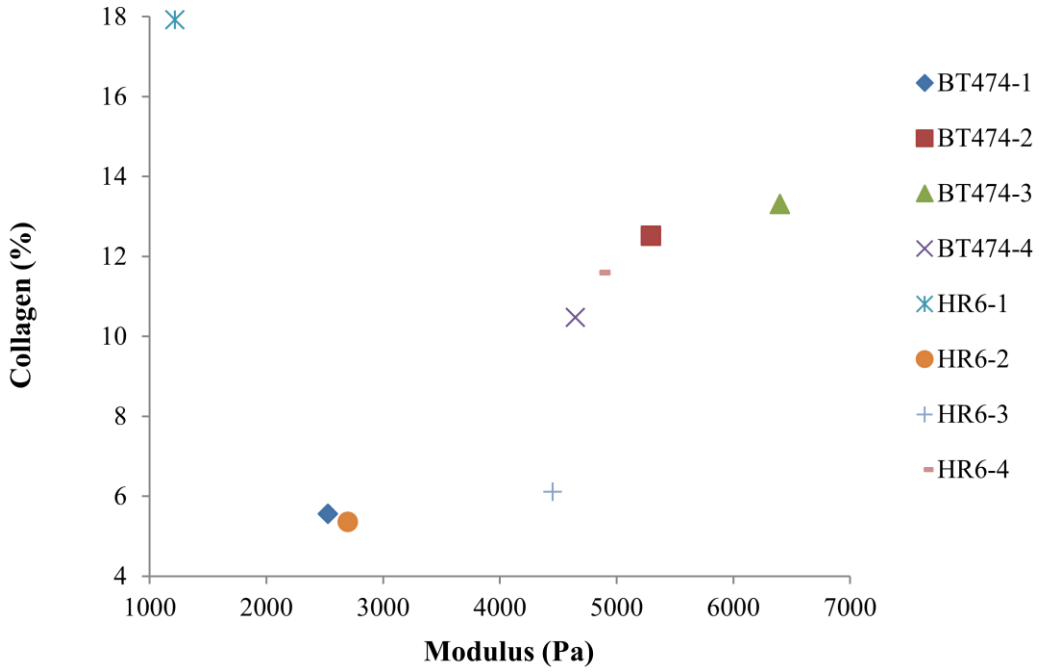

Figure 16. Percent collagen and assay modulus for Herceptin-responsive (BT) and Herceptin-resistant (HR) tumors.

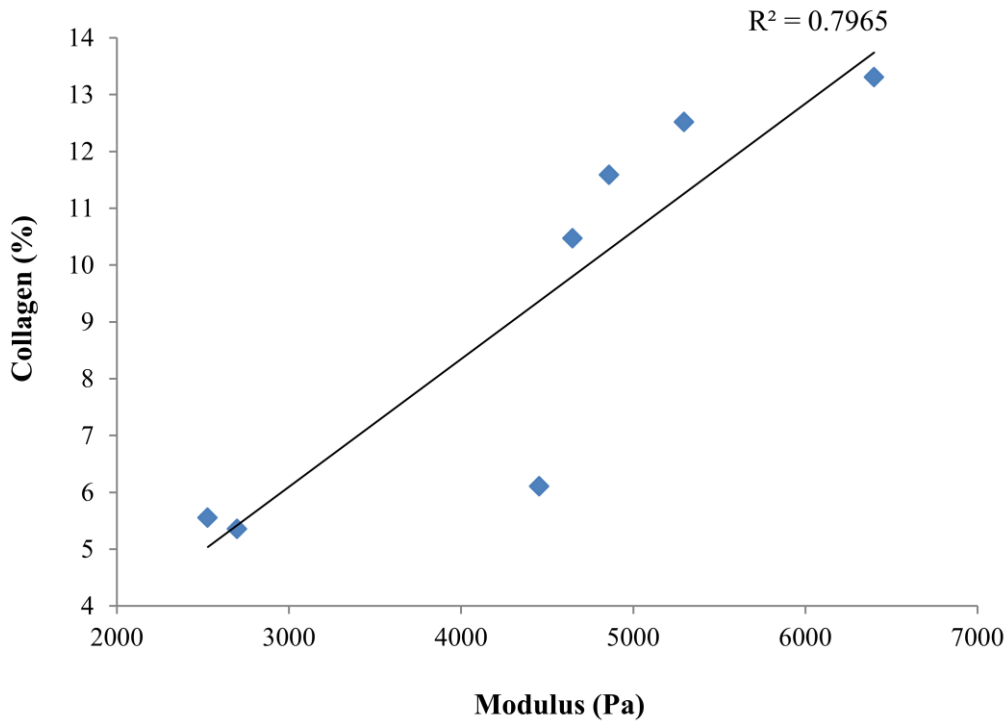

Figure 17. Linear correlation between percent collagen and assay-assigned modulus. Data points represent the seven tumor samples for the combined responsive and resistant lines. The outlier (sample HR6-1) is excluded.

Table 7. Ariol data for percent collagen in each of the three slides from each tumor sample.

	% Collagen			
	Slide 1	**Slide 2**	**Slide 3**	**Average**
BT474-1	5.53	6.67	4.47	5.56
BT474-2	10.31	13.70	13.54	12.52
BT474-3	13.94	12.23	13.77	13.31
BT474-4	8.64	9.72	13.04	10.47
HR6-1	30.82	14.50	8.44	17.92
HR6-2	7.53	4.65	3.91	5.36
HR6-3	8.37	5.51	4.45	6.11
HR6-4	13.96	12.74	8.07	11.59

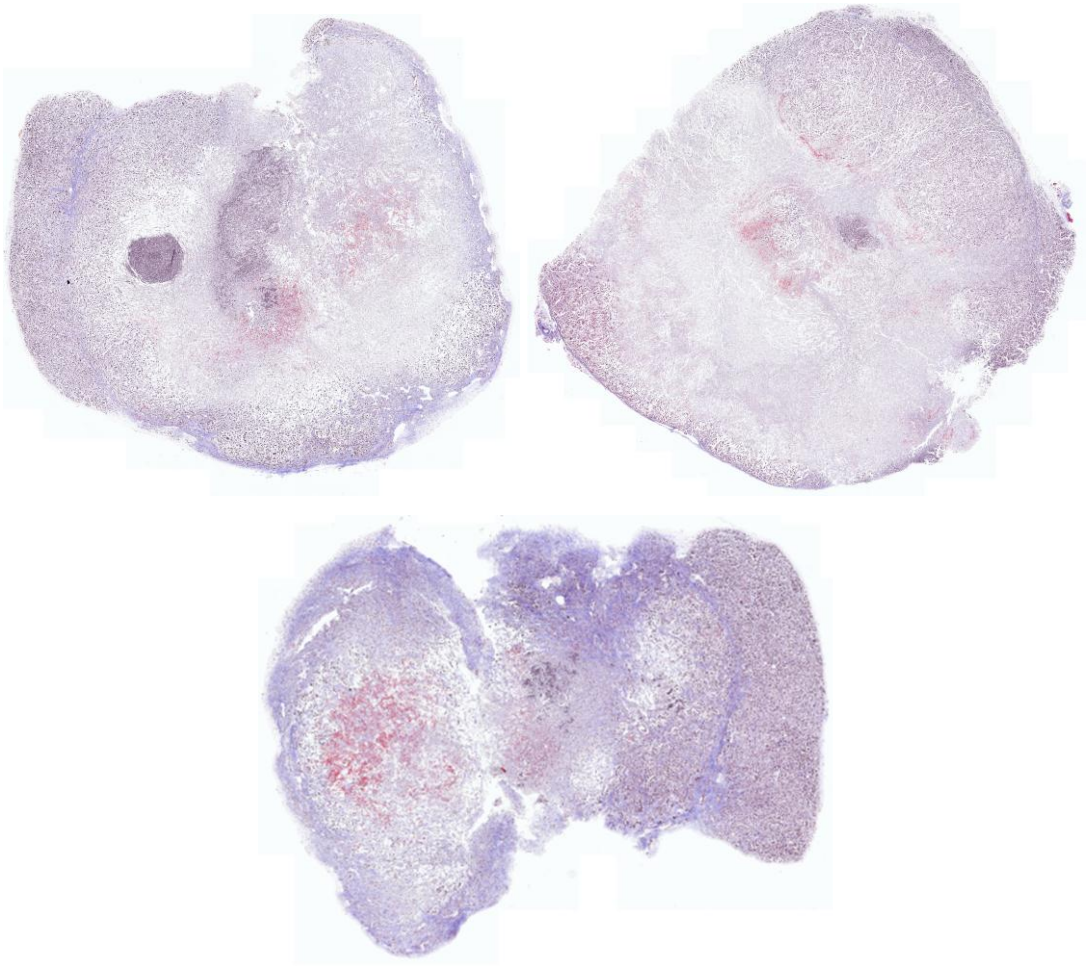

Figure 18. Ariol images of histology slices from tumor sample HR6-1. The actual image set obtained by the Ariol system is significantly higher resolution than the images presented here; the image data had to be down-sampled to be contained in this document.

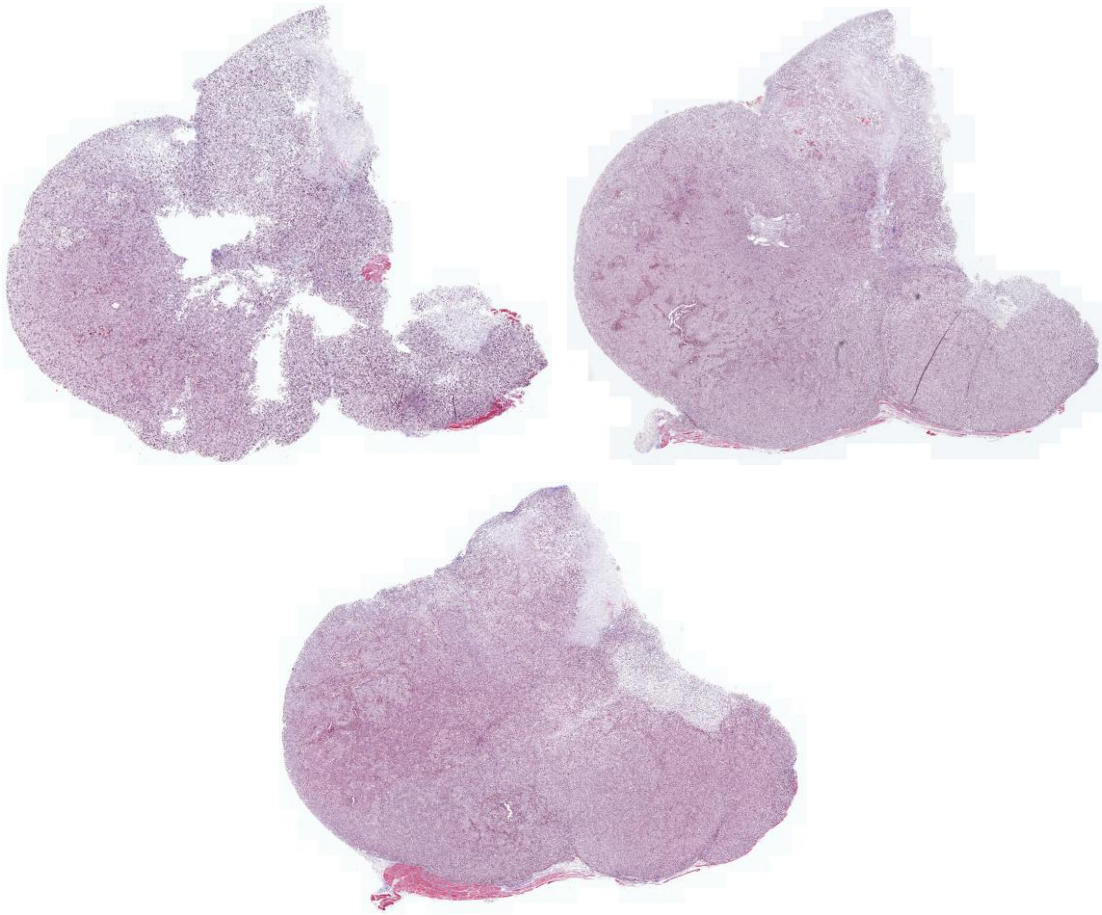

Figure 19. Ariol images of histology slices from tumor sample HR6-3. The actual image set obtained by the Ariol system is significantly higher resolution than the images presented here; the image data had to be down-sampled to be contained in this document.

Discussion

During conception of the responsive versus resistant tumor modulus evaluation study, it was believed that possible cellular and microstructural differences that contributed to the resistant nature of the Herceptin-resistant tumor line would result in perceivable differences in modulus between the tumor lines. However, in the modest population of four tumors of each type presented here, there was not a significant

difference between the responsive and the resistant tumor types. The average modulus for the four responsive samples was slightly higher (4718 Pa) than the average modulus of the resistant tumors (3307 Pa), but a t-test for the difference in means indicated that this was not a significant result. Thus, for this sample set, a difference in modulus between the responsive and resistant tumor types could not be established.

Histological analysis was performed on the tumor tissues in order to probe whether a relationship existed between the collagen content of the tissues and the assay-derived modulus, as was the case in previous work [2]. As indicated in Figure 17, there was an apparent correlation between collagen content and tissue modulus, though the correlation indicated in this work is not as strong as the correlation previously established in the PyV-mT tissue case. One reason for this may be the difference in collagen quantification methods. In the previous work, collagen content was assessed biochemically by hydroxyproline content. In the work presented here, the collagen quantification was performed by means of trichrome staining and image analysis techniques. The image analysis method of collagen quantification is less specific than the hydroxyproline content analysis, as it is susceptible to errant staining and pixel misclassification. Even though the correlation is not as strong as previously experienced, the data still establishes a collagen-modulus correlation in a distinct tissue type and serves as another observation of the link between a microstructural component of the tissue and the clinically relevant macroscopic measurement.

In considering the collagen content to modulus data, there are two data points that elicit specific discussion. As previously stated, sample HR6-1 was verified as an outlier in the data set. The collagen content of this sample was very high relative to the expected

value based on the modulus of the sample. The stained histology slices from this sample are shown in Figure 18. In consideration of these slices, the first slice appears brighter and tonally bluer than the other slices. This may indicate some difference in preparation of this slide, which cannot be verified since the staining was performed by an outside source. Another point of interest is the significant difference in shape of the first slice from the other two slices. Though the intent was to capture a representative slice from the core and each of the ends of the tissue volume, the difference in shape may indicate that the slice was obtained from a section too far toward the end of the tissue volume, which could skew the collagen content. Another issue arose in the second slice of sample HR6-1, wherein a dense blue section is present. This area likely biased the pixel count in the slice, artificially inflating the value. The second sample requiring consideration, sample HR6-3, dissents slightly from the general trend in Figure 17; in this case, the collagen content was lower than the modulus value would imply. The histology slices from this sample (Figure 19) do not immediately point to any obvious reason for the difference. However, it does appear that the cell density of the tissue from sample HR6-3 is high relative to the other samples, which could have an effect on the interstitial collagen. Additionally, it was noted when collecting the tissue that HR6-3 appeared to have a necrotic core. If during sectioning the core was not evenly divided between histological sample and assay sample, the differences in sample composition would skew the data. This could attribute to the observed inconsistency of the HR6-3 data point on the collagen-modulus curve (Figure 17). An interesting observation is that both of these contradictory data points are from the Herceptin-resistant line. Considering the extensive processing to generate the resistant line, wherein the cells survive increased unfavorable

conditions relative to the responsive cells, it is not surprising that aberrant behavior would be present.

Conclusions

The intent of this work was to investigate tumor modulus as a predictor of responsiveness to treatment. In the sample set presented here and using the current protocol, a relationship between the two parameters could not be established. However, it is possible that a more complicated interpretation of responsiveness exists which could not be elicited in this particular investigation. Particularly, a more detailed examination of the heterogeneity of the tissue may prove insightful regarding the modulus as a prognostic indicator. It is possible that the responsiveness of the tumor is indicated by heterogeneity in the tissue which cannot be visualized with CT and which is not assessed via the current assignment of a single modulus to the tumor tissue. In the current state, the MGT assay assigns a single modulus to the entire tumor volume. Additionally, the CT scan does not provide contrast between soft tissues and thus does not allow for identification of the internal structure of the tumor, further limiting the evaluation to only one average modulus assessment. Assessment of tissue heterogeneity may provide further insight into the potential of modulus evaluation as a correlative to disease state.

While this investigation could not determine an observable inherent difference in modulus between Herceptin-responsive and Herceptin-resistant tumors pre-treatment, this does not exclude modulus evaluation as a potential biomarker for responsiveness. All of the tumors contained in this study were grown, resected, and tested, without receiving any treatment via Herceptin. Thus, both sets of tumors (responsive and resistant) were

overexpressing HER2 and experiencing the downstream effects of this signaling in a similar manner. This similarity in condition is reflected in the result that the two groups were not differentiable in modulus value as assessed by the MGT assay. The difference between the two tumor sets lies in their response to Herceptin treatment, wherein the responsive set loses the signaling associated with HER2, while the responsive set eludes the treatment and continues downstream signaling. The signaling associated with HER2+ tumors has effects in cell division, migration, adhesion, differentiation, and apoptosis, and treatment with Herceptin results in cell cycle arrest and subsequent cell death. It is therefore reasonable to conceive that, after (preliminary) treatment, differences between the cellular states of the tumors would alter the tension within the tumor and, subsequently, the stiffness of the stroma. Thus it is possible that, although pre-treatment differences were not detectable, early changes in the tumor due to the effect of Herceptin treatment may be identifiable via modulus evaluation before they are noticeable through the clinical manifestation of treatment response, which is a measurable change in the physical tumor size.

CHAPTER VI

OTHER STUDIES

Introduction

It has been well established in research that understanding the mechanical properties of soft tissue is a challenging endeavor. The inherent irregularity of shape of tissue samples and the relative difficulty in creating a normalized shape is one main source of difficulty in evaluating soft tissue properties. However, in many cases, disease development and progression have been shown to result in changes in the stiffness of the tissue and thus methods of soft tissue modulus evaluation are highly desired [7-21]. In previous work, the MGT assay was developed and utilized [102, 119]. The system was conceived as a union of mechanical testing and modeling with a gel submersion system to allow for uniformity and controllability of the testing shape. To test the feasibility of the system, the MGT assay was initially validated relative to the traditionally accepted method of direct indentation testing [102]. This was accomplished using fibrotic murine liver tissue, and the results demonstrated a correlation between the MGT assay modulus and the modulus calculated from indentation testing. However, the magnitude of the modulus differed between the two techniques, which was attributed to the nature of the testing protocols; i.e. indentation testing manipulates only a small portion of the surface of the tissue, while the MGT assay technique is a whole-volume interrogation of the tissue modulus. After confirming the aptitude of the assay, the technique was utilized to evaluate the modulus of murine mammary tumor tissue relative to the collagen content of

the tissue [119]. This work provided an initial examination of the microstructural contribution of the tissue to the bulk Young's modulus, and the results demonstrated a positive correlation between collagen content and the assay derived modulus.

While the aforementioned work was successful in demonstrating the ability of the MGT assay, a thorough sensitivity study of the MGT Assay had yet to be performed, and hence its capabilities and limitations remained unknown. Previous work has shown a dependency on the tissue volume to gel volume relative ratio for the success of the assay in evaluating the tissue modulus [119]. This observation solidifies the idea that the assay inherently possesses limitations and boundaries attributed to the various components of the assay. These limitations will need to be identified and accounted for in order to successfully utilize the MGT assay as a reliable modulus evaluation technique. Thus, the purpose of the work presented herein was to characterize the MGT assay in order to ensure and validate its rigorousness as a repeatable modulus evaluation technique.

The gel generation process is of main concern to the work presented here regarding assay characterization. The protocol described in Chapter II was utilized for all gel generation in this work. Specifically, the buffer solution was generated using 19.1 mL of deionized water, 0.65 mL of 1 molar Tris buffer, and 0.25 mL of 10% ammonium persulfate (BioRad Laboratories, Hercules, CA). Then, a volume of the buffer solution was combined with 30% Acrylamide/Bis-acrylamide (BioRad Laboratories, Hercules, CA), in a proportion which was dependent on the desired final polyacrylamide percentage, to yield a total combined volume of 16 mL of the bulk solution. The individual gels were created by transferring 1.4 mL of the bulk solution to an individual well in a 24 well cell culture plate (Corning Inc., Corning, NY). The wells were

cylindrical in shape and had a diameter of 16 mm, thus creating a standardized shape among samples. After solution allocation, 0.16 mL of the contrast agent Optiray (Mallinckrodt Inc., Hazelwood, MO) was added to the wells, unless otherwise stated. At this point, if a heterogeneous gel was being created, the object to be embedded was suspended by means of forceps in the gel solution. Finally, 0.02 mL of TEMED, the initiating agent, was added and the sample was pipette-mixed for approximately one minute as the solution solidified in order to promote a uniform mixture.

Gel Selection

Methods

In the heterogeneous gel-tissue sample, the gel modulus is used as the elastic reference for the embedded tissue property assessment. Thus, the initial gel selection was of considerable importance. In considering the role of the gel in the MGT assay, two key characteristics of the gel were required: (1) the gel modulus had to be variable and relatively simple to control, and (2) gel properties needed to be relatively static over time, i.e. shifts due to small protocol variations in testing time and ambient temperature needed to be minimized, and viscoelastic effects need to subside quickly. Two materials are commonly mentioned in literature as being utilized for phantom generation and submersion techniques: agarose (Research Products International Corp, Mt. Prospect, IL) and polyacrylamide (BioRad Laboratories, Hercules, CA). In relation to the aforementioned requirements, both agarose and polyacrylamide materials have the advantage that the stiffness of the gel can be modified by altering the percentage (by weight) of agarose or polyacrylamide in the gel, respectively. However, the

controllability of the resultant modulus was unknown. Additionally, the dynamic behavior of the gel properties relative to the time scale of the MGT evaluation required investigation. Hence, an initial assessment of the agarose and polyacrylamide gels was performed in order to facilitate gel selection. In order to assess the achievable modulus range and controllability for each gel, an array of gels of differing compositions was created. For the agarose samples, eight gels were generated, with agarose percentages of 0.3, 0.4, 0.5, 0.6, 0.75, 1.0 and 1.25. In the polyacrylamide case, six gel samples were tested, ranging from 3 to 6 percent polyacrylamide in 0.5 percent increments. All gels were created in Petri dishes that measured 10 cm in diameter and 1.1 cm deep. The testing protocol consisted of the application of a 5 percent precompression. Step compressions were applied in 0.5 percent increments for a total of 5 percent additional strain, with a 60 second dwell after each compression. The force values were collected at the end of each dwell period, and were utilized with the corresponding compression values to generate stress and strain data for the gels. A linear regression was performed on the stress-strain data to approximate the modulus for each gel sample. The same material testing protocol was implemented to assess the thermal-dependence of the gel moduli. Two samples were manufactured for each gel type. The gels were tested immediately after generation, and then at each subsequent hour for four hours. The modulus values for the samples were calculated as previously described.

Results

The results from the gel selection testing indicated that both were readily controllable in terms of the resultant modulus by regulating the percent of the constitutive

components. In regards to thermal sensitivity, the results showed that agarose was very sensitive to thermal effects; particularly, the modulus of the agarose samples decreased by 15.5% over the first hour and 44.8% over the full four hours of the test. Polyacrylamide, on the other hand, did not demonstrate the same extremity of thermal effects as agarose. The polyacrylamide results showed a decrease in modulus of only 4.8% in the first hour, and a total of 12.6% over the four hours of experimentation.

Discussion

The initial gel testing for the comparison between agarose and polyacrylamide gel proved deterministic in the gel selection. Both gels were able to be controlled for modulus based on the percentage of agarose or polyacrylamide, and could be adapted to generate the desired modulus, so either gel was appropriate in this regard. However, the thermal testing results proved the most decisive. In considering the experimental procedures of the MGT assay, the gel would be exposed to room temperature for prolonged periods of time during imaging and material testing, and thus thermal stability was necessary. Agarose is a hydrogel, and the gel is solidified by cooling the components on ice. As it is exposed to room temperature for prolonged periods of time, the gel liquefies and changes properties, and this was reflected in the material testing results. Polyacrylamide solidifies by way of a polymerization reaction, which limits the thermal dependence. The polyacrylamide gel was thus chosen as the gel matrix based on its insensitivity to thermal fluctuations, rapid congealing properties, and stability. Appendix A contains specifics regarding the chemistry and structure of polyacrylamide.

Gel Generation Reliability Test

Methods

In considering the reliability of the MGT assay, a main component for investigation is the background modulus of the heterogeneous gel. The background modulus utilized for the heterogeneous optimization is defined using a homogeneous reference gel which is generated at the same time and in the same manner as the heterogeneous tissue-containing gels. The homogeneous gel is tested and imaged following the same method described for the assay evaluation, and an optimized modulus value is obtained, which is then assumed to be the modulus of the background gel in the heterogeneous tissue-gel sample. In using the homogeneous gel modulus in the heterogeneous optimization, it is assumed that the gel modulus is consistent from sample to sample, and that the same modulus value can be obtained in a repeatable manner. To validate this assumption, five sets of three homogenous gels were tested. On each occasion, one bulk solution was mixed as previously described, from which each set of homogeneous gels was created. Sets 1 and 2 were created using 4.5 percent polyacrylamide while sets 3 and 4 were generated with 4.8 percent polyacrylamide. Set 5 was also produced with 4.8 percent polyacrylamide, but the CT contrast agent (Optiray) was withheld from the gels. Table 8 gives the required volumes of both the buffer solution and the polyacrylamide for each percent polyacrylamide used for this experiment.

Table 8. Components of the bulk solution for the gel generation reliability testing.

	%PA of Solution	
	4.5	**4.8**
Buffer Solution (mL)	13.6	13.44
30% Acrylamide/Bis-acrylamide (mL)	2.4	2.56

Results

The results for the gel generation reliability tests are shown in Table 9 below. The optimized modulus values for each of the three samples in the five sets are tabulated. The table also includes the average and the standard deviation of each set of samples. The last row of the table gives the standard deviation as a percentage of the average modulus for each set. The average of this value over the five sets is 1%. The largest standard deviation as a percent of the average occurs in set 1, at 1.40%.

Table 9. Gel generation reliability test modulus results.

	Modulus Values (Pa)				
	Set 1	**Set 2**	**Set 3**	**Set 4**	**Set5**
	911	993	1303	1282	1810
	936	1001	1294	1279	1778
	918	1003	1277	1258	1801
Average (Pa)	922	999	1291	1273	1796
Std Deviation (Pa)	12.9	5.3	12.3	13.1	16.5
Std Dev % of Avg	1.40%	0.53%	0.95%	1.03%	0.92%

Discussion

In the gel generation reliability testing, the difference in modulus value between individual gels generated from the same bulk solution was minimal when considering the number in isolation. As previously stated, the average standard deviation as a percent of the mean modulus value over the five sets was 1%. The high repeatability was anticipated since the majority of the components that constitute the gel mixture, and thus the majority of the sources for variance among gel modulus values, are placed into the bulk solution, instituting uniformity among the gels. The contrast agent and the initiator (TEMED) are added separately to the gels after they have been proportioned to the individual well plates, and thus are both possible sources of the constituent differences that result in different gel modulus values. The contrast agent is added by means of syringe, and though every effort is made to keep the amount uniform, very slight differences in volume are not only possible but likely. Since the contrast agent adds to the volume of the gel and thus in essence dilutes the polyacrylamide percentage of the volume, differences in the contrast agent volume will create slight differences in the modulus values of the individual gels. In considering the reference gel sets, the first four sets contained a contrast agent, but set 5 did not. Even without the contrast agent, the modulus values of set 5 still vary among the three samples, resulting in a standard deviation as a percent of the average modulus of 0.92%. Since the potential error due to the addition of the contrast agent has been eliminated in this case, other sources must be responsible for the differences. The addition of the initiator, TEMED, though added to the individual gel is not a likely source of error. Previous experiments have shown that the amount of initiator affects the final modulus of the gel, so if the amount added to each

gel were not constant, then it is possible that the TEMED would have an effect. However, the TEMED measurement is highly controlled by means of a micropipette and thus should be invariant. Other possible sources of the disparity in modulus values outside of the gel generation process include the material testing and the segmentation of the CT images. These aspects of the assay are highly controlled and automated in all possible cases in order to minimize induced error. However, the material testing and segmentation are still user-controlled and hence have the potential to generate error.

Effect of Gel Generation Reliability on Modulus Reconstruction

Methods

After evaluating the repeatability of the gel generation, the progression of tests led to an evaluation of the extent of the effect of the background modulus on the optimized embedded tissue modulus. Since the model calculated surface stress (and hence force) is dependent on both the background modulus and the embedded modulus, a change in the background modulus will consequently have an effect on the optimized embedded modulus. To investigate this effect, nine heterogeneous meshes from a previous study were utilized. These meshes were from the second evaluation of the MGT assay wherein the modulus values of murine mammary tumors derived from mouse mammary tumor virus polyomavirus middle T (PyV-mT) transgenic lines were compared to the collagen content of the tissue. In evaluating the tissues via the MGT assay, heterogeneous meshes were created for each sample with a corresponding assigned background modulus and an optimized tissue modulus. The background modulus and the optimized tissue modulus values from the previous study were utilized as the baseline for the background modulus

dependency interrogation presented here. In the previous study, the nine tumor samples were evaluated in three different groups at various times, so there were three groups of baseline background modulus values: 4164, 2346, and 989. The baseline background modulus values and baseline tissue modulus values are shown in Table 10. The respective background modulus was altered both above and below the baseline value by a percentage consistent with the results from the gel generation reliability test, or 1%. The optimization process was initiated with the altered background modulus and the resultant tissue modulus was recorded and compared to the value obtained in the baseline case.

Table 10. Tumor data for effect of gel generation reliability on modulus reconstruction analysis.

Tumor Number	Background Modulus (Pa)	Tissue Modulus (Pa)
1	4164	746
2	4164	974
3	4164	3841
4	2346	2427
5	2346	1049
6	989	2728
7	989	1840
8	989	886
9	989	650

Results

The results are shown in Tables 11 and 12 and Figures 20 and 21 below. In Table 11, the percent change is given for each of the 9 tumor samples. The percent change is calculated as:

$$\% \, Change = \frac{(E_{opt}^{below} - E_{baseline}) + (E_{opt}^{above} - E_{baseline})}{2 * E_{baseline}} \qquad (22)$$

where E_{opt}^{below} is the optimized tissue modulus value when the background modulus is decreased by 1%, E_{opt}^{above} is the optimized tissue modulus value when the background modulus is increased by 1%, and $E_{baseline}$is the baseline tissue modulus. For a 1% alteration in the background modulus, the average change over all nine samples was 0.144, or approximately 14 percent. The maximum value over the samples was 0.300 and the minimum value was 0.050. Other parameters of interest for the nine samples, including baseline background modulus, baseline tissue modulus, tissue volume, gel volume, and tissue-gel volume ratio are also tabulated (Table 12). Figures 20 and 21 depict the data for the 1% range in graphical form. Figure 20 shows the normalized optimized tissue modulus as a function of the normalized background modulus (or percent change in background modulus) for each incremental background modulus evaluation. Figure 21 shows the normalized average tissue modulus change as a function of the tissue to gel volume ratio. The nine samples are grouped by baseline background modulus, as indicated by the marker style.

Table 11. Effect of gel generation on modulus reconstruction results – 1% range.

Tumor Number	Percent Change
1	11.7%
2	11.0%
3	5.0%
4	21.9%
5	30.0%
6	13.5%
7	8.6%
8	16.8%
9	10.8%
Average	14.4%

Table 12. Tumor data for effect of gel generation on modulus reconstruction analysis.

Tumor Number	**Background Modulus (Pa)**	**Tissue Modulus (Pa)**	**Tissue Volume (mm^3)**	**Gel Volume (mm^3)**	**Tissue-Gel Volume Ratio**
1	4164	746	303.4	2000	0.152
2	4164	974	284.3	2000	0.142
3	4164	3841	329.5	2000	0.165
4	2346	2427	63.3	1500	0.042
5	2346	1049	65.9	1500	0.044
6	989	2728	66.9	1400	0.048
7	989	1840	134.6	1400	0.096
8	989	886	88.6	1400	0.063
9	989	650	158.7	1400	0.113

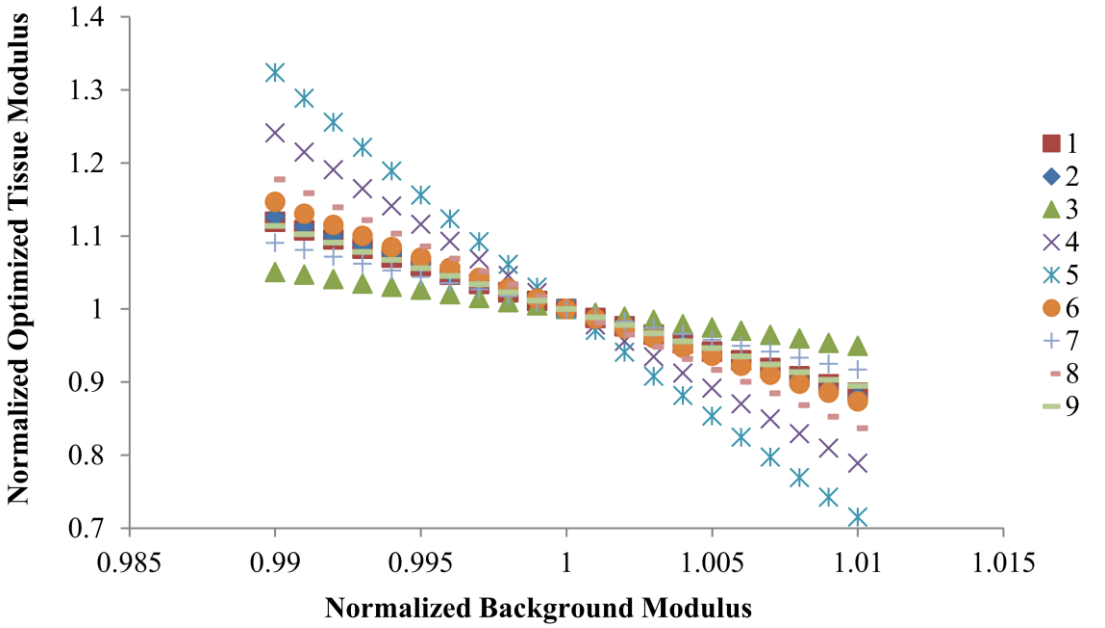

Figure 20. Normalized tissue modulus as a function of percent background modulus noise for each of the nine PyV-mT tumor samples in the effect of gel generation on modulus reconstruction analysis.

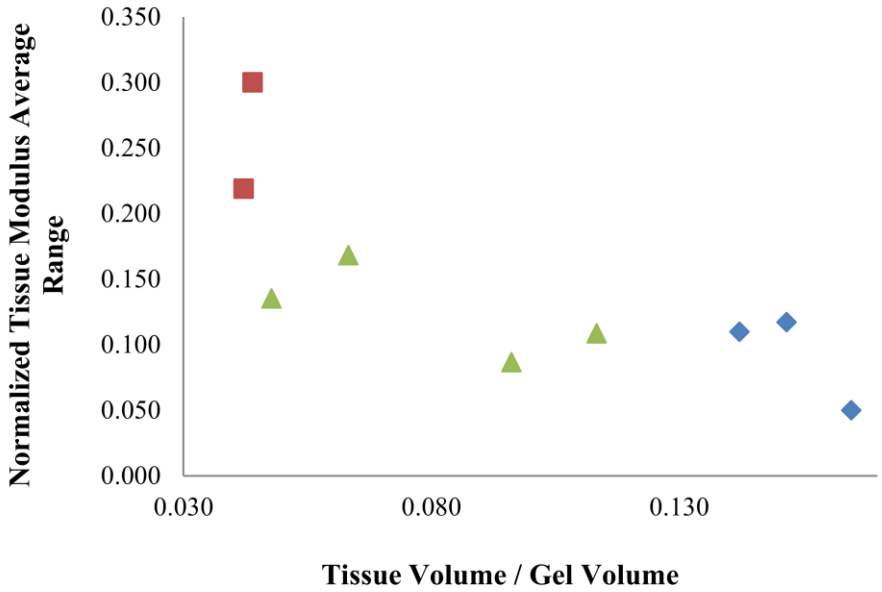

Figure 21. Normalized modulus average range as a function of tissue to gel volume ratio in the effect of gel generation on modulus reconstruction analysis. The different markers indicate the three original background modulus values. The red square indicates an original value of 2346 Pa, the green triangle was originally 989 Pa, and the blue diamond was 4164 Pa.

Discussion

From the previous results, the average standard deviation of the reference sets as a percent of the mean modulus was 1%. This is thus the largest difference between an optimized reference gel modulus utilized as the assumed background modulus and the actual heterogeneous background modulus that would be expected. From this assumption, a ±1% range of the altered background modulus was evaluated. Though the percent change in the background modulus was uniform, the effect on the optimized tissue modulus varied. Figure 20 shows the normalized tissue modulus (optimized modulus divided by baseline modulus) as a function of normalized background modulus (altered modulus divided by baseline modulus). From this figure, it is apparent that the extent of the effect of the background modulus is not a simple relationship, but rather is a complicated dependency on parameters such as the tissue-volume-to-gel-volume-ratio, the tissue modulus, the ratio between the tissue modulus and background modulus, and the boundary between the tissue and gel. Many options were considered in trying to find a universal relationship between the altered background modulus and the optimized tissue modulus for all of the samples, but the relationship is inherently complicated and relies on a complex combination of the parameters that could not be elicited. Figure 21 shows the average 1% range divided by the baseline tissue modulus as a function of tissue volume to gel volume ratio. This figure implies a slight relationship between these two parameters, with a general increase in the range as the tissue volume to gel volume ratio decreases; however, it is clear that they do not completely describe the relationship. Even without a clear descriptive relationship, the normalized average range is insightful. This value spans from 0.050 to 0.300, with an average value of 0.141. This means that, in the

worst case, a 1% change in the background modulus results in a 30% change in the optimized tissue modulus, and on average it results in a 14% change in the modulus. These results emphasize that the optimized embedded modulus is highly sensitive to the background modulus. Unfortunately, the gel creation process is susceptible to slight differences that cannot be controlled beyond the repeatability demonstrated by the gel generation repeatability testing. An option that had been considered to address this issue was eliminating the homogeneous gel for background modulus assignment and rather performing a dual optimization of both the background modulus and the embedded modulus. This would allow the background modulus to vary for each sample, and thus could account for the slight differences in background modulus. However, implementation of the dual optimization has proven difficult due to the range of modulus combinations that can produce the same error. In the single optimization case, where the background modulus is assigned, a minimum error is associated with one single embedded modulus value. In the dual optimization case, a basin of minimum error values occurs wherein various combinations of modulus values produce the same error. This is due to a lack of information relative to the input parameters (ie force, displacement). Based on the work presented here, it may be beneficial and even necessary to further consider ways to restrict the dual optimization process so that the error due to the assigned background modulus could potentially be eliminated.

Reliability and Repeatability of Modulus Reconstruction

Methods

The assumption in utilizing the MGT assay for embedded tissue modulus evaluation is that the assay can accurately evaluate the modulus of the embedded item. The feasibility of this assumption has been previously checked in a secondary nature by comparing the results of the assay to the traditionally accepted soft tissue evaluation method of indentation testing. However, in order to concisely evaluate the assay, it was opted to directly check the accuracy and repeatability of the embedded modulus evaluation. It has been previously established that a gel-volume-to-tissue-mass ratio dependency exists for the assay, and a limiting ratio was suggested based on the data available from previous work [119]. Due to this realization, a volume-modulus-ratio (VMR) evaluation was produced which consisted of embedding multiple objects with the same modulus value but different volumes. The VMR evaluation was conceived to serve three purposes: (1) test the ability of the assay to repeatedly assign the 'correct' modulus to the embedded component, (2) analyze whether a relationship existed between the ratio of embedded volume to overall gel volume and the evaluated embedded modulus, and (3) investigate the dependency of a successful reconstruction on the ratio between embedded modulus and background modulus. In order to achieve these objectives, it was necessary to ensure uniformity among the embedded pieces. To this avail, a gel-in-gel system was devised wherein polyacrylamide gel phantoms were used to represent the embedded soft tissue sample, and were subsequently embedded in the traditional polyacrylamide background. Each VMR evaluation consisted 11 total gels: a reference gel, a sample of the embedded gel compatible for material testing, and three sets of three heterogeneous

gels, with small, medium, and large embedded pieces. The sample preparation process for this experiment occurred in two parts. First, the gels for embedding were generated; a 5.5% bulk solution was created as previously detailed. In this experiment, barium sulfate was used in place of Optiray to provide both CT and visual contrast. The consistency of the barium sulfate made it difficult to measure volumes small enough to add to the individual gels, so 0.16 mL of barium sulfate was added to the bulk solution to ensure consistency among gel samples. From the bulk solution, three gels were generated: one which was utilized as the sample of the embedded gel, providing a measure of the expected reconstructed embedded modulus, and the other two which were cut into pieces to create the embedded samples. Nine embedded segments were utilized, with three each of a large mass, a medium mass, and a small mass. Each large embedded gel weighed approximately 150 mg, the medium embedded gels weighed around 120 mg, and the small embedded gels weighed 90 mg. The second portion of the sample preparation process consisted of generating the background gel and embedding the gel segments. As in all gel generation cases, the bulk solution was generated with the desired percent polyacrylamide, from which the homogenous gel and nine heterogeneous gels were created. The nine heterogeneous gels, the reference gel, and the sample of the embedded gel were evaluated using the MGT assay protocol, and the optimized modulus from the sample of the embedded gel was used to assess the fidelity of the embedded modulus evaluations. Three distinct sets of the VMR analysis were evaluated; the difference between the three sets existed in the percent polyacrylamide, and hence the modulus, of the background gels. The percent polyacrylamide of the embedded gel remained constant at 5.5% in all cases, while the background gel percent polyacrylamide was varied

between 4%, 4.5%, and 5% PA. The component volumes for the polyacrylamide percentages used in this portion of the experimentation are given in Table 13. The combinations of background %PA and embedded %PA for each set are given in Table 14, and examples of the homogeneous embedded and background gels as well as the heterogeneous gel are shown in Figure 22.

Table 13. Components of the bulk solution for the VMR analysis.

	% PA of Solution			
	4	**4.5**	**5**	**5.5**
Buffer Solution (mL)	13.87	13.6	13.33	13.07
30% Acrylamide/Bis-acrylamide (mL)	2.13	2.4	2.67	2.93

Table 14. Percent polyacrylamide for VMR analysis.

	Set Number		
	1	**2**	**3**
Background % PA	4.5	5	4
Embedded % PA	5.5	5.5	5.5

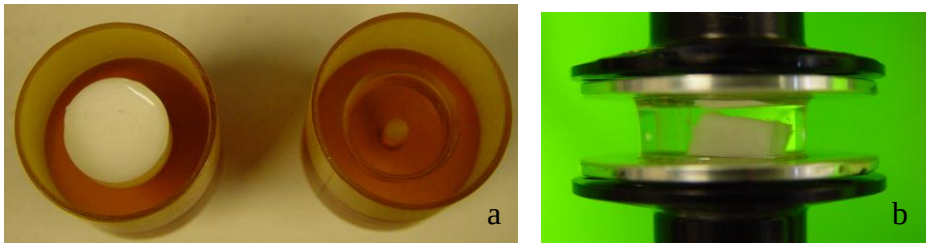

Figure 22. (a) Sample of embedded modulus gel with barium sulfate (left) and background reference gel (right). (b) Heterogeneous gel with embedded polyacrylamide sample from the VMR analysis.

Results

The results for the VMR analysis are presented in Table 15. Table 15 consists of the homogeneous gel modulus value for each set as well as the modulus of the sample of the embedded gel for each set. Additionally, it gives the optimized modulus values for each of the nine embedded gel segments in each of the three sets. Figures 23 and 24 below show the force values from the material testing protocol as a function of the displacement for each sample in sets 1 and 2 of the VMR analysis. The dashed curves indicate the unsuccessful modulus reconstructions from each set, while the other samples in the set are represented by the solid lines. Tables 16 and 17 provide the slope of the force-displacement curves for each sample in VMR set 1 and 2, respectively. The highlighted slopes correspond to the dashed force-displacement curves from Figures 23 and 24.

Table 15. Results for the reliability and repeatability of modulus reconstruction (VMR) analysis.

	Modulus (Pa)		
	Set 1	**Set 2**	**Set 3**
Reference	1327	2890	941
Sample of Embedded Gel	4453	5137	4478
Sample 1	4620	5821	94
Sample 2	2946	2293	322
Sample 3	4503	5217	562
Sample 4	4316	1324	138
Sample 5	4720	2686	1583
Sample 6	4063	5137	644
Sample 7	1667	5314	559
Sample 8	4340	4779	444
Sample 9	4486	5308	403

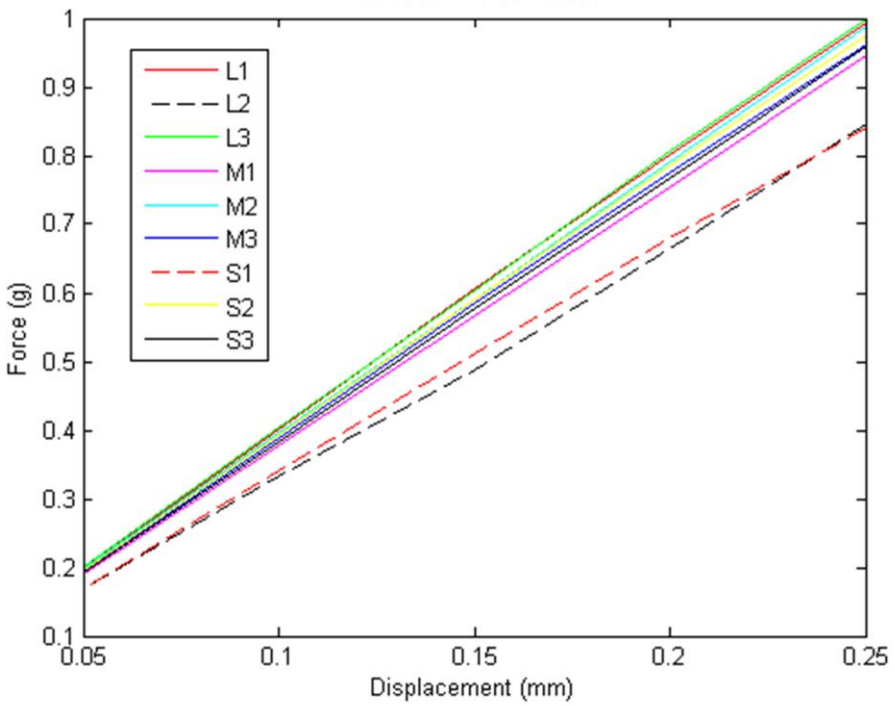

Figure 23. Force values as a function of displacement for VMR set #1.

Table 16. Slope of force versus displacement curve for VMR set #1.

Sample Number	Slope (force vs disp)	Absolute Difference from Average
1	3.98	1.98%
2	3.37	13.70%
3	4.00	2.53%
4	3.78	3.09%
5	3.96	1.36%
6	3.85	1.21%
7	3.37	13.55%
8	3.91	0.11%
9	3.84	1.67%
Average	3.90	

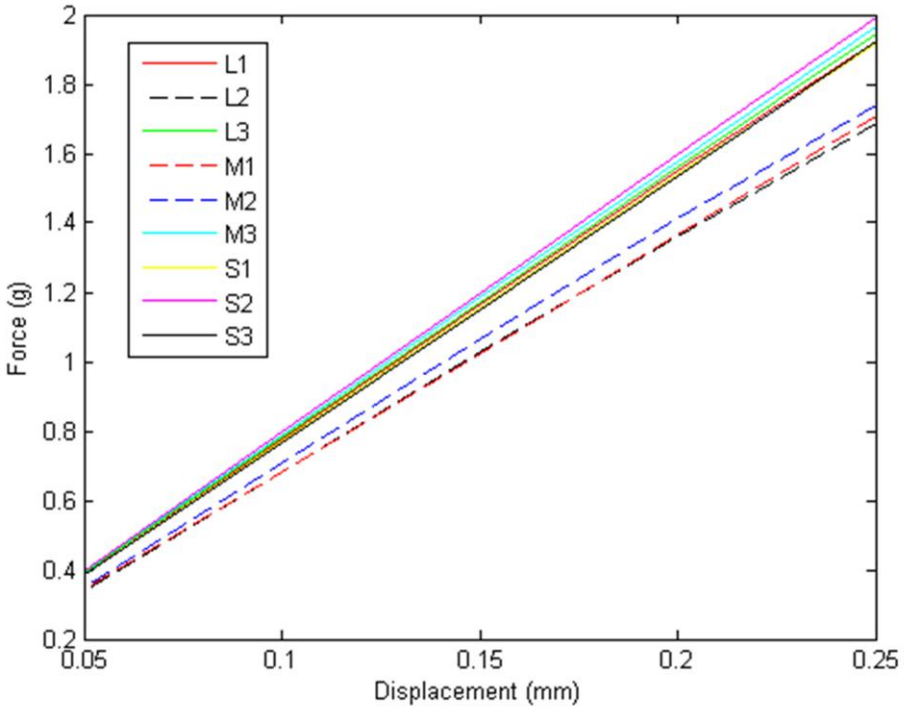

Figure 24. Force values as a function of displacement for VMR set #2.

Table 17. Slope of force versus displacement curve for VMR set #2.

Sample Number	Slope (force vs disp)	Absolute Difference from Average
1	7.71	0.90%
2	6.76	13.14%
3	7.78	0.01%
4	6.83	12.28%
5	6.98	10.32%
6	7.87	1.08%
7	7.68	1.39%
8	7.97	2.33%
9	7.70	1.12%
Average	7.78	

Discussion

The results of the reliability and repeatability of modulus reconstruction proved very interesting. Based on the previous realization of the importance of the gel-volume-to-tissue-volume ratio, it was expected that there would be a trend concerning embedded volume. Specifically, it was hypothesized that embedded volume would affect the accuracy of the reconstructed modulus of the embedded specimen; for the samples that succeeded in reconstructing, this trend was not observed. The average difference between the optimized embedded modulus and the sample embedded gel did not depend on the volume of the embedded segment. In the first set, the average absolute difference was 109 Pa for the large samples, 264 for the medium samples, and 73 for the small samples (excluding those that did not test appropriately, i.e. 'large 2' and 'small 1'). In the second set, the average difference values were 67 for the large samples and 235 for the small samples (excluding 'large 2'). Of the three medium samples in the second set, only 1 tested appropriately, and that sample had an error of zero. These values comprise a very limited sampling due to the failure of the modulus optimization in some of the cases. However, as an initial estimation, it is implied that there is no correlation between modulus optimization error and embedded volume. This statement is tempered, though, by the fact that the sensitivity of the transducer must be sufficient to quantify the force differences achieved based on gel-volume-to-tissue-mass-ratio.

The notable result from the VMR evaluation is the behavior of 'large 2' and 'small 1' from set 1, 'large 2', 'medium 1', and 'medium 2' from set 2, and the entirety of set 3. These samples produced very large embedded modulus evaluation errors, in some cases to the extent where the evaluation does not sense the embedded volume. After

viewing these results, it was hypothesized that the reason for this behavior is that the gel-in-gel configuration lacked the bonding at the interface that the tissue-in-gel system possesses. In other words, it appears that as the heterogeneous gel-in-gel sample is compressed, the background gel is decoupled from the embedded gel due to a weak interface bond and hence the assay cannot accurately evaluate the embedded gel. Though this does not happen in all cases, the faltered evaluations indicate that the interface is unreliable. Figures 23 and 24 show the force values as a function of the step displacements for sets 1 and 2, respectively. In these figures, the samples which did not test appropriately are indicated by the dashed line, whereas those which had successful reconstructions are indicated by the solid lines. From this depiction, it is obvious that the force values are lower for all of the samples which failed to reconstruct appropriately. This observation is further confirmed by Tables 16 and 17, which present the slopes of the force-displacement curves. Here again the unsuccessful samples are distinct in that the slopes are noticeably lower than the successful samples. These would seem to support the hypothesis that the background gel and embedded gel decoupled. Without a bond between the two surfaces, as the top surface of the background gel is compressed, the internal motion of the gel will not be coupled to the embedded gel, and instead will deform around the embedded gel. Since the background gel modulus is lower than the embedded gel modulus in all cases, a lack of strain transfer to the embedded gel would result in a lower force experienced by the material tester as compared to the coupled case. In considering the third set, all nine of the samples evaluated to very low (near zero) embedded modulus values. This is most likely due to the high contrast between the embedded and background modulus values, which exasperated the inadequate bond and

caused all of the samples to fail. Due to the modulus evaluation failure in some of the sample cases, the VMR analysis did not prove successful in its intended three-fold purpose. However, it did manage to highlight the previously understated importance of the bond between the embedded tissue and the polyacrylamide gel.

The gel-in-gel approach to the VMR analysis proved to be ineffective due to the presumed interface issues; however, the bonding in the tissue-in-gel case had not previously presented an issue. The reason for this was hypothesized to be the surface texture and porosity of the tissue that is not mimicked in the embedded gel case. Previous experiments with murine liver and murine breast tumor tissue have displayed effective bonding between the gel and the tissue, with no outward signs of inadequacy as in the gel-in-gel case. If interface issues had occurred in these cases, then the optimized tissue modulus would be lower than the actual tissue modulus, which would not be identifiable based on modulus value alone. It is not likely that this occurred in either of the soft tissue cases, though, due to the experimental protocol. In the murine liver case, indentation testing was performed to validate the assay-derived modulus. In the non-diseased case, the two measures were almost identical. In the diseased case, the magnitude of the measures differed, but a correlation existed between the two. A similar correlation was found in the mammary tumor work, wherein the modulus of the tissue correlated tightly to tissue collagen content. If the gel-tissue interface were decoupling in either of these evaluations, random noise would have effectively been added to the optimized tissue values and such strong correlations to other measures would not have been observed.

Soft Tissue Boundary Effect

Methods

The gel-in-gel approach to the assay evaluation process was conceptualized as a baseline evaluation system due to the controllable nature of the embedded gel size and modulus. Additionally, embedded gels produced from the same bulk gel provided a uniform modulus across samples, allowing for a separate calculation of the expected embedded modulus by means of the sample of the embedded gel, and providing a standard for calculation of the assay modulus optimization error. However, the gel analysis did not prove entirely successful. It was hypothesized that the problem with the gel-in-gel analysis could be attributed to the gel-gel interface, which was potentially not indicative of the bond experienced in the soft tissue case. Based on this hypothesis, the VMR analysis was extended in a more representative manner using soft tissue, the result of which was an experiment involving chicken liver samples. The experimental protocol was similar to the gel-in-gel VMR analysis previously described. A single lobe of a chicken liver purchased from the grocery store was sectioned into 10 samples, nine of which were used for embedding for assay analysis, and one of which was underwent indentation testing for modulus confirmation. The nine samples for embedding were divided into three groups of three samples – named large, medium, and small – based on the sample mass. The large tissue samples weighed an average of 245 mg, the medium samples registered an average of 197 mg, and the small samples weighed an average of 144 mg. A 4.8% polyacrylamide bulk solution was produced and utilized for the background gel, from which the homogeneous gel and the heterogeneous chicken liver gels were created. After solidification, the gels were tested, imaged, and evaluated as

previously described. For corroboration of the assay-evaluated modulus values, indentation testing was performed on the final liver sample. The indentation protocol was the same as that described in the murine liver paper [1]. Briefly, a spherical indenter tip with a radius of 1.5 mm was used to indent the tissue a distance of 0.4 mm. The indentation was held for a 60 second dwell and then released for 60 seconds; this was repeated three times for each test. The indentation test was repeated twice – once before the gels were tested and the second time after half of the gel testing had been performed. Analysis of the data for modulus extraction was performed in the manner previously described, using the correlation model suggested by Stevanocić et al. [60].

Results

The results for the soft tissue boundary effect analysis are given in Table 18. Presented here are the optimized modulus values for each of the nine embedded samples as well as the resulting modulus from the indentation testing of the liver segment. The average modulus value assessed by the MGT assay was 547 Pa with a standard deviation of 22.7 Pa. Also given in Table 18 are the absolute differences between the optimized modulus and the indentation-based modulus. The maximum difference between the indentation-derived modulus and the assay-assigned modulus occurs in sample ‘M2’ with a magnitude of 44 Pa, which equates to an 8.2% error. The average absolute difference over all nine samples is 17.8 Pa, or 3.31%.

Table 18. Optimized modulus values for chicken liver tests.

	Modulus (Pa)	Absolute Difference from Indentation (Pa)
Indentation	538	
Sample 1	531	7.2
Sample 2	526	12.4
Sample 3	540	2
Sample 4	572	33.5
Sample 5	582	44
Sample 6	543	4.5
Sample 7	528	10.4
Sample 8	529	9
Sample 9	575	37.3

Discussion

To verify the suspected inferiority of the gel-gel system, a soft tissue test utilizing chicken liver was implemented. This test was performed in the same manner as the VMR analysis, except soft tissue (specifically chicken liver) was substituted for the embedded gel. As shown in Table 18, the results for this experiment indicate a successful evaluation of the embedded liver tissue. All nine samples optimized successfully with an average modulus of 547 Pa and a standard deviation of 22.6 Pa. Additionally, the assay derived modulus values for the nine embedded samples mirrored the separately evaluated indentation modulus, with a maximum error of 44 Pa, or 8.18%, and an average error of 17.8 Pa, or 3.31%. This strong correspondence between the indentation testing and the assay assessment parallels the initial experiments with murine liver which demonstrated a

very high correlation between the assay modulus and the indentation modulus in the non-diseased case. In the evaluation performed here, some spread of the modulus was expected due to the nature of the soft tissue. Liver tissue was chosen due to its relative homogeneity, though heterogeneity inherently still exists which could account for some of the spread in the data. Additionally, the previously established dependency on background modulus could account for some of the modulus spread experienced in the chicken liver evaluation. Overall, the values presented here provide a secondary confirmation of the ability of the assay to evaluate a modulus that corresponds to a traditionally accepted soft tissue modulus evaluation technique. Additionally, these results speak to the repeatability of the MGT in assessing the 'correct' modulus value to the embedded tissue. Finally, this data makes a strong argument toward validating the assumption that the issues in the gel-in-gel case were not a function of the MGT assay protocol, but could be attributed to the interaction between the embedded gel and the background gel.

CHAPTER VII

SUMMARY AND RECOMENDATIONS

The work described here has been a collection of evaluations and trials of the newly developed soft tissue modulus evaluation technique termed the MGT assay. The assay has been utilized for a variety of tissue evaluations, including fibrotic murine liver and murine mammary tumor tissue. Additionally, it has been validated relative to a standard mechanical testing technique in the murine liver case, and the results of the assay have been correlated to microstructural composition by comparison to collagen content in the PyV-mT murine mammary tumor case. These investigations provided the utility and initial validation of the MGT assay. In the latest work, the assay was utilized to evaluate the modulus difference between responsive and resistant lines of the BT-474 tumor tissue. Though mechanical properties did not prove to provide a statistically significant biomarker between the lines, a correlation between modulus and collagen content of the samples was established. Finally, an investigation of the limitations and capabilities of the MGT assay was conducted to ensure its aptitude and reliability as a modulus evaluation technique. This analysis brought to light some aspects of the assay that need to be further considered or adapted as well as some areas which had previously been undervalued.

Investigations utilizing the MGT assay have not reached their pinnacle, as there are other aspects of the assay to investigate, and ways to further the analysis paradigm. For example, it is intuitive to think that the segmentation of the CT scans and the

resulting gel and embedded volumes would affect the modulus optimization. This has, in fact, proven to be the case in previous work, where, purely for the sake of observation, the segmented volumes of a sample were manipulated to survey the effect on the modulus evaluation. To present the effect in an organized manner, a theoretical example of the dependency is shown in Figure 25 and Tables 19 and 20 below. A simulation was created which consisted of an ellipsoid embedded in a cylindrical volume with a paraboloid top to mimic a tissue sample embedded in the polyacrylamide gel. A modulus was assigned to the background and to the embedded volume, and a forward evaluation of the forces was performed. The embedded volume was then varied from the baseline state, both by increasing and decreasing the volume, and the resulting system was utilized with the previously established force values to obtain an optimized embedded modulus. This analysis was performed with two different baseline embedded volumes; one was 140 mm^3, which corresponds to the average tumor volume in previous studies, and one was 102 mm^3, to consider the case of smaller embedded volumes. As expected, the changing embedded volume, representing the changing segmentation volume, has an effect of the reconstructed modulus. This can be visualized in Figure 25. The effect appears fairly linear in this case, but that is most likely due to the smooth surfaces and lack of noise in the simulation. It would be expected that the relationship would be more complex in the tissue case. In all evaluations utilizing the MGT assay, segmented gel volumes and segmented embedded volumes have been recorded. However, data for actual volume of the tissue and gel have not been collected due to the difficulty associated with obtaining it as well as the possible destructive effects on the samples. In all cases, masses were recorded, but since the density value of the samples is unknown, the mass only provides a

broad idea of where the segmented volume should fall. The correlation between segmented volume and optimized modulus should be further evaluated and consideration should be given as to how to assess the segmented volume for accuracy.

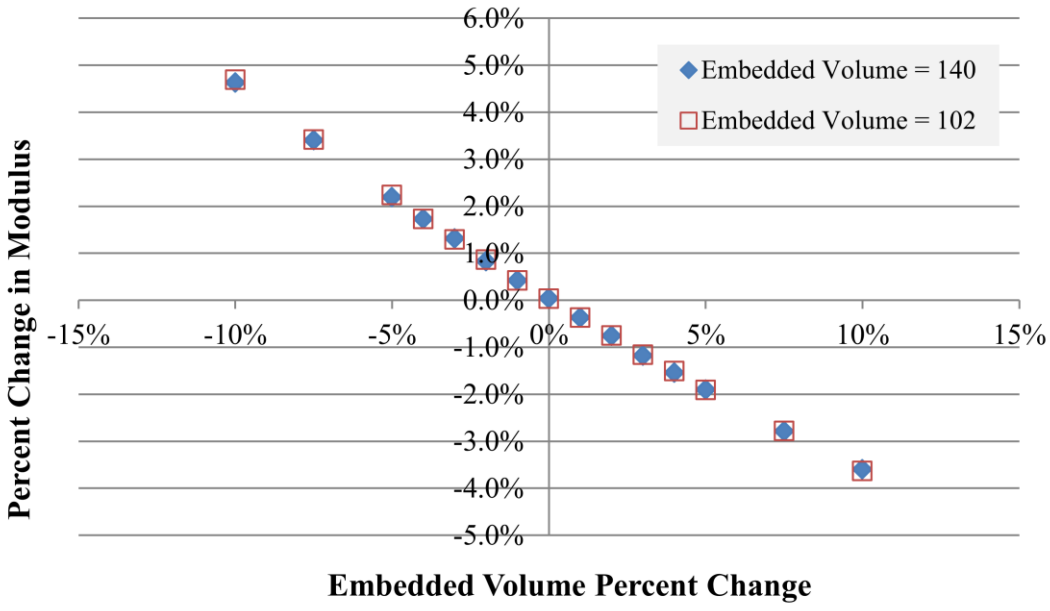

Figure 25. Effect of Embedded Volume on Optimized Modulus.

Table 19. Effect of Embedded Modulus Segmented Volume on Modulus, embedded volume =140 mm^3.

Embedded Volume = 140 mm^3			
Optimized Modulus	Percent Volume change	Difference	Difference Percent of Actual
1.8757	0%	0.0007	0.04%
1.8681	1%	-0.0069	-0.37%
1.8608	2%	-0.0142	-0.76%
1.8528	3%	-0.0222	-1.18%
1.8462	4%	-0.0288	-1.54%
1.8394	5%	-0.0356	-1.90%
1.8227	7.5%	-0.0523	-2.79%
1.8075	10%	-0.0675	-3.60%
1.8828	-1%	0.0078	0.42%
1.8906	-2%	0.0156	0.83%
1.8996	-3%	0.0246	1.31%
1.9074	-4%	0.0324	1.73%
1.9161	-5%	0.0411	2.19%
1.9387	-7.5%	0.0637	3.40%
1.9619	-10%	0.0869	4.63%

Table 20. Effect of Embedded Modulus Segmented Volume on Modulus, embedded volume =102 mm^3.

Embedded Volume = 102 mm^3			
Optimized Modulus	Percent Volume change	Difference	Difference Percent of Actual
1.8755	0%	0.0005	0.03%
1.8681	1%	-0.0069	-0.37%
1.8609	2%	-0.0141	-0.75%
1.8533	3%	-0.0217	-1.16%
1.8466	4%	-0.0284	-1.51%
1.8392	5%	-0.0358	-1.91%
1.8228	7.5%	-0.0522	-2.78%
1.807	10%	-0.068	-3.63%
1.8828	-1%	0.0078	0.42%
1.8911	-2%	0.0161	0.86%
1.8992	-3%	0.0242	1.29%
1.9074	-4%	0.0324	1.73%
1.917	-5%	0.042	2.24%
1.9392	-7.5%	0.0642	3.42%
1.963	-10%	0.088	4.69%

The MGT assay was developed as an adaptable method, insomuch as the mechanical testing protocol and the model utilized can be adjusted. A logical next step in advancing the assay would be to consider the viscoelastic nature of the components. Biological tissues are inherently viscoelastic, and the polyacrylamide gel has demonstrated this behavior in the exponential decay of the force curve with prolonged compression (Figure 27). Work until this point has assumed a steady-state of the system after the dwell period and implemented a linear elastic model of the gel-tissue system. The data points extracted at the end of the dwell period demonstrate a linear stress-strain relationship and hence a linear evaluation of the data as an initial examination was validated. However, the time-dependent data contains information that is lost in the linear evaluation and which may prove insightful in evaluating the tissue. Since the mechanical testing protocol is at the discretion of the investigator and can be adapted at will to the situation, it would be feasible to implement a viscoelastic description of the gel and tissue in the modeling portion of the MGT assay and adapt the mechanical testing accordingly. As an initial investigation of the viscoelastic nature of the system, a standard linear solid (SLS) model, as shown in Figure 26, was fit to the experimental data for the BT-474 tissue samples. The current protocol imposes a dwell period during which stress-relaxation occurs. At each step compression, a constant strain is held while the stress responds accordingly. This approach is not ideal for calculating viscoelastic parameters, but it can serve to provide us with some initial evaluation of the viscoelastic tendencies of the system.

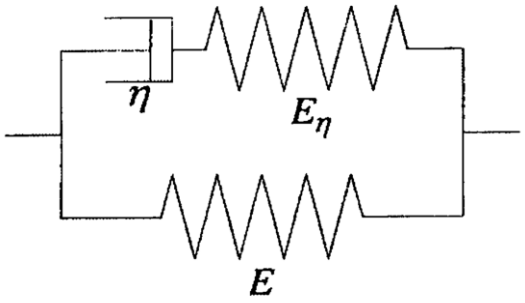

Figure 26. Standard linear solid model.

A sample mechanical testing curve is shown in Figure 27. For this preliminary viscoelastic parameterization, each step compression was considered individually. The constitutive equation for the standard linear solid model is given by:

$$\left(E_\eta + E\right)\varepsilon + \frac{E_\eta E}{\eta}\dot{\varepsilon} = \frac{E_\eta}{\eta}\sigma + \dot{\sigma}$$

When subjected to the conditions of a stress relaxation test (i.e. $\dot{\varepsilon} = 0, \varepsilon = \varepsilon_o$) the time-dependent expression for the stress is given by:

$$\sigma(t) = E\varepsilon_o + E_\eta \varepsilon_o e^{\frac{-t}{\tau_e}}$$

where ε_o is the strain level and τ_e is the stress relaxation time constant and is given by:

$$\tau_e = \frac{\eta}{E_\eta}$$

The relaxation equation was fit to the stress data for the tumor samples, and the coefficients were evaluated using a least squares approximation. A representative curve

fit is presented in Figure 28; the blue line is the testing data and the green line is the SLS fit. The average relaxation time constants for the samples are shown in Table 21.

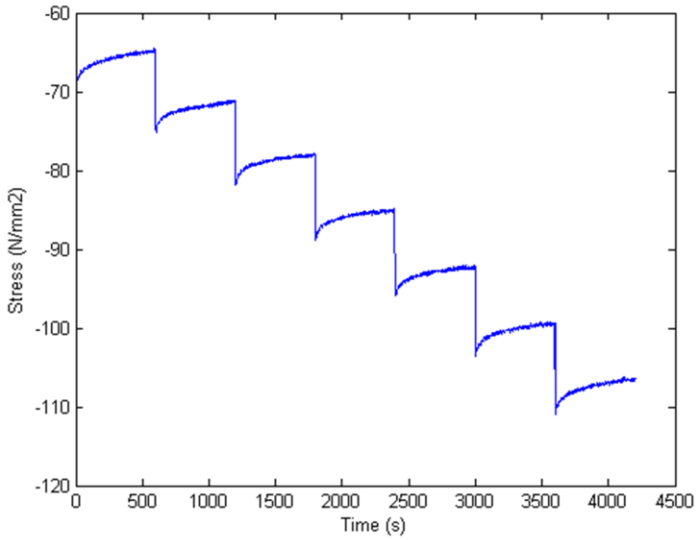

Figure 27. Sample material testing curve.

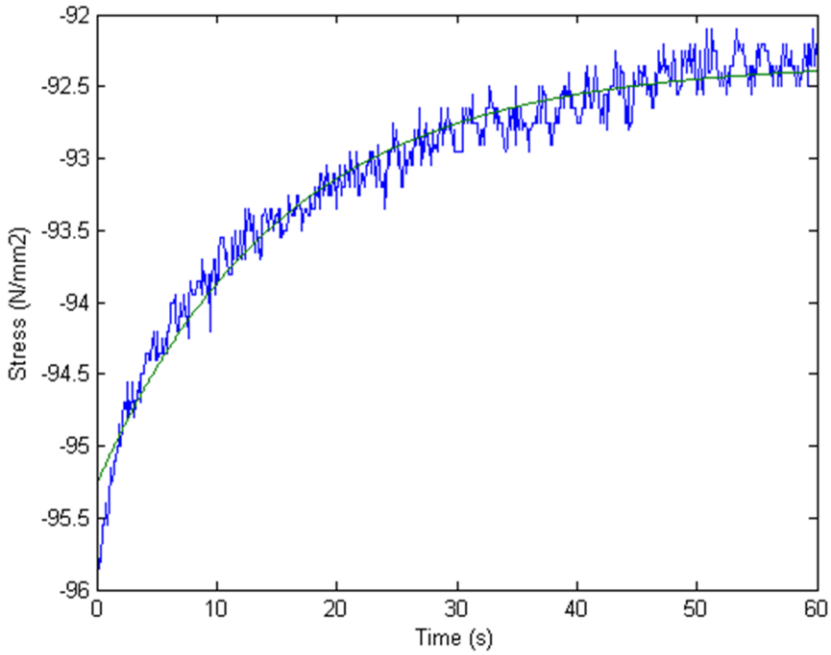

Figure 28. Representative fitting of the SLS model to the experimental data.

Table 21. Stress relaxation time constants for reference gels and heterogeneous gels.

Reference Gel	Average τ_e	Specimen	Average τ_e
Ref1	20.97	BT474-1	23.18
Ref2	21.84	HR6-1	25.13
Ref3	18.63	BT474-2	18.6
		BT474-3	21.27
Ref4	18.82	HR6-2	21.88
		HR6-3	22.72
Ref5	16.76	BT474-4	17.27

From Figure 28, it is obvious that this model is insufficient to describe the data. The main shortcoming is in the initial response, where the model cannot accurately represent the immediate elastic deformation experienced in the mechanical testing. A more detailed model is necessary to fully describe the data, but this simplified model is a suitable first approximation to probe a viscoelastic consideration of the mechanical testing data. Given the data in Table 21, it is interesting to note that in almost all cases the addition of the biological specimen increases the relaxation time of the model fit. This indicates that the tissue is higher in viscosity than the gel and prolongs relaxation of the system. Using dynamic data to assess the tissues as opposed to the static information currently implemented in the MGT assay would allow for further parameterization of the tissue which could provide insight regarding differences among the samples that are lost in the static evaluation.

In regards to the potential for the MGT assay as a component of elastographic techniques, two preliminary evaluations have been performed. Both evaluations were performed using the fibrotic liver samples that were evaluated in Chapter III. The first

preliminary investigation utilized a specially designed compression chamber, as shown in Figure 29(a). The gel-embedded liver sample (created for and used in the MGT assay evaluation) was placed in the chamber, and pre- and post-compression CT images were collected. An elastographic method termed Modality Independent Elastography (MIE) was then utilized to assess the elasticity contrast between the gel and the tissue [120]. The MGT assay analysis of the tissue modulus was also performed, allowing for a direct comparison of the two evaluation techniques. The results are shown in Table 22. The resulting contrast for the two techniques was very similar, with an error of 3.3%. This evaluation provides a prime example of how the MGT assay could potentially be used for validation of elastographic techniques.

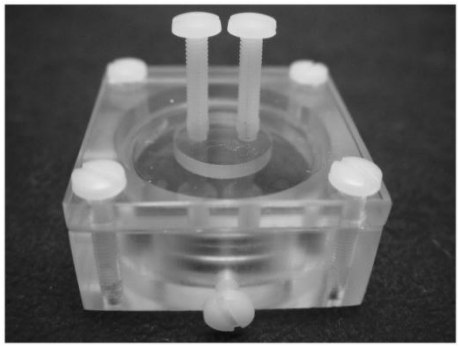
(a)

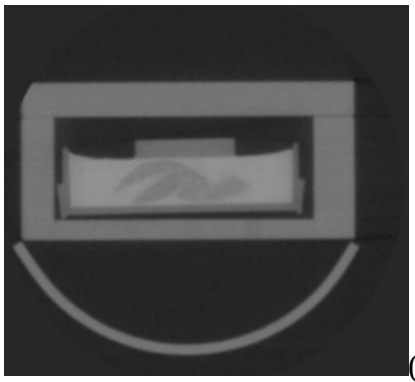
(b)

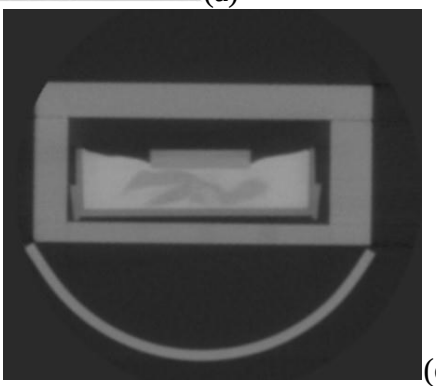
(c)

Figure 29. MIE data acquisition. (a) Photograph of compression chamber, (b) transverse CT slice of setup, and (c) liver-gel block under compression.

Table 22. Elasticity contrast ratios obtained by different material property analyses.

	Elasticity contrast (gel:liver)
MGT Assay	4.23:1
MIE	4.09:1

The second preliminary elastographic evaluation of the MGT system was in the form of ultrasound elastography. As previously mentioned, the gel-tissue heterogeneous system was initially devised in order to provide a sample which was conducive to both ultrasound evaluation and mechanical testing. To this avail, ultrasound images were obtained of one of the gel-embedded fibrotic murine livers. A sample ultrasound image is provided in Figure 30. The resultant strain image is shown in Figure 31. Using the two regions of interest delineated in Figure 31, an average contrast ratio between the gel and the liver was calculated as 2.71. Though the corresponding MGT assay evaluation of the data is not available, this preliminary data set serves to further demonstrate the feasibility of using the gel-embedded tissue system in elastographic techniques, which can then be directly validated using the MGT assay.

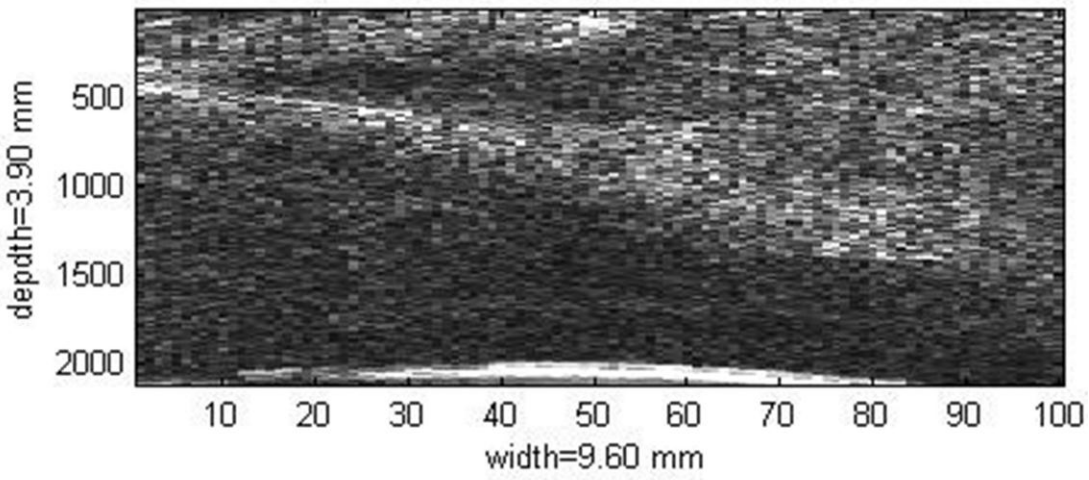

Figure 30. B-mode ultrasound image of gel-liver interface.

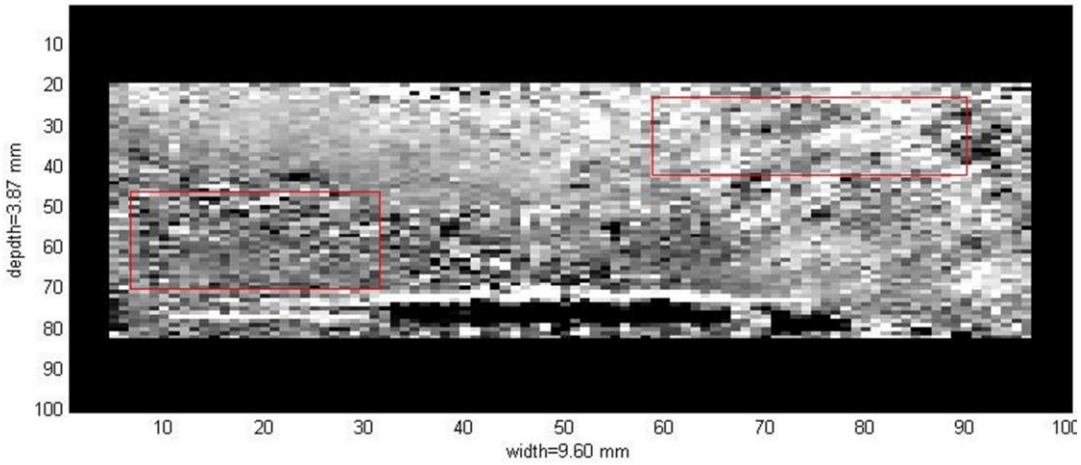

Figure 31. Strain image of gel-liver interface.

Protection of Research Subjects and Societal Implications

In performing any research detailed in this manuscript, all necessary precautions were taken to protect the animals involved. Mice were used frequently in the work presented herein, and their use was always preceded by the appropriate protocol approved by the Institutional Animal Care and Use Committee and following the guidelines for humane care as set forth by the institution. Precautions were taken to minimize pain and ensure quality of life, and the animals were closely monitored to ensure that they were not suffering at any point during their use in the studies.

The utility of the MGT assay lies mainly in research regarding the correlation of disease and tissue modulus. The assay can serve as a stand-alone soft tissue evaluation technique, but it was conceived as a method for validating non-invasive imaging techniques for modulus assessment, and that is most likely how it would find its use in a broad spectrum. It is conceivable that the assay be used in other applications where an evaluation of soft tissue mechanical properties is desired, such as a biopsy evaluation method. However, these methods would be clinical or research-based and hence ethical concerns would be expected to be minimal.

Appendix A: Polyacrylamide

Polyacrylamide gels are formed by the copolymerization of acrylamide monomers and a bifunctional crosslinker, which is typically bisacrylamide (N,N'-methylene-bis-acrylamide). The resulting structure is a three-dimensional network of acrylamide chains, crosslinked by the bisacrylamide. The reaction that produces polyacrylamide is a vinyl addition polymerization initiated by a free radical-producing catalyst (Chramback 1985). The most common catalytic initiator is ammonium persulfate coupled with tetramethylethlenediamine (TEMED). In the presence of TEMED, ammonium persulfate produces free oxygen radicals at an accelerated rate. These free radicals then act as catalysts for the polymerization reaction by converting acrylamide monomers to free radicals. The newly formed acrylamide monomer free radicals then react with unactivated monomers, beginning the polymerization reaction. The concentration of the initiators affects both the rate of polymerization and the properties of the resulting gel; an increase in the concentration of the initiators causes a decrease in the gel elasticity and the average polymer chain length. The polyacylamide polymerization reaction is depicted in Figure 32 [121].

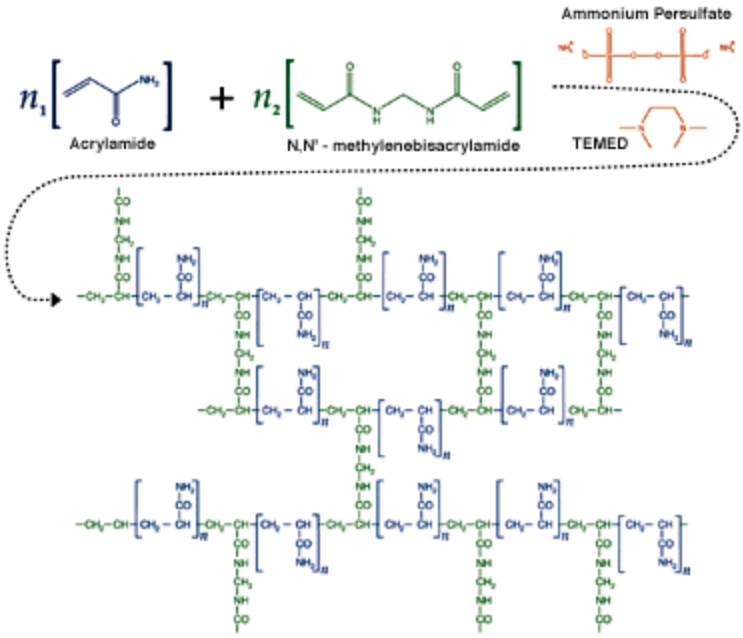

Figure 32. Polyacrylamide gel polymerization reaction and resulting polyacylamide matrix [121].

REFERENCES

1. Kim, J., et al., *Virtual surgery simulation for medical training using multi-resolution organ models.* International Journal of Medical Robotics and Computer Assisted Surgery, 2007. **3**(2): p. 149-158.

2. Basdogan, C., et al., *VR-based simulators for training in minimally invasive surgery.* Ieee Computer Graphics and Applications, 2007. **27**(2): p. 54-66.

3. Delingette, H., *Toward realistic soft-tissue modeling in medical simulation.* Proceedings of the Ieee, 1998. **86**(3): p. 512-523.

4. Szekely, G., et al., *Virtual reality-based simulation of endoscopic surgery.* Presence-Teleoperators and Virtual Environments, 2000. **9**(3): p. 310-333.

5. Buckley, A., K.E. Hill, and J.M. Davidson, *Collagen metabolism.* Methods in Enzymology, 1988(163): p. 674-694.

6. Samani, A., J. Zubovits, and D. Plewes, *Elastic modulus of normal and pathological human breast tissues: an inversion-technique-based investigation of 169 samples.* Phys Med Biol, 2007. **52**: p. 1565-1576.

7. Krouskop, T.A., et al., *Elastic moduli of breast and prostate tissues under compression.* Ultrason Imaging, 1998. **20**(4): p. 260-74.

8. Anderson, W., *Synopsis of pathology*. 1980, St. Louis: Mosby.

9. Levy, M., H. Bass, and R. Stren, *Handbook of Elastic Properties of Solids, Liquids, and Gases*. 2001, San Diego: Academic Press.

10. Yeh, W.C., et al., *Elastic modulus measurements of human liver and correlation with pathology.* Ultrasound Med Biol, 2002. **28**(4): p. 467-74.

11. de Ledinghen, V., et al., *Diagnosis of hepatic fibrosis and cirrhosis by transient elastography in HIV/hepatitis C virus-coinfected patients.* J Acquir Immune Defic Syndr, 2006. **41**(2): p. 175-9.

12. Ziol, M., et al., *Noninvasive assessment of liver fibrosis by measurement of stiffness in patients with chronic hepatitis C.* Hepatology, 2005. **41**(1): p. 48-54.

13. Tilleman, T.R., M.M. Tilleman, and M.H.A. Neumann, *The elastic properties of cancerous skin: poisson's ratio and young's modulus.* Israel Medical Association Journal, 2004. **6**(12): p. 753-755.

14. Herrington, D.M., et al., *Relationship Between Arterial Stiffness and Subclinical Aortic Atherosclerosis.* Circulation, 2004. **110**(4): p. 432-437.

15. Covell, J.W. and J.J. Ross, *Nature and significance of alterations in myocardial compliance.* The American Journal of Cardiology, 1973. **32**(4): p. 449-455.

16. Diamond, G. and J.S. Forrester, *Effect of Coronary Artery Disease and Acute Myocardial Infarction on Left Ventricular Compliance in Man.* Circulation, 1972. **45**(1): p. 11-19.

17. Gaasch, W.H., et al., *Left Ventricular Compliance: Mechanisms and Clinical Implications.* The American Journal of Cardiology, 1976. **38**: p. 645-653.

18. Phipps, S., et al., *Measurement of tissue mechanical characteristics to distinguish between benign and malignant prostatic disease.* Urology, 2005. **66**(2).

19. Nagasaki, T., et al., *Increased pulse wave velocity in subclinical hypothyroidism.* The Journal of Clinical Endocrinology and Metabolism, 2006. **91**(1): p. 154-158.

20. Giannattasio, C. and G. Mancia, *Arterial distensibility in humans. Modulating mechanisms, alterations in diseases and effects of treatment.* Journal of Hypertension, 2002. **20**(10): p. 1889-1899.

21. vanPopele, N.M., et al., *Association Between Arterial Stiffness and Atherosclerosis: The Rotterdam Study.* Stroke, 2001. **32**(2): p. 454-460.

22. Sandrin, L., et al., *Transient elastography: A new noninvasive method for assessment of hepatic fibrosis.* Ultrasound in Medicine and Biology, 2003. **29**(12): p. 1705-1713.

23. Beaugrand, M., *How to assess liver fibrosis and for what purpose?* Journal of Hepatology, 2006. **44**(3): p. 444-445.

24. Bilgen, M., et al., *Elastography imaging of small animal oncology models: a feasibility study.* Ultrasound in Medicine and Biology, 2003. **29**(9): p. 1291-1296.

25. Garra, B.S., et al., *Elastography of breast lesions: Initial clinical results.* Radiology, 1997. **202**(1): p. 79-86.

26. Hall, T.J., *Beyond the basics: Elasticity imaging with US.* Radiographics, 2003. **23**(6): p. 1657-1671.

27. Ophir, J., et al., *Elastography - A quantitative method for imaging the elasticity of biological tissues.* Ultrasonic Imaging, 1991. **13**(2): p. 111-134.

28. Washington, C.W. and M.I. Miga, *Modality independent elastography (MIE): A new approach to elasticity imaging.* Ieee Transactions on Medical Imaging, 2004. **23**(9): p. 1117-1128.

29. Lukes, L., et al., *The Origins of Breast Cancer Prognostic Gene Expression Profiles.* Cancer Research, 2009. **69**(1): p. 310-318.

30. Paik, S., et al., *A multigene assay to predict recurrence of tamoxifen-treated, node-negative breast cancer.* New England Journal of Medicine, 2004. **351**(27): p. 2817-2826.

31. Ramaswamy, S., et al., *A molecular signature of metastasis in primary solid tumors.* Nature Genetics, 2003. **33**(1): p. 49-54.

32. van de Vijver, M.J., et al., *A gene-expression signature as a predictor of survival in breast cancer.* New England Journal of Medicine, 2002. **347**(25): p. 1999-2009.

33. Eckhardt, B.L., et al., *Genomic analysis of a spontaneous model of breast cancer metastasis to bone reveals a role for the extracellular matrix.* Molecular Cancer Research, 2005. **3**(1): p. 1-13.

34. Stamenkovic, I., *Matrix metalloproteinases in tumor invasion and metastasis.* Seminars in Cancer Biology, 2000. **10**(6): p. 415-433.

35. Duffy, M.J., et al., *Metalloproteinases: role in breast carcinogenesis, invasion and metastasis.* Breast Cancer Research, 2000. **2**(4): p. 252-257.

36. Wang, W.G., et al., *Single cell behavior in metastatic primary mammary tumors correlated with gene expression patterns revealed by molecular profiling.* Cancer Research, 2002. **62**(21): p. 6278-6288.

37. Somasundaram, R. and D. Schuppan, *Type I, II, III, IV, V, and VI collagens serve as extracellular ligands for the isoforms of platelet-derived growth factor (AA, BB, and AB).* Journal of Biological Chemistry, 1996. **271**(43): p. 26884-26891.

38. Kuo, C.J., et al., *Oligomerization-dependent regulation of motility and morphogenesis by the collagen XVIII NC1/endostatin domain.* Journal of Cell Biology, 2001. **152**(6): p. 1233-1246.

39. Daniels, K.J., et al., *Expression of type VI collagen in uveal melanoma: Its role in pattern formation and tumor progression.* Laboratory Investigation, 1996. **75**(1): p. 55-66.

40. Colpaert, C., et al., *The presence of a fibrotic focus is an independent predictor of early metastasis in lymph node-negative breast cancer patients.* American Journal of Surgical Pathology, 2001. **25**(12): p. 1557-1558.

41. Hasebe, T., et al., *New prognostic histological parameter of invasive ductal carcinoma of the breast: Clinicopathological significance of fibrotic focus.* Pathology International, 2000. **50**(4): p. 263-272.

42. Chen, E.J., et al., *Young's modulus measurements of soft tissues with application to elasticity imaging.* Ieee Transactions on Ultrasonics Ferroelectrics and Frequency Control, 1996. **43**(1): p. 191-194.

43. Hoyt, K., et al., *Tissue elasticity properties as biomarkers for prostate cancer.* Cancer Biomarkers, 2008. **4**(4-5): p. 213-225.

44. Kiss, M.Z., T. Varghese, and T.J. Hall, *Viscoelastic characterization of in vitro canine tissue.* Physics in Medicine and Biology, 2004. **49**(18): p. DOI 10.1088/0031-9155/49/18/002|PII S0031-9155(04)75297-5.

45. Kallel, F., et al., *Elastographic imaging of low-contrast elastic modulus distributions in tissue.* Ultrasound in Medicine and Biology, 1998. **24**(3): p. 409-425.

46. Erkamp, R.Q., et al., *Measuring the Elastic Modulus of Small Tissue Samples.* Ultrasonic Imaging, 1998. **20**: p. 17-28.

47. Carter, F.J., et al., *Measurements and modelling of the compliance of human and porcine organs.* Med Image Anal, 2001. **5**(4): p. 231-6.

48. Samani, A., et al., *Measuring the elastic modulus of ex vivo small tissue samples.* Phys Med Biol, 2003. **48**: p. 2183-2198.

49. Samani, A. and D. Plewes, *An inverse problem solution for measuring the elastic modulus of intact ex vivo breast tissue tumours.* Phys Med Biol, 2007. **52**: p. 1247-1260.

50. Paszek, M. and V. Weaver, *The tension mounts: mechanics meets morphogenesis and malignancy.* Journal of Mammary Gland Biology and Neoplasia, 2004. **9**(4): p. 325-342.

51. Butcher, D., T. Alliston, and V. Weaver, *A tense situation: forcing tumour progression.* Nature Reviews Cancer, 2009. **9**.

52. Levental, K., et al., *Matrix crosslinking forces tumor progression by enhancing integrin signaling.* Cell, 2009. **139**: p. 891-906.

53. Lo, C., et al., *Cell movement is guided by the rigidity of the substrate.* Biophysical Journal, 2000. **79**: p. 144-152.

54. Sullivan, J.M., G. Charron, and K.D. Paulsen, *A three-dimensional mesh generator for arbitrary multiple material domains.* Finite Elements in Analysis and Design, 1997. **25**(3-4): p. 219-241.

55. Joachimowicz, N., C. Pichot, and J.P. Hugonin, *Inverse scattering - an interative numerical-method for electromagnetic imaging.* Ieee Transactions on Antennas and Propagation, 1991. **39**(12): p. 1742-1752.

56. Wells, R.G., *The role of matrix stiffness in hepatic stellate cell activation and liver fibrosis.* Journal of Clinical Gastroenterology, 2005. **39**(4): p. S158-S161.

57. Yeh, W.C., et al., *Elastic modulus measurements of human liver and correlation with pathology.* Ultrasound in Medicine and Biology, 2002. **28**(4): p. 467-474.

58. Sandrin, L., et al., *Transient elastography: A new noninvasive method for assessment of hepatic fibrosis.* Ultrasound in Medicine and Biology, 2003. **29**(12): p. 1705-1713.

59. Gomez-Dominguez, E., et al., *Transient elastography: a valid alternative to biopsy in patients with chronic liver disease.* Alimentary Pharmacology & Therapeutics, 2006. **24**(3): p. 513-518.

60. Klatt, D., et al., *In vivo determination of hepatic stiffness using steady-state free precession magnetic resonance elastography.* Investigative Radiology, 2006. **41**(12): p. 841-848.

61. Kruse, S.A., et al., *Tissue characterization using magnetic resonance elastography: preliminary results.* Physics in Medicine and Biology, 2000. **45**(6): p. 1579-1590.

62. Bamber, J.C., et al., *Quantitative-Evaluation of Real-Time Ultrasound Features of the Breast.* Ultrasound in Medicine and Biology, 1988. **14**: p. 81-87.

63. Cespedes, I. and J. Ophir, *Reduction of Image Noise in Elastography.* Ultrasonic Imaging, 1993. **15**(2): p. 89-102.

64. Nightingale, K.R., et al., *A finite element model of remote palpation of breast lesions using radiation force: Factors affecting tissue displacement.* Ultrasonic Imaging, 2000. **22**(1): p. 35-54.

65. Steinberg, B.D., D.C. Sullivan, and D.L. Carlson, *Disparity mapping applied to sonography of the breast: Technical note.* Radiology, 1998. **207**(2): p. 545-550.

66. Sumi, C., K. Nakayama, and M. Kubota, *An effective ultrasonic strain measurement-based shear modulus reconstruction technique for superficial tissues - demonstration on in vitro pork ribs and in vivo human breast tissues.* Physics in Medicine and Biology, 2000. **45**(6): p. 1511-1520.

67. Lorenz, A., et al., *Ultrasound elastography of the prostate: An innovative technique for tumour-detection.* Ultraschall in Der Medizin, 2000. **21**(1): p. 8-15.

68. Kallel, F., et al., *Elastographic imaging of the normal canine prostate in vitro.* Ultrasonic Imaging, 1999. **21**(3): p. 201-215.

69. Lyshchik, A., et al., *Thyroid gland tumor diagnosis at US elastography.* Radiology, 2005. **237**(1): p. 202-211.

70. de Korte, C.L., et al., *Characterization of plaque components and vulnerability with intravascular ultrasound elastography.* Physics in Medicine and Biology, 2000. **45**(6): p. 1465-1475.

71. Bom, N., et al., *Quantification of plaque volume, shear stress on the endothelium, and mechanical properties of the arterial wall with intravascular ultrasound imaging.* Zeitschrift Fur Kardiologie, 2000. **89**: p. 105-111.

72. Cao, L., et al., *Compressive properties of mouse articular cartilage determined in a novel micro-indentation test method and biphasic finite element model.* J Biomech Eng, 2006. **128**(5): p. 766-71.

73. Delalleau, A., et al., *Characterization of the mechanical properties of skin by inverse analysis combined with the indentation test.* Journal of Biomechanics, 2006. **39**: p. 1603-1610.

74. Klaesner, J.W., et al., *Accuracy and reliability testing of a portable soft tissue indentor.* IEEE Trans Neural Syst Rehabil Eng, 2001. **9**(2): p. 232-40.

75. Ishak, K., et al., *Histological grading and staging of chronic hepatitis.* Journal of Hepatology, 1995. **22**: p. 696-699.

76. Stevanovic, M., M. Yovanovich, and J.R. Culham, *Modeling contact between rigid sphere and elastic layer bonded to rigid substrate.* IEEE Trans on Components and Package Technologies, 2001. **24**(2): p. 207-212.

77. Chen, W.T. and P.A. Engel, *Impact and contact stress analysis in multilayer media.* International Journal of Solids and Structures, 1972. **8**: p. 1257-1281.

78. Cash, D.M., et al., *Image-guided liver surgery: Concepts and initial clinical experiences.* Journal of Gastrointestinal Surgery, 2006. **(in press)**.

79. Cash, D.M., et al., *Compensating for intraoperative soft-tissue deformations using incomplete surface data and finite elements.* Ieee Transactions on Medical Imaging, 2005. **24**(11): p. 1479-1491.

80. Miga, M.I., et al., *In vivo quantification of a homogeneous brain deformation model for updating preoperative images during surgery.* IEEE Transactions on Biomedical Engineering, 2000. **47**(2): p. 266-273.

81. Miga, M.I., et al., *Model-updated image guidance: Initial clinical experiences with gravity-induced brain deformation.* IEEE Transactions on Medical Imaging, 1999. **18**(10): p. 866-874.

82. Bramley, R. and X. Wang. *SPLIB: A library of iterative methods for sparse linear system*. [Technical Report] 1995.

83. Sheskin, D.J., *Handbook of Parametric and Nonparametric Statistical Procedure*. 2nd ed. 2000, New York: Chapman & Hall/CRC.

84. Wang, B., et al., *An experimental study on biomechanical properties of hepatic tissue using a new measuring method* Biomed Mat Eng, 1992. **2**(3): p. 133-138.

85. Miga, M.I., et al., *Model-updated image guidance: Initial clinical experiences with gravity-induced brain deformation.* IEEE Transactions on Medical Imaging, 1999. **18**: p. 866-874.

86. Sinkus, R., et al., *Potential of MRI and ultrasound radiation force in elastography: applications to diagnosis and therapy.* Proceeding of the IEEE, 2008. **96**: p. 490-499.

87. Souchon, R., et al., *Visualization of HIFU lesions using elastography of the human prostate in vivo: preliminary results.* Ultrasound in Medicine and Biology, 2003. **29**(7): p. 1007-1015.

88. Garra, B.S., et al., *Elastography of breast lesions: intial clinical results.* Radiology, 1997. **202**(1): p. 79-86.

89. Venkatesh, S.K., et al., *MR elastography of liver tumors: preliminary results.* American Journal of Roentgenology, 2008. **190**(6): p. 1534-1540.

90. Fahey, B.J., et al., *In vivo visualization of abdominal malignancies with acoustic radiation force elastography.* Physics in Medicine & Biology, 2008. **53**: p. 279-293.

91. Muthupillai, R., et al., *Magnetic-resonance elastography by direct visualization of propagating acoustic strain waves.* Science, 1995. **269**: p. 1854-1857.

92. Provenzano, P.P., et al., *Collagen density promotes mammary tumor initiation and progression.* BMC Medicine, 2008. **6**(11).

93. Naylor, C., *The rational clinical examination: physical examination of the liver.* Journal of the American Medical Association, 1994. **271**(23): p. 1859-1865.

94. Mahoney, L. and A. Csima, *Efficiency of palpation in clinical detection of breast cancer.* Canadian Medical Association Journal, 1982. **127**(8): p. 729-730.

95. Ghany, M. and E. Doo, *Assessment of liver fibrosis: palpate, poke, or pulse?* Hepatology, 2005. **42**(4): p. 759-761.

96. McCormick, P. and N. Nolan, *Palpable epigastric liver as a physical sign of cirrhosis: a prospective study.* European Journal of Gastroenterology & Hepatology, 2004. **16**(12): p. 1331-1334.

97. Delos, D., et al., *The effects of RANKL inhibition on fracture healing and bone strength in a mouse model of osteogenesis imperfecta.* Journal of Orthopaedic Research, 2008. **26**: p. 153-164.

98. Shefelbine, S.J., et al., *Prediction of fracture callus mechanical properties using micro-CT images and voxel-based finite element analysis.* Bone, 2005. **36**: p. 480-488.

99. Huddleston, P.M., et al., *Ciprofloxacin Inhibition of Experimental Fracture-Healing.* The Journal of Bone & Joint Surgery, 2000. **82**: p. 161-173.

100. Campos, A.C., A.K. Groth, and A.B. Branco, *Assessment and nutritional aspects of wound healing.* Current Opinion in Clinical Nutrition & Metabolic Care, 2008. **11**(3): p. 281-288.

101. Gal, P., et al., *Early changes in the tensile strength and morphology of primary sutured skin wounds in rats.* Folia Biologica, 2006. **52**(4): p. 109-115.

102. Barnes, S.L., et al., *Development of a mechanical testing assay for fibrotic murine liver.* Medical Physics, 2007. **34**(11): p. 4439-4450.

103. Hines, W.W. and D.C. Montgomery, *Probability and Statistics in Engineering and Management Science*. Third ed. 1990, New York: John Wiley & Sons, Inc.

104. Montgomery, D.C. and G.C. Runger, *Applied Statistics and Probability for Engineers*. 2003, New York: John Wiley & Sons, Inc.

105. Group, U.S.C.S.W. *United States Cancer Statistics: 1999-2006 Incidence and Mortality Web-based Report*. 2010; Available from: http://www.cdc.gov/uscs. <http://apps.nccd.cdc.gov/uscs/>.

106. Slamon, D., et al., *Studies of the HER-2/neu Proto-oncogene in Human Breast and Ovarian Cancer.* Science, 1989. **244**(4905): p. 707-712.

107. Yarden, Y. and M.X. Sliwkowski, *Untangling the ErbB signaling network.* Nature Reviews Molecular Cell Biology, 2001. **2**(2): p. 127-137.

108. Chang, H.R., *Trastuzumab-based neoadjuvant therapy in patients with HER2-positive breast cancer.* Cancer, 2010. **116**(12): p. 2856–2867.

109. Cho, H.S., M. K., and K.X. Ramyar, *Structure of the extracellular region of HER2 alone and in complex with the herceptin fab.* Nature, 2003. **421**: p. 756-60.

110. Angus, D.B., R.W. Akita, and W.D. Fox, *Targeting ligand activated ErbB2 signaling inhibits breast and prostate tumor growth.* Cancer Cell, 2002. **2**: p. 127-137.

111. Lu, Y., et al., *Insulin-like growth factor-I receptor signaling and resistance to trastuzumab (herceptin).* Journal of the National Cancer Institute, 2001. **93**: p. 1852-1857.

112. Nahta, R., et al., *Insulin-like growth factor-I receptor/human epidermal growth factor receptor 2 heterodimerization contributes to trastuzumab resistance of breast cancer cells.* Cancer Research, 2005. **65**: p. 11118-11128.

113. Jerome, L., N. Alami, and S. Belanger, *Recombinant human insulin-like growth factor binding protein 3 inhibits growth of human epidermal grwoth factor receptor-2-overexpressing breast tumors and potentiates herceptin activity in vivo.* Cancer Research, 2006. **66**: p. 7245-7252.

114. Isakoff, S.J., E. J.A., and H.Y. Irie, *Breast cancer-associated PIK3CA mutatoins are oncogenic in mammary epithelial cells.* Cancer Research, 2005. **65**(10992-11000).

115. Berns, K., H.M. Horlings, and B.T. Hennessy, *A functional genetic approach identifies the PI3K pathway as a major determinant of trastuzumab resistance in breast cancer.* Cancer Cell, 2007. **12**: p. 395-402.

116. Nagata, Y., K.H. Lan, and X. Zhou, *PTEN activation contributes to tumor inhibition by trastuzumab, and loss of PTEN predicts trastuzumab resistance in patients.* Cancer Cell, 2004. **6**(117-127).

117. Sandrin, L., et al., *Transient elastography: a new noninvasive method for assessment of hepatic fibrosis.* Ultrasound Med Biol, 2003. **29**(12): p. 1705-13.

118. Ritter, C.A., et al., *Human breast cancer cells selected for resistance to trastuzumab in vivo overexpress epidermal growth factor receptor and ErbB Ligands and remain dependent on the ErbB receptor network.* Clinical Cancer Research, 2007. **13**(16): p. 4909-4919.

119. Barnes, S., P. Young, and M. Miga, *A novel model-gel-tissue assay analysis for comparing tumor elastic properties to collagen content.* Biomechanics and Modeling in Mechanobiology, 2009. **8**(4): p. 337-343.

120. Ou, J., *Development of modality-independent elastography as a method of breast cancer detection*, in *Biomedical Engineering*. 2007, Vanderbilt University: Nashville. p. 165.

121. *The Polyacrylamide Matrix*. 2010; Available from: http://www.nationaldiagnostics.com/article_info.php/articles_id/6.